Inês Alexandra Manata Antunes Valente

Licenciada em Ciências da Engenharia Química e Bioquímica

Adsorption equilibria of flue gas components on activated carbon

Dissertação para obtenção do Grau de Mestre em

Engenharia Química e Bioquímica

Orientador: Doutora Isabel Alexandra de Almeida Caneto Esteves Esperança

Co-orientadores: Professor Doutor José Paulo Barbosa Mota

Doutor Rui Pedro Pinto Lopes Ribeiro

Monte da Caparica, Faculdade de Ciências e Tecnologia, Universidade de Lisboa

Março 2014

Adsorption equilibria of flue gas components on activated carbon

Acknowledgments

No limiar do final de mais uma etapa deste caminho de longos anos, não podia deixar passar a oportunidade de agradecer às pessoas que me acompanharam até aqui e aquelas que se destacaram no desfecho deste Mestrado. Gostaria então de agradecer:

Ao Professor Doutor José Paulo Mota e à Doutora Isabel Esteves pela orientação e, por me terem convencido a fazer a minha tese em Adsorção Gasosa, um tema ao qual me afeiçoei e do qual tantos conhecimentos adquiri.

Ao Doutor Rui Ribeiro, pela orientação, paciência e disponibilidade contínua para as minhas "questões mais esotéricas".

À Faculdade de Ciências e Tecnologia, da Universidade Nova de Lisboa, local que tanto contribuí-o para o meu desenvolvimento pessoal e profissional.

Ao Professor Mário Eusébio pelos seus conselhos.

Ao Doutor Ricardo Silva pela boa disposição e ajuda na parte informática. À Eliana Orfão, pela sua constante alegria e positivismo.

Aos meus colegas, vocês que partilharam comigo as dificuldades destes últimos meses: João Gomes, pela companhia, boa disposição e apoio; e à Bárbara Camacho, pela orientação, disponibilidade e amizade.

Ao Nuno Costa, à Inês Matos e à Professora Isabel Fonseca que tanto me ajudaram no capítulo de caracterização do material.

À Dª Palminha e à Dª Maria José Carapinha, pela vossa ajuda.

Aos meus amigos, ao pessoal do BEST Almada, às/aos minhas/meus colegas da Duplix | Impressão e Imagem pela vossa força, apoio e compreensão.

Aos meus pais, avós, irmão e ao Diogo pelo vosso apoio e amor incondicional para o qual não existem palavras para descrever.

A todos vós, muito obrigada!

Inês Valente

"*Attitude is a little thing that makes a big difference.*"

Winston Churchill

Gostaria de dedicar esta tese aos meus pais e avós, que sempre fizeram de tudo para me darem a melhor educação.

Abstract

Carbon dioxide (CO_2) is the greenhouse gas which can be found at higher concentrations in the atmosphere. This is mainly due to emission of CO_2 from anthropogenic sources as the flue gases fossil fueled power stations.

Adsorption processes are considered as a viable alternative to perform the capture of the CO_2 emitted from flue gases. The development of adsorption-based technologies depends on the knowledge of the adsorption equilibrium properties of the flue gas components over potential adsorbent materials This work consisted in the characterization of two activated carbons: ANGUARD 6, 1 mm, in the form of extruded (Sutcliffe Speakman Carbons Ltd., UK) and a honeycomb monolith (Mast Carbon International Limited, UK). Surface chemistry characterization of both carbons was performed. Characterization of the surface area, pore volumes and pore size distribution was also performed for the ANGUARD 6 sample.

Adsorption equilibrium of carbon dioxide (CO_2), nitrogen (N_2) and butane (C_4H_{10}) at 303.15K, 323.15K and 353.15K in a pressure range of 0-35 bar was measured on ANGUARD 6. Adsorption equilibrium of CO_2 on the activated carbon honeycomb monolith was also measured in the same temperature and pressure ranges as for the ANGUARD 6 sample. The Sips isotherm model was employed to fit the experimental data and the model could fit the data successfully. The isosteric heats of adsorption for each of the studied species were also determined.

Keywords: adsorption equilibrium, activated carbon, carbon dioxide, gravimetric method.

Resumo

O dióxido de carbono é um gás com efeito de estufa que pode ser encontrado em maiores concentrações na atmosfera. Este facto deve-se, principalmente, a emissões de origem antropogénica nas quais se inclui a emissão de gases de chaminé de centrais de produção de energia a partir de combustíveis fósseis.

Processos de adsorção são considerados como uma opção viável para aplicação na captura de CO_2 de gases de chaminé. O desenvolvimento de processos de separação por adsorção depende no conhecimento das propriedades de equilíbrio de adsorção dos componentes dos gases de chaminé por potenciais adsorventes.

Este trabalho consistiu na caracterização de dois carvões activados: ANGUARD 6, 1 mm, em forma de extrudados (Sutcliffe Speakman Carbons Ltd., UK) e um monólito de estrutura tipo "favo de mel" (Mast Carbon International Limited, UK). A química de superfície de ambos os carvões foi caracterizada. Caracterização da área superficial, volume de poros e distribuição de tamanho de poros foi efectuada para a amostra de ANGUARD 6.

Foi estudado o equilíbrio de adsorção de dióxido de carbono (CO_2), azoto (N_2) e butano (C_4H_{10}) a temperaturas de 303.15K, 323.15K e 353.15K, na gama de pressão de 0 a 35 bar, na amostra de ANGUARD 6. Equilíbrio de adsorção de CO_2 no monólito de carvão activado foi também estudado, na mesma gama de pressão e temperatura. O modelo de isotérmica de Sips foi utilizado para descrever os dados obtidos experimentalmente. Os calores isostéricos dos vários adsorbatos estudados foram também determinados.

Palavras-chave: equilíbrio de adsorção, carvão activado, dióxido de carbono, método gravimétrico.

Contents

List of Figures

List of Tables

List of Symbols

Notation

A_A - Dispersion constants for the adsorbate calculated from Kirkwood-Muller formulae (erg^2.cm^6)

A_S - Dispersion constants for the adsorbent calculated from Kirkwood-Muller formulae (erg^2.cm^6)

b - Affinity constant (bar^{-1})

b_0 - Affinity constant at a reference temperature, T_0 (bar^{-1})

C – BET Constant

d_A - Gas molecular diameter ($\dot{A}$)

d_s - Adsorbent atom diameter ($\dot{A}$)

d_0 - Average of the adsorbate and adsorbent molecule diameters ($\dot{A}$)

L - Distance between the nuclei of two parallel infinite lattice planes or pore width ($\dot{A}$)

m - Weight read from the balance at any time (g)

m_h - Mass of the sample holder (g)

m_s - Mass of the sample adsorbent (g)

mc^2 - Kinetic energy of electron (0.8183x10^{-6} erg)

n – Sips isotherm model parameter

n_0 - Sips isotherm model parameter n at the same reference temperature, T_0

n_a - Amount adsorbed (cm^3/g)

n_m^a - Monolayer capacity (cm^3/g)

n_{CFS} - Number of moles of carbon surface functionalities at the carbon surface

N_A - Number of gas molecules per unit area (molecules/cm^2)

N_{Av} - Avogadro's number (6.023x10^{23} molecules^{-1})

N_S - Number adsorbent molecules per unit area (molecules/ cm^2)

P – Absolute pressure (bar or mmHg)

P^0 - Saturated vapor pressure (bar or mmHg)

q_i - Adsorbed quantity of the more adsorbed specie (mol/kg)

q_j - Quantity of the less adsorb quantity (mol/kg)

q_{ex} - Specific excess adsorbed (mol/kg)

q_{net} - Net adsorption (mol/kg)

q_t - Total amount adsorbed (mol/kg)

q_{ts} - Maximum amount adsorbed (mol/kg)

Q – Heat of adsorption (kJ/mol)

R or R_g - Ideal gas constant (8.31441x10^7 ergs/mole.K)

S_{BET} – BET surface area (m^2/g)

S_{ext} – Surface external area (m^2/g)

T - Temperature (K)

t - Standard multilayer thickness on the reference non-porous material at the corresponding relative pressure ($\dot{A}$)

V_B – Bulk volume (mL/g)

V_h - Volume of all moving parts present in the measuring cell (cm^3/g)

V_{MP} – Microporous volume (cm^3/g)

V_p - Accessible pore volume of the adsorbent (cm^3/g)

V_{PT} - Total porosity (%)

V_S – Skeletal volume in Hg porosimetry (mL/g)

V_s - Specific adsorbent volume impenetrable to the adsorbate (cm^3/g)

X_s - Diamagnetic susceptibility of an adsorbate atom (cm^3)

X_A - Diamagnetic susceptibility of gas molecule (cm^3)

$(-\Delta H)$ - Isosteric heat of adsorption (kJ/mol)

Greek Letters

α - Sips isotherm model parameter

α_A - Polarizability of gas molecule (cm^3)

α_s - Polarizability of adsorbent atoms (cm^3)

$\alpha_{i/j}$ - Selectivity

σ - Cross-sectional area that each adsorbate molecule occupy in the completed monolayer (nm^2)

ρ_h - Density of the sample holder (g/cm^3)

ρ_s - Skeletal density of the sample adsorbent (g/cm^3)

θ - Fractional loading

Chapter 1

1. Introduction

1.1. Motivation

Carbon dioxide (CO_2) is naturally present in the atmosphere as part of the Earth's carbon cycle (the natural circulation of carbon among the atmosphere and life beings). But since the Industrial Revolution, human activities have been altering the carbon cycle, by adding more CO_2 to the atmosphere. It is now estimated that around 90% of the carbon dioxide present in the atmosphere is from anthropogenic origin [1].

According to the *Inventory of U.S Greenhouse Gas Emissions and Sinks (1990-2011)* electricity production (38%), transportation of people and goods (31%) and industry (14%) are the sectors that most contribute to the emission of carbon dioxide to the atmosphere. This results from the burning of fossil fuels like coal, oil and natural gas [2]. Since carbon dioxide is a greenhouse gas, which can contribute to global climate change, it is imperial to reduce its emissions. In the past few decades many projects and possible solutions have been proposed to mitigate this problem. This includes improvements in energy efficiency and utilization of renewable and greener sources of energy [3].

Nowadays, CCS (CO_2 Capture and Storage) is starting in several power plants [4]. CCS process consists in the capture of the carbon dioxide resulting from the burning of fossil fuels. CCS can be performed using pre-combustion or post-combustion techniques [5]. Then, after being separated from other gases, CO_2 is compressed and transported through a net of pipelines or ships so it can be injected in underground geological formations, where it will be safely storage for several years. It is estimated that CCS process can reduce the emissions of carbon dioxide by 90% [6].

The leading technology for implementation of post-combustion CO_2 capture is an absorption-based capture process where the flue gas resulting from the burning of fossil fuels (mainly constituted by carbon dioxide, nitrogen and water vapor) is fed to reactor that contains a solvent, usually amines. This process is called *amine scrubbing* [7]. The solvent will react with the CO_2 and then is pumped to another tank where carbon dioxide and the solvent will be separated (amine regeneration), so the solvent can be recycled to the first tank and the gas

compressed. Despite being a mature process, amine scrubbing presents some drawbacks. Amine regeneration is very energy intensive, corrosion problems as well as the emission of carcinogenic compounds. Therefore, alternative processes are needed to overcome these difficulties [8].

Adsorption-based separation processes are present important alternatives for CO_2 capture from flue gases. Among this processes, Pressure Swing adsorption (PSA) is an important option. In this process the pressurized flue gas stream is passed through a porous solid that preferentially adsorbs CO_2. After this, by decreasing the pressure, CO_2 is desorbed and ready to be compressed [9].

The PSA performance and the power consumption of PSA is highly related with the adsorbents used. This is why the development of adsorbents with high adsorption capacities, high selectivity and good regenerability for CO_2 adsorption/desorption is so important in the design of the adsorption process. Many adsorbents have been studied for PSA application, including zeolites, activated carbons and, more recently metal organic frameworks. Among these materials activated carbons combine the advantages of being robust and also unexpansive materials [10].

1.2. Thesis Structure

This thesis is divided in five chapters:

Chapter 1: Introduction

The content of this chapter intends to advertise the reader about the problems related with the growing emissions of carbon dioxide to the atmosphere and how adsorption can be a viable alternative solution to help solve this problem.

This chapter also summarizes the organization of this work.

Chapter 2: Background

This chapter begins with a small review of adsorption-related concepts and the techniques traditionally employed in adsorption equilibrium studies. Finally, some of the adsorbent materials available in the market are described. Since activated carbons were the materials employed in this work, a more detailed section is devoted to this type of materials.

Chapter 3: Adsorbent Characterization

This chapter briefly explains the characterization methods used (Point of Zero Charge – PZC - method, Bohem titrations, N_2 adsorption at 77K (BET Surface Area Method, t-Plot Method, Horvath-Kawazoe Method and Density Functional Theory Method) and Mercury Porosimetry and summarizes the results obtained for the activated carbons studied.

Chapter 4: Adsorption Equilibrium

In this chapter adsorption equilibrium data for carbon dioxide, nitrogen and butane on activated carbons are presented.

The apparatus and experimental procedure employed are described. Then, an explanation is given about the equations behind the several amounts adsorbed considered. The concepts of absolute, excess and net amount adsorbed are discussed and the corresponding results obtained are presented. The experimental data obtained was fitted with the Sips isotherm model and the obtained results are presented and discussed.

Chapter 5: Conclusions and Suggestions for Future Work

In this chapter all the conclusions obtained along this study are presented and some suggestions are left to the future.

Chapter 2

2. Background

2.1. Adsorption

2.1.1. Definition

Adsorption can be defined as the process where some atoms, ions or molecules present in a given fluid, gas or a liquid (*adsorptive*), adhere to the surface of a solid material (*adsorbent*). Due the increase of the adsorptive compound concentration, the solid material will be enriched with the molecules of the fluid phase. This molecules adsorbed on the surface of the solid material can be referred as *adsorbate*.

The reverse process, called desorption, can be defined as the removal of adsorbate from the adsorbent. Desorption can be promoted by the decreasing the pressure and/or increasing the system temperature [11].

2.1.2. Some Applications

Adsorption phenomena is related with important technology processes used nowadays, not only because some adsorbents are used in large scale as desiccants, catalysts or catalyst supports but also because adsorption can be used in areas so diverse like separation of gases, purification of liquids and pollution control, like the removal of aqueous contaminants from groundwater [12]. This phenomenon is also useful for the determination of the surface area and pore size distribution of a diverse range of powders and porous materials [13].

2.1.3. Chemisorption and Physisorption

Adsorption can be defined according to the nature of the interactions adsorbate/adsorbent. Adsorption can be divided in two types: *Chemisorption* and *Physisorption*. Chemisorption consists in the adsorption of molecules of a fluid on the surface of a solid caused by covalent or ionic bonding. In physisorption the fluid molecules are retained due to Van der Waal forces (including dipole–dipole, dipole-induced dipole and London forces). Due to their different nature, physisorption and chemisorption can be distinguished by [11], [13]:

a) Since in chemisorption the molecules of the fluid phase react with the adsorbent molecules, its original form is not kept. On the other hand, in physisorption, the molecules are adsorbed and desorbed without any chemical reaction.

b) Physisorption has a relatively low degree of specificity and for that adsorbate molecules can be linked to other adsorbate molecules and to the adsorbent, forming multilayers. On the other hand, chemisorption is dependent on the reactivity of the adsorbent and adsorptive, so adsorbate molecules can only linked to specific sites of the adsorbent surface, being confined to a monolayer.

c) The energy of chemisorption has the same order of magnitude as the energy change in a comparable chemical reaction. Physisorption is always exothermic, but the energy involved is, generally, not much higher than the energy of condensation of the adsorptive.

2.1.4. Adsorption Isotherms

The relation, at constant temperature, between the amount adsorbed and the equilibrium pressure (for gases) is known by *adsorption isotherm*. When the adsorptive pressure stabilizes, the equilibrium is reached, which means that the quantity of molecules adsorbed and the molecules in the fluid phase will not vary with time

In order to describe this relation there are several models of isotherms. However the isotherm models of Freudlich, Langmuir and BET (Brunauer, Emmett and Teller) are the most commonly observed [14]. A typical gas adsorption isotherm is represented by a plot of the amount adsorbed versus the adsorptive pressure. The pressure can also be expressed as a ratio of the adsorptive pressure, P, to the saturated vapor pressure, P^0.

Despite the multitude of different gas-solid systems available, the majority of the isotherms obtained can be conveniently grouped into six classes according to the International Union of Pure and Applied Chemistry (IUPAC) classification which is based on the original Brunauer, Deming, Deming and Teller (BDDT) classification (1940) [13] . The different types can be seen in **Figure 2.1**.

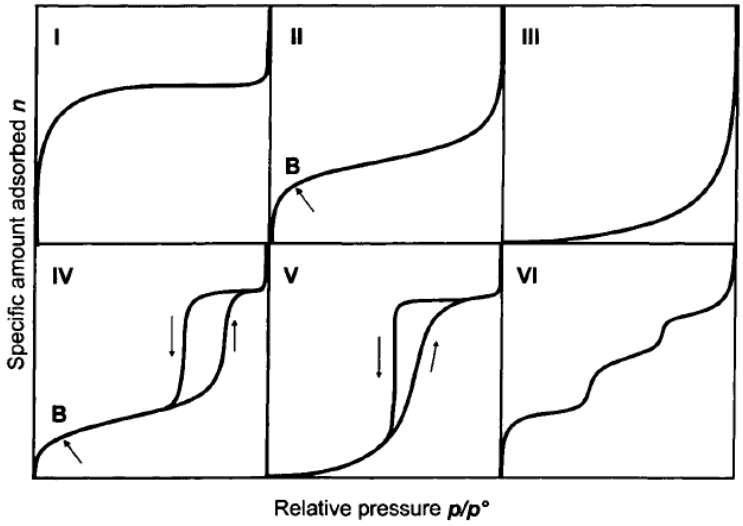

Figure 2.1 - IUPAC gas physisorption isotherm classification [13].

The different adsorption isotherm types are related with the adsorbent and adsorbate properties. The differences between them can be listed as follow.

Type I - Observed in the physical adsorption of gases on microporous solids, in which the pore size is not much greater that the molecular diameter of the adsorbate molecule. This type of adsorption isotherm is common in activated carbons and black carbons [15].

Type II – Typically observed in non-porous or macroporous adsorbents. An inflexion point, or knee, is indicated by point B in **Figure 2.1**. This point indicates the stage at which the monolayer coverage is complete and multilayer adsorption begins to occur [16].

Type III – Observed in macroporous solids. This isotherm is convex to the (p/p^0) axis over its entire range and therefore does not exhibit a point B. This feature is indicative of weak adsorbent/adsorbate interactions. These kinds of isotherms are not common [13], [16].

Type IV – Characteristic of mesoporous adsorbents, this kind of adsorption isotherm possess a hysteresis loop (which means that the adsorption isotherm is different from the desorption isotherm). *Type IV* isotherms are common but the exact shape of the hysteresis loop varies with the system properties [13], [15].

Type V – Like the previous type, this isotherm is observed mesoporous solids and possesses a hysteresis loop. As *Type III* isotherm this kind of isotherm indicatives weak adsorbent/adsorbate interactions. This type of isotherms is relatively rare [13], [15].

Type VI – Usually observed on porous solids with uniform surfaces, this kind of isotherm is relatively rare and is associated with layer-by-layer adsorption on a highly uniform surface [13].

This type of isotherm classification is only applicable to the adsorption of a single-component gas within its condensable range of temperature. Such measurements are extremely useful for the characterization of porous materials [13].

2.1.5. Measuring Adsorption Isotherms

In order to determine the adsorption isotherms and the energies associated with the adsorption phenomena, experimental measurements must be made. Depending on the gas-solid system in study and the operational conditions there are several gas adsorption methods to quantify the amount adsorbed. The most used are the volumetric and gravimetric methods.

2.1.5.1. The Volumetric Method

The name volumetric method dates from the Emmett and Brunauer (1937) [13] experiments which were made using a mercury burette and a manometer. This technique is based on the measurement of the gas pressure in a calibrated constant volume at a known temperature.

A typical volumetric apparatus, shown in **Figure 2.2**, possess two different chambers: one for the adsorbent sample is placed and other for the calibrated charge volume. Initially, the adsorbent contained in the adsorption cell (or chamber) is activated under the appropriate conditions in order to remove the previously adsorbed species. Both the column and the reservoir are maintained at the desired temperature. After this, the reservoir is charged with the gas to a predetermined pressure. The valve between the reservoir and the column is then opened, and the adsorption equilibrium is established between the solid and the gas; the final equilibrium pressure is recorded [17].

One big advantage of the volumetric technique is that the apparatus is less costly than the gravimetric method. Volumetric units only require high precision pressure transducers and high precision volume measurements. On the other hand, modern gravimetric units provide more precise measurements than the ones obtained by volumetric method.

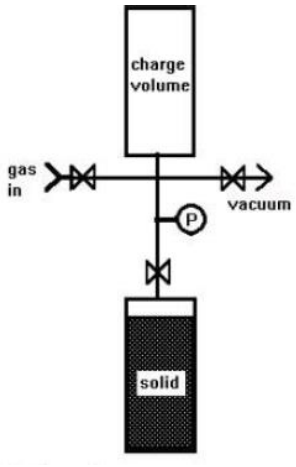

Figure 2.2 - Generic volumetric apparatus [17].

2.1.5.2. The Gravimetric Method

The determination of the amount adsorbed by the gravimetric method using a spring balance was first use by McBain and Bakr in 1926. The apparatus consisted in an adsorbent bucket attached to the lower end of a fused silica spring, which was suspended within a vertical glass tube. Nowadays, spring balances have been substituted by suspension magnetic balances (MSB) [13].

The process is initiated by placing the adsorbent sample inside a basket. The material is then activated preferentially in-situ, in vacuum at a desired temperature. After the sample is cleaned from impurities, the first measurement will give weight of the pair basket + clean adsorbent sample. After this, adsorbate is fed to the adsorption chamber and the sample is then allowed to equilibrate at the desired pressure and temperature (at a gas molar density). The signal from the microbalance is recorded under equilibrium conditions (pressure and temperature are constant). The change in the microbalance signal is a result of adsorption occurring on the solid surface and the total buoyancy force [17]. A generic gravimetric apparatus is shown in **Figure 2.3**.

The gravimetric technique has some advantages and disadvantages. The primary disadvantage is the cost; microbalances are very expensive. In spite of that, this equipment has a high precision and accuracy which made it very useful for high-quality research work and pore analysis. That is the reason why the gravimetric method was chosen for this experimental work.

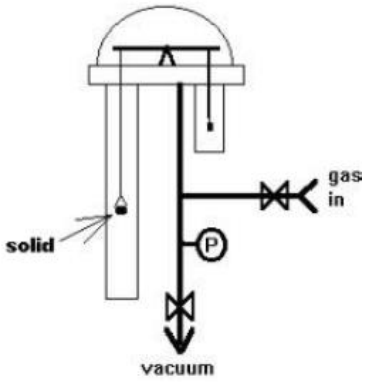

Figure 2.3 - Generic gravimetric apparatus [17].

2.2. Adsorbates

The following gases were selected for the present work since they are adsorbates with interest in typical adsorption applications. Moreover, those gases are of extreme importance in the mitigation of the greenhouse gas emissions.

2.2.1. Carbon Dioxide

Carbon dioxide, CAS number [*124-38-9*], CO_2, *M*r 44.010 g/mol, with a boiling point of -329.72K (56.57ºC) and a melting point of 193.33K (-78.92ºC) is a colorless, odorless, non-flammable gas with a sour taste. At normal temperature, the carbon dioxide molecules are relatively stable and do not readily break down into simpler compounds. However, the substance is very sensitive to high temperatures, ultraviolet light, and electrical discharge [18].

Like it was referred in Chapter 1, the majority of the carbon dioxide present in the atmosphere is a result of human activities as energy production, transportation of people and goods and from the industrial processes [2]. Several measures and protocols, like the Kyoto Protocol [19], to reduce the emissions of greenhouse gases that lead to global warming, are being applied nowadays. Despite this fact, the emissions of CO_2 to the atmosphere grow each day. According to data from the Mauna Loa Observatory and the NOAA-ESRL (National Oceanic & Atmospheric Administration, from U.S Department of Commerce), last year (data from February 2013) the concentration of carbon dioxide present in the atmosphere was 396.88 ppm and this year, by the same time was 397.38 ppm instead of the 350 ppm, which is the goal imposed since 1988 [20].

2.2.2. Nitrogen

When two molecules of elemental nitrogen, N (atomic number 7, *A*r 14.0067 g/mol) form a stable diatomic molecule they origin a molecular substance named nitrogen, CAS number [*7727-37-9*], N_2, *M*r 28.0134 g/mol. At atmospheric pressure and room temperature, nitrogen is a colorless, odorless, noncombustible gas. Nitrogen has a boiling point of 77K (at 1.01 bar) and a melting point of 63.29K (−209.86 ºC).

Nitrogen, which means “lifeless” in Greek, was named by Lavoisier. This molecule is obtained from air and is one of its major constituents (78%). In industry, cryogenic (low-temperature) processes, adsorption processes (such as PSA – Pressure Swing Adsorption), and membrane separation are used to separate nitrogen from air [18]. Also, N_2 is one of the main components of flue gases and, therefore, the knowledge of its adsorption properties is extremely important for the modelling of adsorption-based processes for CO_2 capture from flue gases [1].

2.2.3. Butane

Butane, CAS number [*106-97-8]*, C_4H_{10}, *M*r 58.122 g/mol, with a boiling point of 273.65K (0.5ºC) is a gaseous hydrocarbon with a colorless and odorless aspect. This substance currently known as *n*-butane (to indicate that the carbon atoms are linked in a straight chain) occurs in natural gas and in crude oil. It is formed in large quantities, by catalytic cracking in the refining of petroleum to produce gasoline. Commercially, *n*-butane can be added to gasoline to increase its volatility [21]. Removal of butane from natural gas and biogas is extremely important, reason why the study of its adsorption equilibrium is of major importance for the design of adsorption based processes [22].

2.3. Adsorbents

2.3.1. General Adsorbents

Adsorbents are porous solid materials which have the ability to adsorb molecules from a liquid or gas [14]. According to IUPAC [23], the pore size generally specified as *pore width (*the available distance between two opposite walls) of a porous material can be classified as:

Micropore – Pore of internal width less than 2 nm;
Mesopore - Pore of internal width between 2 and 50 nm;
Macropore - Pore of internal width greater than 50 nm.

The potential of adsorbents has been studied since the 18th century [14] and the applications for the use of adsorbents have grown with the years. For this reason, it became necessary to design new adsorbents in order to face the specificity of the processes, which they are applied. Some of the most important application for adsorbents are:

a) Gas separation processes like the upgrading of biogas [24];

b) Cleaning processes, sewage gas purification [25], removal of contaminants from groundwater through adsorption [12] and the cleaning of industrial effluents [26];

c) Gas storage processes like Adsorbed Natural Gas (ANG) [22];

According to the gas adsorption process, a proper selection of the adsorbent must be made. Nowadays there are several adsorbents available. Some of them are listed next.

The name **activated alumina** is generally applied to an alumina adsorbent prepared by the heat treatment of some hydrated alumina (i.e. a crystalline hydroxide, oxide-hydroxide or hydrous alumina gel) [13]. This material presents a good mechanical resistance and can be used in moving bed applications [27]. The surface chemistry of activated alumina, as well as its pore structure, can be modified by the use of a controlled thermal treatment [28].

Silica Gel has a granular and amorphous form. It is produced by heating a gel, product of the acidification of a solution of sodium silicate. This glassy material is highly porous and it is used to dry liquids and gases and also to recover hydrocarbons [27]. In addition, its surface can be modified by reacting (or grafting) with a monomolecular layer of organic ligand. These modified silica gels can be applied in several chromatographic applications [28].

Zeolites, also referred to as molecular sieves, are microporous crystalline solids with well-defined structures. Generally they contain silicon, aluminum and oxygen in their framework and cations, water and/or other molecules within their pores. Many zeolites occur naturally as minerals as others are synthetic. The major use of zeolites are in petrochemical cracking, ion-exchange (water softening and purification), and in the separation and removal of gases and solvents [29].

Metal-Organic Frameworks (MOFs) are crystalline materials composed of two components: metal ions or ion clusters and organic molecules known as linkers. The choice of metal and linker has significant effects on the structure and properties of the particular MOF. These materials have broad potential for industrial applications because of their attributes: large surface-areas and the flexibility with which their structures can be varied [30]. These structures can be used in studies for high-density storage of gases, including methane (natural gas) and hydrogen. [31], [32], [33] .

Once the adsorbents used in this work are two activated carbons, a special section will be dedicated to these materials.

2.3.2. Activated Carbon

2.3.2.1. Historical Aspects

The first known use for carbon dates from Egyptian time, where this material was used for oil purification and medicinal purposes. By the early 19th century both wood and bone charcoal were used in large-scale for the decolorization and purification of cane sugar [27], [28], [34].

However, it was only in the beginning of the First World War (WWI) that the potential of activated carbon was really capitalized upon. The advent of gas warfare necessitated the development of suitable respiratory devices for personnel protection. Granular activated carbon was used to this end as, indeed, it still is today [35]. By the late 1930's there was considerable industrial-scale use of carbon for gaseous and liquid phase application. During the Second World War (WWII), a more sophisticated chemically impregnated carbon for entrapment of nerve gases was produced [34].

2.3.2.2. Structure and Precursor Materials

Among all the adsorbents used in industry**, activated carbon,** also called activated charcoal, is one of the most used. This microporous adsorbent can be obtained from several carbon containing materials. Its high surface area (activated carbons can have BET-areas larger than 2000 m^2/g) [13] and its microporore volume, associated with the presence of variety of functional groups on its surface, make activated carbon materials powerful adsorbent. The structure of carbon it is basically comprised by graphitic plates, as showed in **Figure 2.4**. The vertices and the edges can accommodate a range of elements such as oxygen, nitrogen and hydrogen which comprises the surface functional groups. Its graphite structure is very important from the adsorption capacity point of view, because it provides space on the slit-pore channels to accommodate adsorbate molecules [36], [37].

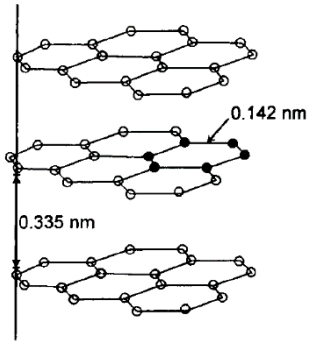

Figure 2.4 - Hexagonal structure of graphite [13].

Depending on the raw materials used for its production, several types of activated carbon can be obtained. Almost all materials containing high fixed carbon content can potentially be activated. The most used carbonaceous source materials are coal (anthracite, bituminous, sub-bituminous and lignite), coconut shell, peanut shell, wood, peat, coals, petroleum coke, bones and fruit nuts. Among these, anthracite and bituminous coals have been the major sources employed [27], [28], [38], [39].

2.3.2.3. Carbonization and Activation

The process for the production of activated carbon usually involves three steps: **a)** Raw material preparation, **b)** Carbonization and **c)** Activation. In order to achieve the desired pore structure and mechanical strength, the activation conditions must be carefully controlled. There are two kinds of activation: physical activation and chemical activation. In both a step of carbonization is required. This step allows the pure carbon to be extracted by pyrolysis [12], [40].

In **physical activation**, once the material is carbonized it is exposed to oxidizing gases like carbon dioxide, oxygen or steam, under a temperature usually between 1073.15K and 1273.15K. This activation step serves to create porosity allowing the tailoring of the desired size distribution and surface area.

In **chemical activation** the material is first impregnated with chemicals agents such as phosphoric acid or zinc chloride and then is carbonized [12], [28], [41].

During the manufacturing process, macropores are the first to be formed. This occurs due the oxidation of weak points (edge groups) on the external surface area of the raw material. Mesopores are then shaped and are, essentially, secondary channels formed in the walls of the macropore structure. Finally, the micropores are molded by attack of the planes within the structure of the raw material. All activated carbons contain micropores, mesopores, and macropores (**Figure 2.5)** within their structures but the proportion vary according with the precursor material and the activation conditions [39].

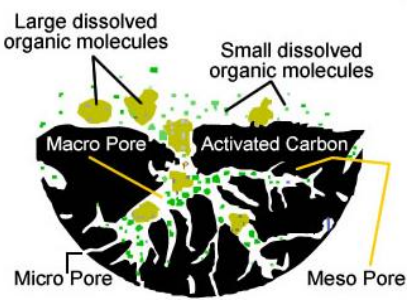

Figure 2.5 - Schematic representation of an activated carbon porous matrix [42].

2.3.2.4. Applications

Due to its unique adsorptive characteristics, activated carbon plays an important role in many liquid and gas phase applications [43]. Some of the processes that use this adsorbent are listed as following:

Because of its large surface area, purity and relative hardness, activated carbon is an ideal **carrier for catalytic metals**, for example in batteries [44]. In the **environmental field**, adsorption over activated carbon it is used for several applications. Some of these applications are effluent treatment of industrial and municipal waste waters, air purification and capture of volatile organic compounds (VOC's) from diverse streams, and the removal of pesticides from contaminated soils [12], [44]. In **medicine,** activated carbons can be employed in poisoning treatments. Through its ingestion, this material prevents the poison from being absorbed in the stomach. Sometimes, several doses of activated charcoal are needed to treat severe poisoning [45].

Activated carbons present a great option for **gas storage**, especially for natural gas. Because they have a large microporous volume, are efficiently compacted into a packed bed, and can be cheaply manufactured in large quantities [22], [46]. This procedure permits storing the gas at lower pressures, improving the safety criteria and reducing the compression costs associated to the traditional storage methods [22].

Cane and sugar syrups require **decolorization** before being ready for final use. Activated carbons are specially processed to develop pore structures that readily adsorb plant pigments from the sugar (polyphenols) [47].

In summary, the characteristics of activated carbons make this type of materials one of the best adsorbents that can be used in adsorption processes. Not only because of it high surface areas and micropore volumes, but also because activated carbons can be produced in several morphologies (beds, pellets, monoliths, fibers, etc. [8]). Activated carbons are also

available at low, prices, and being present in industry for so long, they are considered a robust material for adsorption applications. In **Table 2.1** it is possible to see some typical characteristics of activated carbons.

Table 2.1 - Typical characteristics of activated carbons [36].

True density	2.2 g/cm^3
Particle density	0.73 g/cm^3
Total porosity	0.71
Macropore porosity	0.31
Micropore porosity	0.40
Macropore volume	0.47 cm^3/g
Micropore volume	0.44 cm^3/g
Specific surface area	1200 m^2/g
Mean macropore radius	800 nm
Mean micropore half width	1-2 nm

In the next chapter, the adsorbents characteristics of the two activated carbons used in this work will be properly study by using standard procedures.

Chapter 3

3. Adsorbent Characterization

3.1. Introduction

The design of a separation or purification process by adsorption begins with the choice of a suitable adsorbent. The success or failure of the process is strictly related with the performance of the adsorbent in both adsorption equilibria and kinetics. To satisfy these two requirements the adsorbent must have [36]:

a) A reasonable high surface and a micropore volume, so it can have a good adsorption capacity;

b) Relatively large pore network: If the pore size is too small the transport of the gas molecules to the particle interior can take too long influencing the kinetics;

c) An easy desorption: If the adsorbent does not have properties that allow an easy desorption, it will be necessary to expose the material to high temperatures or extremely low pressure for its regeneration. This will contribute to reduce the adsorbent life due to thermal ageing [15] and increases the energy consumption related to adsorbent regeneration.

Therefore, in order to evaluate the adsorbent, adsorbent characterization must be performed. Density, surface area, pore size distribution, pore volume, and the surface chemistry are usually determined. In this study, an activated carbon, ANGUARD 6 (ANG 6), in the form of extrudates with 1mm diameter, supplied by Sutcliffe Speakman Carbons Ltd. (UK) was characterized at FCT/UNL using N_2 adsorption at 77K, Mercury porosimetry, Bohem Titration Method, Point of Zero Charge Method (PZC) and Thermogravimetric Analysis (TGA).

During the realization of this work, another carbonaceous material became available and, therefore, was possible to perform the PZC and Bohem titrations analysis for this sample. This material consists in an activated carbon honeycomb monolith (ACHM) purchased from Master Carbon International Limited (UK). The monolith is cylindrical and presents 20 mm of external diameter and 300 cells per square inch. Erro! Auto-referência de marcador inválida. shows the two carbon samples.

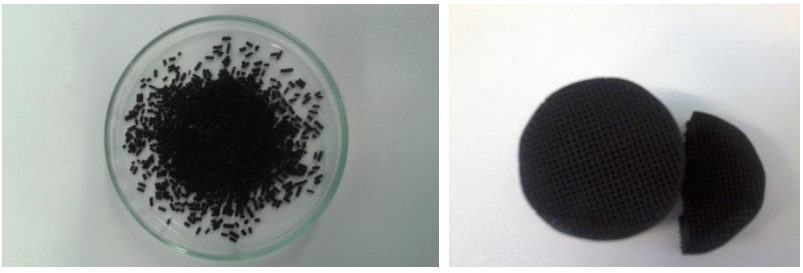

Figure 3.1 - Activated carbons used in this study: ANGUARD 6 (on the left) and activated carbon honeycomb monolith (ACHM).

3.2. Characterization Methods

3.2.1. Point of Zero Charge (PZC)

3.2.1.1 General Description

The surface of a carbon particle is basic or acidic depending on the functional groups that are in majority on its surface. When a small amount of well crushed activated carbon is mixed with water, the ions H^+ and OH^- from the dissociation of the functional groups are given to the solution until the acid/base equilibrium is achieved. PZC (Point of Zero Charge) is a widely used method to determine the surface nature of a carbonaceous adsorbent and can be defined as the pH value at which a solid submerged in an electrolyte exhibits zero net electrical charge [12], [48].

3.2.1.2. Experimental Procedure

Conditions:

An aqueous solution with 0.5 g of well crushed ANGUARD 6 and 50 mL of distillated water was prepared. The glass container in which the solution was kept covered with an aluminum sheet to prevent the oxidation of the carbon. After that, the solution was subject to agitation during 48 hours, at 200 rpm. Thereafter, the agitation was stopped and the solution allowed standing. Then, using a graduated pipette an aliquot was collected from the solution and its pH value was determined using a digital pHmeter, CRISON 2001.

To secure the data reproducibility, three PZC experiments were made. In the first two, the carbon was allowed to settle in the bottom of the vessel and the aliquots were collected from the solution above the settled carbon. However, for the third experiment the solution was subject to centrifugation and the supernatant removed. This procedure enhanced the time needed to read pH in the digital pHmeter employed, since there were less carbon particles in suspension.

PZC analysis was also performed for the activated carbon monolith. Since the amount of material available for the experiments was less than for ANGUARD 6, the experimental protocol had to be modified. This way, half the quantity of activated carbon and distilled water were employed. Also, after the agitation step the carbon solutions were centrifuged.

.

3.2.1.3. Experimental Results and Data Analysis

The results obtained from PZC experiments for ANGUARD 6 and the ACHM are presented in **Table 3.1** and **Table 3.2** respectively.

Table 3.1 - PZC results obtained for ANGUARD 6.

Experiment	Weight of ANG 6 (g)	pH value
1*	0.513	7.08 at 293.55K
2*	0.512	7.06 at 292.35K
3**	0.513	6.81 at 293.15K

*without centrifugation, ** with centrifugation, pH of distillated water: 5.35 at 293.55K.

Table 3.2 - PZC results obtained for the ACHM.

Experiment	Weight of ANG 6 (g)	pH value
1*	0.256	6.15 at 293.15K
2*	0.254	6.67 at 293.15K
3*	0.257	6.50 at 293.15K

* with centrifugation, pH of distillated water: 4.89 at 293.15K.

From the results obtained, the average pH value obtained for ANGUARD 6 was 6.98 and for the ACHM the average pH was 6.44. It can be concluded that the surface of both activated carbons is amphoteric, which means that the acid and basic surface functional groups are in equilibrium.

3.2.2. Bohem Titration Method

3.2.2.1 General Description

Many properties of carbon materials, in particular their adsorption behavior are influenced by the chemisorbed oxygen. The oxygen present on the surface of an activated carbon can bond with several elements such as oxygen, nitrogen, hydrogen and sulphur to form functional groups. According to the activation method used, the functional groups present in the surface of a carbon can be different. Acidic and basic surface sites usually coexist, but the concentration of basic sites decreases with the increasing acid character of the surface and vice-versa. The functional groups usually found in activated carbons are: carboxyl, carboxylic anhydride, lactone, lactol, phenol, carbonyl (acidic groups) and chromene, ketone and pyrones (basic groups) [15], [48] . Some of these functional groups can be seen in **Figure 3.2** and **Figure 3.3**.

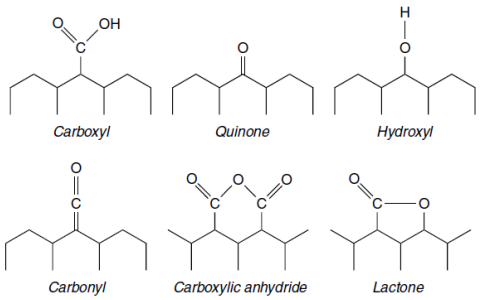

Figure 3.2 - Simplified schematic of some acidic surface groups on an activated carbon [28].

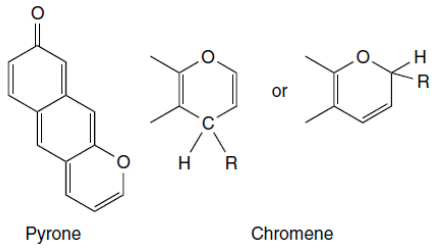

Figure 3.3 - Schematic of some possible basic groups on an activated carbon [28].

The Boehm titration method permits the identification of the functional groups present in the carbon surface. For this purpose, a small amount of activated carbon is mixed with some strong bases in order to neutralize the phenols, lactonic groups and carboxylic acids. These basic substances are NaOH, Na_2CO_3 and $NaHCO_3$. Sodium hydroxide (NaOH) is the strongest base and neutralizes all the Brönsted acids, while sodium carbonate (Na_2CO_3) neutralizes carboxylic acids and lactonic groups (e.g. lactone) and sodium bicarbonate ($NaHCO_3$) neutralizes carboxylic acids. The number of basic sites is calculated from the amount of HCl required to the titration [48].

3.2.2.2. Experimental Procedure

For determination of the acidic and basic surface functional groups of ANGUARD 6 three laboratorial experiments were performed. The experimental procedure was initiated by the preparation of the basic and acidic solutions.

Solutions preparation:

Four solutions (three basic and one acidic) of 100 mL with concentration of 0.05 M were prepared. For this purpose NaOH (Akzo Nobel, Eka Chemicals), Na_2CO_3 (Riedel-de-Häen, 99.5%), $NaHCO_3$ (VR–V. Reis, Lda.) and HCl (Riedel-de-Häen, 37%) and distillated water (with a pH of 5.35 at 293.55K) were used. The solutions were stored and used along the three experiments in glass containers.

RUN A Procedure:

From each solution, 10 mL were extracted to glass containers and 1.0 g of well crushed ANGUARD 6 was added. The glass containers were covered with an aluminum sheet to prevent the oxidation of the carbon particles through the exposure to humid air. The solutions were subjected to a period of agitation of 48 hours, at 200 rpm.

After this period, the agitation was stopped and the solutions were left to settle, during 10 to 15 minutes. In order to remove most of the carbon particles the solutions were decanted several times. Then, aliquots were extracted with a graduated pipette and their pH values were measured. Finally, the basic and acidic titrations were made, using as titrants an aqueous solution of NaOH (0.1 M) and an aqueous solution of HCl (0.1 M). Two drops of phenolphthalein were used as pH indicator.

RUN B Procedure:

The conditions and procedure used in this experiment were the same as the ones used for **RUN A**, with the difference that after the agitation, the solutions were centrifuged to obtain a better separation between the two phases (liquid and solid).

RUN C Procedure:

From each solution, 10 mL were extracted and 1.0 g of non-crushed ANGUARD 6 was added. The glass containers were covered with aluminum sheet to prevent the oxidation of the carbon particles through the exposure to air humidity. The solutions were subjected to a period of agitation of 24 hours, at 200 rpm.

Thereafter, the agitation was stopped and the solutions were subject to centrifugation. The aliquot was then extracted and the pH values were measured. Finally, the basic and acidic titrations were made, using as titrants aqueous solutions of NaOH (0.1 M) and HCl (0.1 M). Again, phenolphthalein was employed as pH indicator.

The calculations used for this analysis can be consulted in **APPENDIX A.1**.

3.2.2.3. Experimental Results and Data Analysis

The first attempt to perform these experiments was made using the Bohem titration general procedure. Therefore, in the first experiment (**RUN A**), after the agitation was stopped, the basic solutions with the carbon were left to settle for a period of time (10-15 minutes). Then a volume from the supernatant was extracted to use in the pH measurement. This procedure is

inefficient because not only the waiting for the carbon mixture to settle adds substantial time to the experiment but also the carbon particles left in the supernatant add difficulty the pH lecture.

The mass, volume and concentrations values obtained for the four experimental procedures can be seen in **APPENDIX A.2, Table A.1** to **Table A.3** (for ANGUARD 6) and in **Table A.4** (for the ACHM). The values of n_{CFS} for each functional group per gram of adsorbent are presented in **Table 3.3** and **Table 3.4**.

After the analysis of the results obtained for the four experiments, it was observed that the values of $n_{CFS}$for the lactones were always negative. Since there is no such thing as negative number of moles, the values were considered to be zero. This means that the surface of both activated carbons is not characterized by lactonic groups.

Along the four experiments it could be seen that the values for the quantity of basic groups are always larger than the values for the quantities of carboxylic groups and phenols isolated. But the overall quantity of the acidic groups is similar to the quantity of basic groups. This is consistent with the PZC results, which showed that both ANGUARD 6 and the ACHM have an amphoteric surface. In sum, the surface of both activated carbons is characterized by basic groups (chromene, ketone and pyrones) and by acidic groups (carboxylic groups and phenols, but not by lactonic groups).

Table 3.3 - Values of nCFS for RUN A, RUN B, RUN C and RUN D.

RUN A (ANGUARD 6)					
	nCFs (moles/g of ANG6)	**Carboxilic Acids (moles/g of ANG6)**	**Lactones (moles/g of ANG6)**	**Phenols (moles/g of ANG6)**	**Total Basic Groups (moles/g of ANG6)**
NaOH	2.03E-04	2.61E-04	0	5.42E-05	3.61E-04
$NaHCO_3$	2.61E-04				
Na_2CO_3	1.49E-04		**Total Acidic groups =**	3.16E-04	
HCl	3.61E-04		**(moles/g of ANG6)**		

RUN B (ANGUARD 6)					
	nCFs (moles/g of ANG6)	**Carboxilic Acids (moles/g of ANG6)**	**Lactones (moles/g of ANG6)**	**Phenols (moles/g of ANG6)**	**Total Basic Groups (moles/g of ANG6)**
NaOH	2.21E-04	3.64E-04	0	1.77E-04	4.43E-04
$NaHCO_3$	3.64E-04				
Na_2CO_3	4.35E-05		**Total Acidic groups =**	5.41E-04	
HCl	4.43E-04		**(moles/g of ANG6)**		

RUN C (ANGUARD 6)					
	nCFs (moles/g of ANG6)	**Carboxilic Acids (moles/g of ANG6)**	**Lactones (moles/g of ANG6)**	**Phenols (moles/g of ANG6)**	**Total Basic Groups (moles/g of ANG6)**
NaOH	1.90E-04	2.65E-04	0	1.83E-04	3.87E-04
$NaHCO_3$	2.65E-04				
Na_2CO_3	7.68E-06		**Total Acidic groups =**	4.48E-04	
HCl	3.87E-04		**(moles/g of ANG6)**		

Table 3.4 - (Continued) Values of nCFS for RUN A, RUN B, RUN C and RUN D.

	RUN D (ACHM)				
	nCFs (moles/g of ACHM)	**Carboxilic Acids (moles/g of ACHM)**	**Lactones (moles/g of ACHM)**	**Phenols (moles/g of ACHM)**	**Total Basic Groups (moles/g of ACHM)**
NaOH	1.17E-04	1.32E-04	0	8.45E-05	3.04E-04
$NaHCO_3$	1.32E-04				
Na_2CO_3	3.30E-05		**Total Acidic groups =**	2.17E-04	
HCl	3.04E-04		**(moles/g of ACHM)**		

3.2.3. Thermogravimetric Analysis (TGA)

3.2.3.1 General Description

Thermogravimetric analysis (TGA) is a procedure that allows the evaluation of the physical and chemical properties of materials with the increase in temperature. Usually, the weight of the analyzed sample is measured while the temperature is increased. The results are generally plotted in a curve of the weight percentage *versus* temperature. Through this analysis is possible to know the percentage of the impurities or volatile components, including humidity, lost in the degassing process of an adsorbent. It is also possible to know which is the maximum temperature to which an adsorbent can be subjected without contributing for its decomposition [49]. This analysis can be performed in equipments that combine extremely precise balance and a programmable furnace for temperature control.

3.2.3.2. Experimental Results and Data Analysis

A sample of ANGUARD 6 (8.4720 mg) was analyzed by TGA (TGA model Q50 V6.7 Build 203, Universal V4.4A TA Instruments - USA) to determine the temperature interval over which the sample decomposes. This was done by recording the weight loss as a function of increasing temperature. The analysis was performed under a nitrogen atmosphere at a heating rate of 278.15K/min (5ºC/min).

The TGA profile obtained is showed **Figure 3.4**:

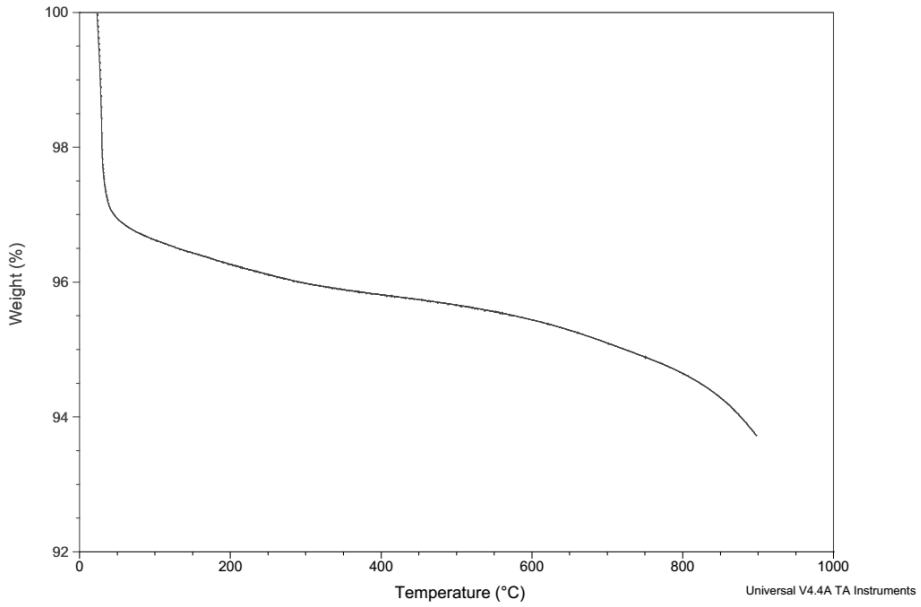

Figure 3.4 – TGA analysis of ANGUARD 6.

The TGA curve showed that the weight of ANGUARD 6 decreases steeply at 323.15K (50ºC), and from about 323.15K to 823.15K (50ºC to 550ºC) the weight decreases slowly. After

873.15K (600ºC) the sample starts to decompose so it is clearly not advisable to heat the adsorbent sample in the activation process more than 823.15K (550ºC). Employing adsorbent activation temperatures between 323.15K and 473.15K (50ºC and 200ºC) the weight decrease is around 3 to 4%.

3.2.4. Nitrogen adsorption at 77K

3.2.4.1 General Description

Nitrogen adsorption at 77K was performed for the activated carbon ANGUARD 6. The experiment was performed using a static volumetric apparatus (ASAP 2010, Micromeritics Adsorption Analyzer, USA) in a range of relative pressure $10^{-6}<P/P_0<0.99$. The sample weight used in the experiment was 0.1418 g. The data from the isotherm was then analyzed using the software DataMaster™, V4.00 (2004). The data obtained from the isotherm of N2 at 77K measured are presented in **APPENDIX A.3, Table A.5**. **Figure 3.5** shows the isotherm obtained.

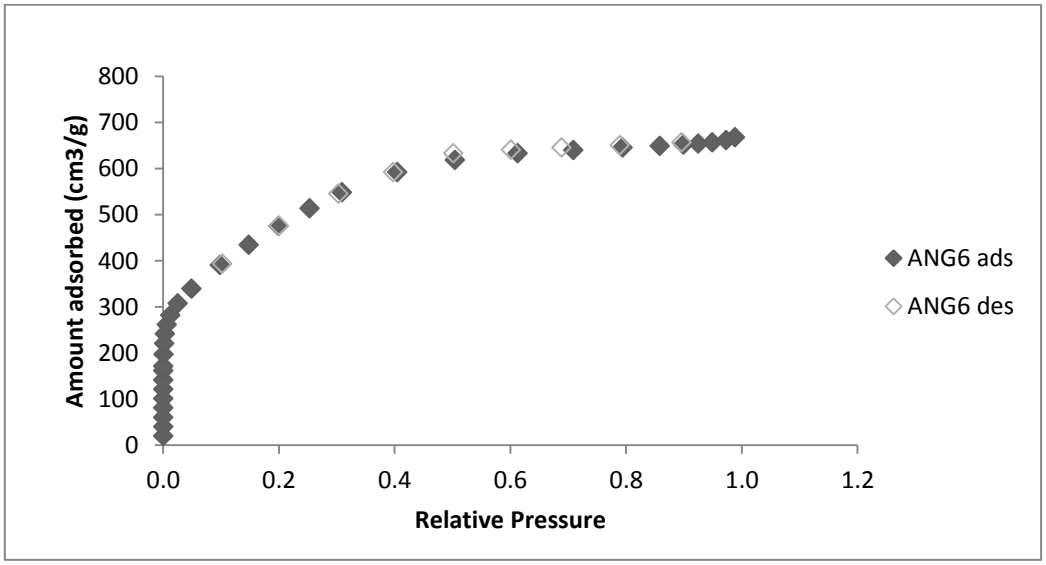

Figure 3.5 - Adsorption isotherm of N_2 at 77K for ANGUARD 6.

3.2.4.1.1. BET Surface Area Method

Brunauer, Emmett and Teller (BET) method is commonly used to determine the surface area of porous materials. Brunauer, Emmett and Teller (1938) extended the Langmuir mechanism to multilayer adsorption and obtained an isotherm equation (BET equation). It is assumed that the adsorbate molecules can settle on the adsorbent surface or on the top of another adsorbate molecule [13].

The first step is to determine the monolayer capacity, n_m^a through the BET Equation [13], [50]:

$$\frac{P}{n_a(-P)} = \frac{1}{n_m^a\, C} + \frac{C-1}{n_m^a\, C}\,\frac{P}{P^0} \qquad \textbf{(Equation 3.1)}$$

Where, n_a is the amount adsorbed in cm^3/g, P is the absolute pressure in mmHg, P^0 is the saturation pressure in mmHg and C is the BET constant.

By simplifying **Equation 3.1,** a linear relation can be established between $\frac{1}{n_a\,(\frac{P^0}{P}-1)}$ and $\frac{P}{P^0}$.

$$\frac{1}{n_a\,(\frac{P^0}{P}-1)} = \frac{1}{n_m^a\, C} + \frac{C-1}{n_m^a\, C}\,\frac{P}{P^0} \qquad \textbf{(Equation 3.2)}$$

This relation can be plotted, where the slope is $s = \frac{C-1}{n_m^a\, C}$ and the intercept is $a = \frac{1}{n_m^a\, C}$. By solving these two equations simultaneously, it can be obtained:

$$n_m^a = \frac{1}{s+a} \qquad \textbf{(Equation 3.3)}$$

$$C = \frac{s}{a} + 1 \qquad \textbf{(Equation 3.4)}$$

To guarantee the linear region of a BET plot it is recommended to restrict the values of relative pressure to a range of 0.05-0.3 $P/\,P^0$. However, the advisable procedure is to obtain, by a statistical analysis, the best linear fit for the initial part of the isotherm [13].

Then, next step is to calculate the BET surface area, $A(BET)$, the surface area that will be available for adsorption, using n_m^a that was obtained from **Equation 3.3**:

$$A(BET) = n_m^a\; N_A\, \sigma \qquad \textbf{(Equation 3.5)}$$

Where N_A is the Avogadro's number and σ is the cross-sectional area that each adsorbate molecule occupy in the completed monolayer. For the nitrogen adsorption at 77 K the value of $\sigma(N_2)$ is normally assumed to be 0.162 nm^2. The value of σ is dependent on the nature of the adsorbent-adsorbate and adsorbate-adsorbate interactions, the structure of the adsorbent surface, and the operational temperature [13].

By restricting the relative pressure range between 0.025 to 0.31 P/P^0, DataMaster™ generated a BET Surface Area Report and a BET Surface Area Plot, shown in **APPENDIX A.4, Figure A.1**.

The recommended procedure is to obtain the best linear fit for initial part of the isotherm. Using only the experimental points in the BET relative pressure range, the fitting obtained was not so good. By extending the relative pressure range, using the previous point (P/P^0 = 0.025), the correlation coefficient obtained was higher (0.9976), indicating a better fitting.

According to the BET theory, the BET constant C is related exponentially to the enthalpy (heat) of adsorption in the first adsorbed layer [51]. Because of this, the C value must be positive. If the value is negative this means that the relative pressure range chosen is not adequate [13]. Since the value for C obtained for this analysis was C=106.50 (>0), the choice of the relative pressure range was assumed to be adequate. Also, since the BET theory is an extension of the Langmuir mechanism to multilayer adsorption, to consider the n_m^a value reliable, it is necessary that the knee of the isotherm is fairly sharp (i.e. the BET constant C is not less than ~100) (12).The BET surface area obtained for ANGUARD 6 is 1699.79 m²/g which is within the typical range for activated carbons (between 300 and ~ 4000 m^2/g) [28].

3.2.4.1.2. t-plot Method

The t-plot method was proposed by Lippens and Boer in 1965. This method allows the determination of micropore volume, external surface and micropore area. The experimental from the isotherm is redrawn in a t-curve, i.e., a plot of the quantity of gas adsorbed as a function of t, the standard multilayer thickness on the reference non-porous material at the corresponding P/P^0. These t-values are calculated using a thickness equation (**Equation 3.6**). When the shape of the reference t-curve and experimental isotherm do not coincide, that is an indication that a non-linear region was reached. From the point where the non-linear region begins, a line is drawn (extrapolated) to intercept the yy axe (t=0). The values of external surface area and micropore volume can be determined from the intercept and slope obtained [13].

DataMaster™ V4.00 uses Harkins and Jura Equation (1944) to determine the values of thickness [52].

$$t(\dot{A}) = \sqrt{\frac{13.99}{0.034 - \log\left(\frac{P^0}{P}\right)}} \qquad \textbf{(Equation 3.6)}$$

Through the slope, *s*, of the extrapolation is possible to calculate the external surface area in m^2/g and from the intercept, *a*, the micropore volume in cm^3/g [16].

$$V_{MP} = 0.001547\ a \quad \textbf{(Equation 3.7)}$$

$$S_{ext} = 15.47\ s \quad \textbf{(Equation 3.8)}$$

The micropore area, in m^2/g can be calculated through the difference between the BET surface area and the external surface area.

$$S_{micro} = S_{BET} - S_{ext} \quad \textbf{(Equation 3.9)}$$

According to the literature [16] the t-plot method is valid for a relative pressure range of 0.08 to 0.75 P/P^0. The results obtained for ANGUARD 6 can be seen in **APPENDIX A.5, Figure A.2**. By restricting the relative pressures to the range recommended, the obtained correlation coefficent was close to 1, which indicates a good fitting. According to the results found in the literature [13], the values obtained are in acordance with the values for several activated carbons. **Table 3.5** presents a resume of micropore volume, external surface area and micropore surface area for the activated carbon ANGUARD 6:

Table 3.5 - Results obtained from t-plot method for ANGUARD 6.

Micropore Volume (cm^3/g)	External surface area (m^2/g)	Micropore surface area (m^2/g)
0.94	52.50	1647.29

3.2.4.1.3. Horvath-Kawazoe (HK) Method

Horvath and Kawazoe (HK) described a semi-empirical, analytical method for the determination of effective pore size distributions from N_2 adsorption isotherms in microporous materials. In its original form, the HK analysis was applied to nitrogen isotherms determined on molecular sieve carbons, over the assumption that these adsorbents contained slit-shaped graphitic pores. However, nowadays it can be applied to other adsorbents with different pore geometries like zeolites [13], [16].

Horvath and Kawazoe found that the average potential could be related to the free energy change of adsorption, creating a relation between filling pressure and the effective pore width. Since the analysis is about an activated carbon, the following equation is based in the slit-pore geometry [16]:

$$RT\ln\left(\frac{P}{P_o}\right) = N_{Av}\ \frac{N_s\ A_s + \ N_A\ A_A}{\sigma^4(L-2d_0)}\ \left[\frac{\sigma^4}{3(L-\ d_0)^3} - \frac{\sigma^{10}}{9(L-\ d_0)^9} - \frac{\sigma^4}{3(\ d_0)^3} + \ \frac{\sigma^{10}}{9(\ d_0)^9}\right] \quad \textbf{(Equation 3.10)}$$

Much of the physical parameters present in this equation can be easily found in the literature [28], [53], [54]. The nomenclature for equations **Equation 3.10** to **Equation 3.14** can be found in *List of Symbols* (Page XXI to Page XXIII). Others like the dispersion constants and the inter-nuclear distances must be calculated employing [16], [55]:

$$A_A = \frac{3}{2}\ mc^2\alpha_s\alpha_A \quad \textbf{(Equation 3.11)}$$

$$A_S = \frac{6\ mc^2\alpha_s\alpha_A}{\frac{\alpha_s}{X_s} + \frac{\alpha_A}{X_A}} \quad \textbf{(Equation 3.12)}$$

$$\sigma_s = \left(\frac{2}{5}\right)^{\frac{1}{6}} d_s \quad \textbf{(Equation 3.13)}$$

$$\sigma_A = \left(\frac{2}{5}\right)^{\frac{1}{6}} d_A \quad \textbf{(Equation 3.14)}$$

DataMaster™ analysis allowed obtaining the results presented in **Table 3.6**:

Table 3.6 - Results obtained by HK method for ANGUARD 6.

Maximum Pore Volume (cm^3/g)	**Medium Pore Diameter** $\dot{A}$
0.98	18.4

The Horvath-Kawazoe detailed report for ANGUARD 6 is present in **APPENDIX A.6., Figure A.3**. The micropore size distribution can be seen in **Figure 3.6**.

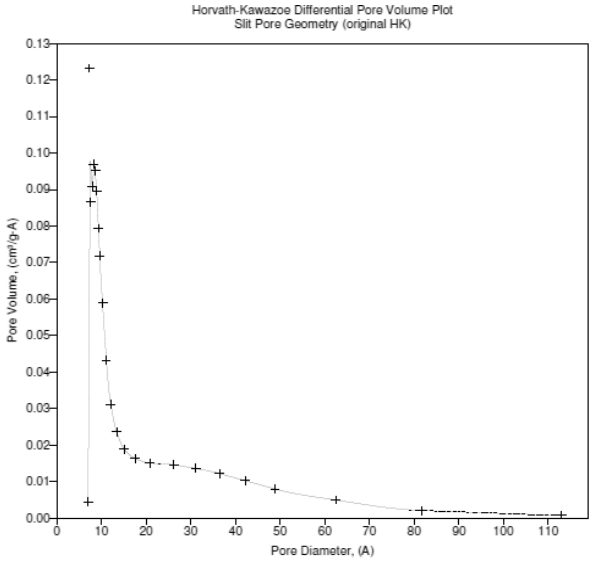

Figure 3.6 - Micropore size distribution obtained from Horvath-Kawazoe Method for ANGUARD 6.

The pore size distribution results obtained from HK Method for ANGUARD 6 shows that most of the pores lie in the micropore region (<20 $\dot{A}$), but also reveals the existence of small mesopores for pore widths slighty higher than 20 $\dot{A}$.

3.2.4.1.4. Density Functional Theory (DFT) Method

Density functional theory (DFT) is a quantum mechanical modelling method mostly used in physics and chemistry areas. In chemistry, it has a great use for predicting a great variety of molecular properties like molecular structures, vibration frequencies, atomization energies, ionization energies, electric and magnetic properties, reactions paths, etc. [56] .

In adsorption science, this statistical method attempts to extend the accuracy of pore size distribution analysis in both micropore and mesopore range [15]. DFT and Gibbs Ensemble Monte Carlo molecular simulation (GEMC) represent an alternative to the classical methods, like the HK method. Usually, for activated carbon it is assumed that the material is composed of non-interconnected, slit-shapes pores with chemically homogeneous graphitic surfaces.

The pore size distribution obtained from DFT method is shown in **Figure 3.7**. The DFT report for ANGUARD 6 can be seen in **APPENDIX A.7, Figure A.4**.

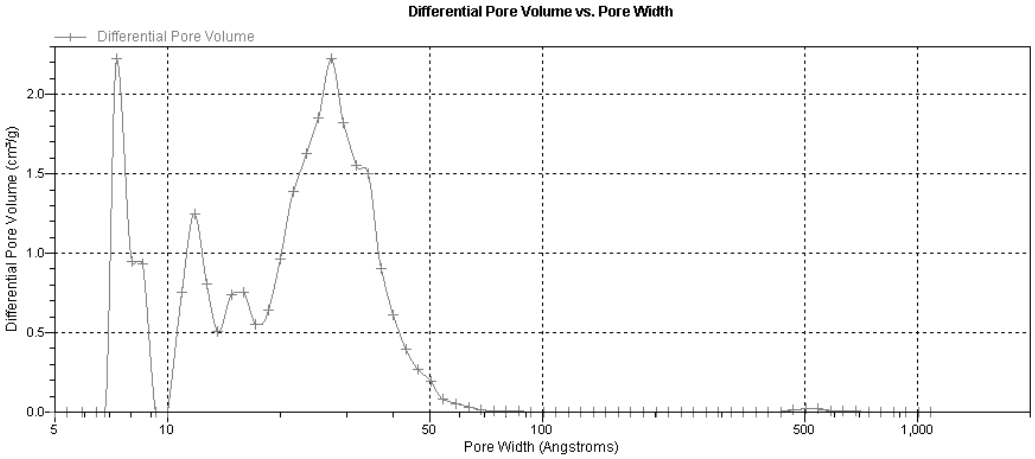

Figure 3.7 - Pore size distribution obtained from DFT Method for ANGUARD 6.

As it was seen for the HK Method, the DFT analysis confirms that the sample adsorbent is mostly microporous, but the existence of mesopores with pore widths slightly above 20 $\dot{A}$ is confirmed.

3.2.5. Mercury Porosimetry

3.2.7.1 General Description

Mercury porosimetry characterizes the porosity of a given material by applying various levels of pressure to a sample immersed in mercury. The pressure required to intrude mercury into the sample pores is inversely proportional to the size of the pores. This indicates that at first, macropores and mesopores are filled with mercury and just then, the mercury enters in the micropores. In spite of the pressure applied, this method is reserved to the analysis of the characteristics of larger pores, instead of the smaller pores [57].

3.2.7.2. Experimental Procedure

To perform this analysis, the sample is first loaded into a penetrometer and then, the penetrometer is sealed and placed in a low pressure port, where the sample is evacuated to remove air and moisture. The penetrometer's cup is then automatically backfield with mercury. As pressure increases, mercury intrudes into the sample's pore, beginning with the pores that have the large diameter. The instrument automatically collects low pressure measurements over a range of pressures specified by the operator. Then, the penetrometer is moved to the high pressure chamber, where high pressure measurements are taken [57].

3.2.7.3. Experimental Results and Data Analysis

A sample of ANGUARD 6 (0.1380 g) was subjected to mercury intrusion porosimetry, using a mercury porosimetry penetrometer (model AutoPore IV 9500 V1.07) from Micromeritics Instrument Corporation (USA).

The intrusion data summary from Hg porosimetry can be consulted in **APPENDIX A.8**, **Figure A.5.** The intrusion-extrusion cycle can be seen in **Figure 3.8**.

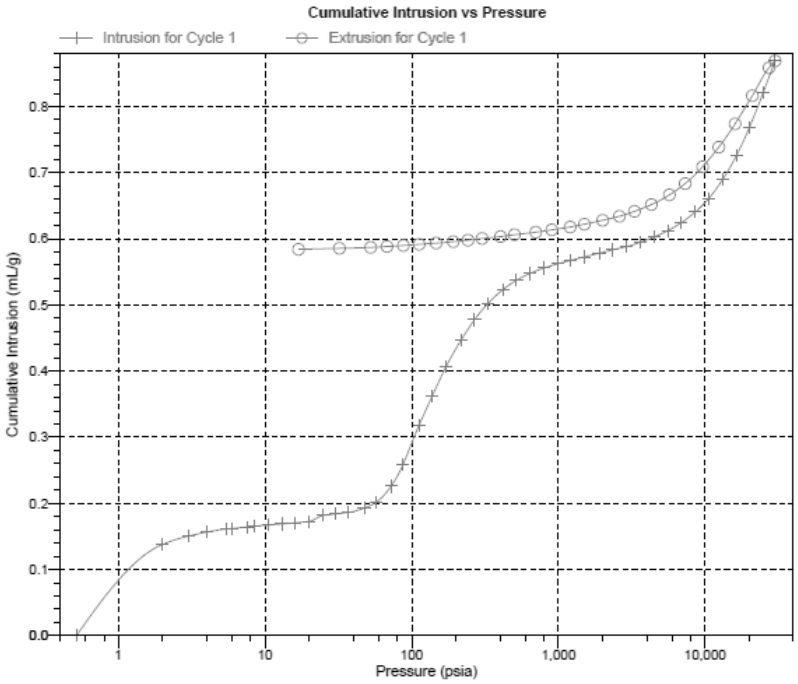

Figure 3.8 - Experimental mercury intrusion-extrusion cycle for ANGUARD 6.

The curves give the volume of mercury (mL Hg/g of carbon sample) penetrated at a given external pressure *P* into the measuring cell. The curve represented by the symbols (−+−+−) indicates the intrusion curve and the other curve, represented by the symbols (−⊖−⊖−) shows the extrusion curve. The results obtained in the mercury porosimetry analysis are summarized in **Table 3.7.**

Table 3.7 - Results obtained from Mercury Porosimetry for ANGUARD 6.

Total Intrusion Volume (cm^3/g)	Bulk Density (g/cm^3)	Apparent Density (g/cm^3)	Porosity (%)
0.87	0.56	1.10	48.87

The **total intrusion volume** is the volume of mesopores and macropores (in case of ANGUARD 6, the percentage of macropores it is very little, which can be seen in **Figure 3.6** and **Figure 3.7**). **Bulk density** is the ratio between the mass of the sample to the sum of all the volumes of the solid material (open, closed and blind pores), **apparent density** is the ratio between the mass of the sample to sum of all the volumes, excluding open pores (closed and blind). **Figure 3.9** illustrates the definition of bulk and apparent densities. The percentage of porosity is calculated through the **Equation 3.15** [58].

$$\%\, Porosity = \frac{V_{PT}}{V_B}.100\% \qquad \textbf{(Equation 3.15)}$$

Where V_{PT} is the total porosity, determined by difference between the bulk volume, V_B and the skeletal volume, V_S , (which only considers the blind pores) [58].

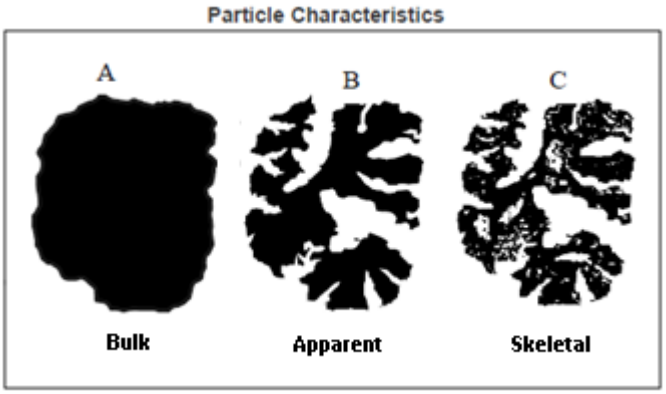

Figure 3.9 - Illustration of bulk, apparent and skeletal densities [58].

Since the micropore volume was obtained through the HK method, it is now possible to calculate the total pore volume for the carbon sample. By summing the micropore volume (0.98 cm^3/g) and the total intrusion volume obtained by mercury porosimetry, the total pore volume for ANGUARD 6 is 1.85 cm^3/g.

3.3. Summary

With the purpose of summarizing the information obtained through the several methods reported in this chapter (excluding PZC method, Bohem Titration method and TGA), **APPENDIX A.9**, is presented.

Based on the information collected for the chemistry surface both activated carbons, ANGUARD 6 and the ACHM, proved to have amphoteric surfaces, characterized by acidic (except lactonic groups) and basic groups.

The thermogravimetric analysis showed that when heated until 323.15K (50ºC), the weight of ANGUARD 6 decreases steeply, loosing at least 3% of its weight. Between 323.15K to 823.15K (50ºC to 550ºC), the weight decreases slowly and after 873.15K (600ºC), the carbon sample starts to decompose.

Through the BET Surface Area Method it was determined that ANGUARD 6 has a high surface area, $A(BET)$=1699.79 m²/g, a micropore volume of 0.98 cm^3/g. The pore size distribution, resulting from the Horvath-Kawazoe (HK) and Density Functional Theory (DFT) methods, determined the existence of micropores, but also a small amount of mesopores with pore widths slightly above 20$\dot{A}$. The total pore volume of ANGUARD 6 was calculated by the sum of the micropore volume (0.98 cm^3/g) and the volume obtained from Mercury Porosimetry (0.87 cm^3/g) as a total of 1.85 cm^3/g. The high surface area and high micropore volume obtained are good indicators that ANGUARD 6 will have a good adsorption capacity.

Chapter 4

4. Adsorption Equilibrium

4.1. Introduction

Adsorption equilibrium data is determinant information to understand an adsorption process. No matter how many components are present in the system, the adsorption equilibrium of pure components knowledge is essential to determine how much of those components can be adsorbed on a solid adsorbent. This information can be used in the modelling and optimization of adsorption separation processes [36].

4.2. Experimental Description

Adsorption equilibrium of carbon dioxide (CO_2), nitrogen (N_2) and butane (C_4H_{10}) at 303.15K, 323.15K and 353.15K and helium (H_e) pycnometry at 353.15K, in a range of 0 – 35 bar, were measured using an activated carbon, ANGUARD 6, as adsorbent. Additionally, a structured activated carbon was purchased (an activated carbon honeycomb monolith) and, therefore, adsorption data of carbon dioxide was also measured.

The adsorption equilibrium data were measured gravimetrically using a high-pressure magnetic suspension balance (MSB) model ISOSORP 2000, from Rubotherm GmbH (Germany), with automated online data acquisition in an *in-house*-developed Labview software [59]. The advantage of the MSB is the possibility of accurately contactless weighing the adsorbent samples, under nearly all environments. Instead of hanging the sample containing baskets directly at the balance, the sample is coupled to a suspension magnet, achieving a constant vertical position in a closed measuring cell. Using this freely suspension coupling, the measuring force is transmitted contactless from the adsorption chamber to a Sartorius microbalance, located outside, under ambient atmosphere.

Also, the MSB available in the group's laboratory includes two baskets to allow the measurement of adsorption equilibrium information for two adsorbents at the same time. The device has a resolution of 0.01 mg, uncertainty lower than 0.002% of the measured value, and a reproducibility of less than 0.03 mg to a maximum load of 25 g [60].

All gases employed were obtained from Air Liquide (Portugal) and Praxair (Portugal). The purities of the gases employed are: CO_2 > 99.998%, N_2 > 99.995%, C_4H_{10} > 99.95% and He > 99.999%. **Figure 4.1** shows the MSB and its components.

Figure 4.1 - Magnetic suspension balance components [60].

4.2.1. Adsorbent Sample Pre-Treatment

Prior to adsorption experiments, the adsorbents employed must be degassed (or activated). This procedure ensures the removal of any adsorbed impurities and moisture.

The information obtained for the ANGUARD 6 carbon by thermogravimetric analysis (TGA) showed that the activated carbon should be activated at temperatures between 323.15K

and 473.15K (50ºC and 200ºC). Within this range of temperatures the amount of loss weight is 3 to 4%. The TGA for the ACHM was not performed yet; reason why the temperature of activation employed was the same as for the ANGUARD 6 carbon.

The ANGUARD 6 and ACHM samples were activated *in situ* at a temperature of 323.15K for a minimum of 4 hours, under vacuum. The heating up to 323.15K was performed at a rate of 278.15K/min.

4.2.2. Experimental Apparatus

The measurements were carried out in the apparatus showed in **Figure 4.2**. The gas enters the sealed chamber of the MSB and the pressure is registered at the exit line of the apparatus, by several high accuracy sensors (PT), each one for a given pressure range. The temperature is controlled using a double-jacket connected to a thermostatic bath (BATH). The temperature is acquired using thermocouple (4-wire Pt100 probe) (T). A vacuum pump and a set of valves (ball and check valves) are also coupled to the system in order to manage the entrance and exit of gas, as well as the selection of the pressure transducer to use in each measurement. The apparatus working range is limited to 150 bar and 373.15K. A complete description of the equipment is given in **APPENDIX C**.

The adsorption laboratory apparatus is composed by four main units: **a)** Feed system unit; **b)** Gravimetric unit with data acquisition; **c)** Pressure measuring and **d)** Temperature measuring and control unit.

Feed Unit:

The feed unit is composed by a 1/8" OD SS tubing system prepared with a secondary vacuum line and two feed lines, one for an inert, and another for the studied component.
The vacuum line is connected to a vacuum pump Edwards 5C. There is also a HiP pressure generator to be applied whenever the desired pressure is higher than the available feed pressure.

Gravimetric Unit:

The gravimetric unit is composed by the MSB, with acquisition of the weight values from the microbalance, and simultaneous pressure data acquisition with a National Instruments PCI-6023E Board. Acquisition is made using Labview construction, where the measurements are monitored in order to see when equilibrium conditions have been reached.

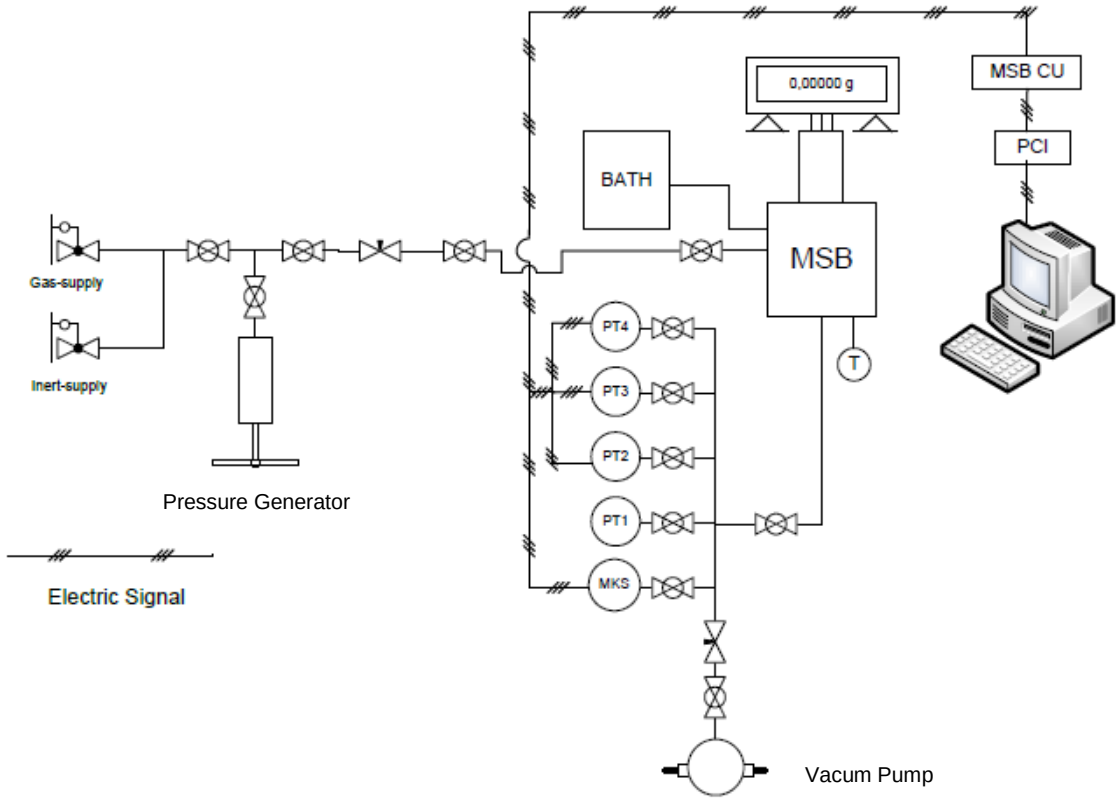

Figure 4.2 - Schematic diagram of the experimental apparatus used in the equilibrium measurements.

Temperature Measuring and Control Unit:

The temperature control unit is composed by:

a) a refrigerator F32-HL from Julabo GmbH (Germany), keeping the temperature within 0.1 K of the set-point value;

c) a 4-wire Pt100 temperature probe, connected to the control unit of the MSB four-wire Pt100 probes (RS Amidata, Spain), for temperature measurement on the measuring cell.

Pressure Measuring and Control Unit:

The pressure was monitored by several pressure transducers (PT) of different ranges, granting good measurement accuracy:

1. MKS Baratron Type 627D Absolute Pressure Transducer, from MKS Baratron, used in the pressure range of 2.00E-05 bar-1.32 bar;
2. PT PX01C1-150A5T pressure sensor (OM2), from Omegadyne Inc., used in the range of 0-10 bar;

3. PT PX01C1-500A5T pressure sensor (OM3), from Omegadyne Inc., used in the range of 0-35 bar;
4. PT PX03C1-3KA5T pressure sensor (OM4), from Omegadyne Inc., used in the range of 0-69 bar.

4.2.3. Experimental Procedure

The equilibrium adsorption data of carbon dioxide, CO_2, nitrogen N_2 and butane C_4H_{10} and helium pycnometry was measured according to standard procedures:

a) Isothermal pressurization of the adsorption chamber of the MSB containing the carbon sample with the pure gas up to the desired pressure, after previously preparation of the system (3-4 g previously weighed several times using an analytical balance and an average of these measurements was used to determine an initial mass of the sample; this mass was confirmed at the initial start-up condition of the MSB);

b) With the in-house developed program [59], online measurement of pressure is taken. Adsorption equilibrium is assumed to occur when, for a period of at least one hour, the pressure, temperature, and sample weight do not vary. The measured weight is recorded, and the amount adsorbed is determined. At this time, pressure and temperature are also acquired and the value of the gas density (for this pressure and temperature conditions) is obtained from a web database: NIST (National Institute of Standards and Technology) [61];

c) The gas pressure in the adsorption chamber is then increased, and the sample is allowed to reach equilibrium with this new condition. These measurements are repeated until an entire adsorption isotherm is obtained;

d) After reaching the highest pressure point, the sample is degassed, once more step by step, and the values of measured weight, temperature and pressure are taken, in order to define the desorption isotherm;

e) In the end, after desorption isotherm is defined the sample is heated under vacuum to ensure its complete regeneration.

4.3. Experimental Results and Data Analysis

The adsorption isotherms of carbon dioxide (CO_2), nitrogen (N_2) and butane (C_4H_{10}) at 303.15K, 323.15K and 353.15K and helium pycnometry at 353.15K, in a range of 0 – 35 bar were measured on the ANGUARD 6 sample. Adsorption isotherms of CO_2 in the same temperature and pressure range were measured for the ACHM sample.

The gravimetric measurements, as well as all other conventional adsorption methods, rather than giving the total amount adsorbed, q_t, give the specific excess adsorbed, q_{ex}. The q_{ex} is the total gas amount added into the measuring cell minus the amount that remains in the gas phase upon system equilibration [30].

An alternative concept was developed by Gumma and Talu. This was named net adsorption, q_{net} and it is defined as the total amount of gas present in the measuring cell (with the adsorbent), minus the amount that would be present in the empty cell (without the adsorbent), at the same pressure and temperature (*P*, *T*) conditions. This parameter can be calculated directly from the experimental data since it is independent of the adsorbent characteristics such as pore volume, solid matrix density and impenetrable pore volume [17]. Therefore, this method eliminates the influence of the use of probe molecules in reporting adsorption equilibrium data.

In order to determine the absolute adsorption, the buoyancy corrections must be performed. Buoyancy corrections are considered to correct the influence of the gas density on the measurements of the apparent weight sample. The corrections in the forces acting in the sample holder, solid adsorbent and adsorbed phase are taken in account.

In the case of net adsorption, the buoyancy correction is needed only for the forces acting on the sample holder, obtained through the blank experiments performed at different pressures with the empty holder; for the excess adsorption, the buoyancy correction is necessary for the impenetrable solid volume, which results in an apparent weight loss. This correction is estimated as a product of the skeletal volume of the adsorbent and the gas density; for the absolute adsorption the correction of the buoyancy acting on the pore volume is also needed [17], [22] .

The weight,m, reading from the balance at any time can be written as [22]:

$$m = m_h \left(1 - \frac{\rho_g}{\rho_h}\right) + m_s \left(1 - \frac{\rho_g}{\rho_s} + q_{ex}\right) \qquad \textbf{(Equation 4.1)}$$

With m_h and ρ_h representing the mass and the density of the sample holder, m_s and ρ_s are respectively the mass and skeletal density of the sample adsorbent, ρ_g is the density of the

bulk gas at equilibrium pressure and temperature. The specific excess adsorption, q_{ex} can be calculated by:

$$q_{ex} = \frac{m - m_h}{m_s} - 1 + \left(\frac{1}{\rho_s} + \frac{V_h}{m_s}\right) \rho_g \qquad \textbf{(Equation 4.2)}$$

Here, V_h is the volume of all moving parts present in the measuring cell (such as the holding basket).

The blank experiments with the empty holder give its mass, volume and density from the intercept and the slope of the linear decrease of apparent weight, m, versus the gas density, ρ_g.

$$m = m_h - \frac{m_h}{\rho_h} \rho_g \qquad \textbf{(Equation 4.3)}$$

The values of m_h and ρ_h were estimated at 293.78K using He, helium. **Figure 4.3** and **Figure 4.4** show the results obtained for the blank calibration of the adsorbent sample holders. **Table 4.1** summarizes the obtained results.

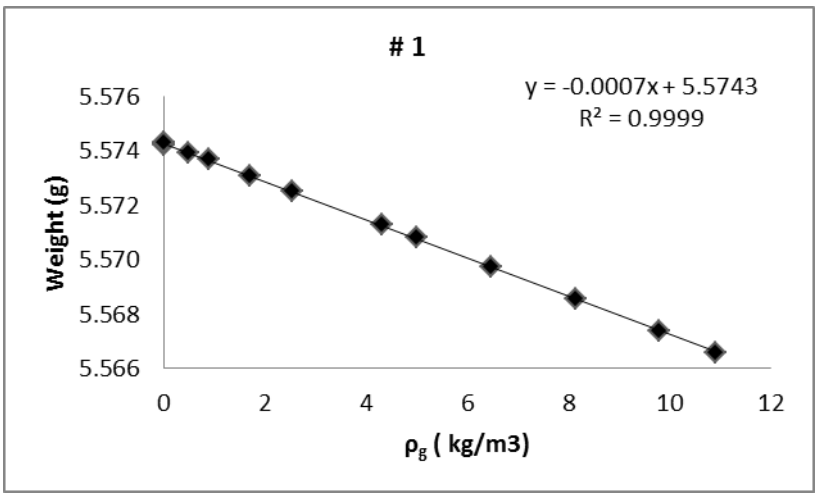

Figure 4.3 - Blank calibration of sample holder #1 used in the adsorption, using helium at 293.63K.

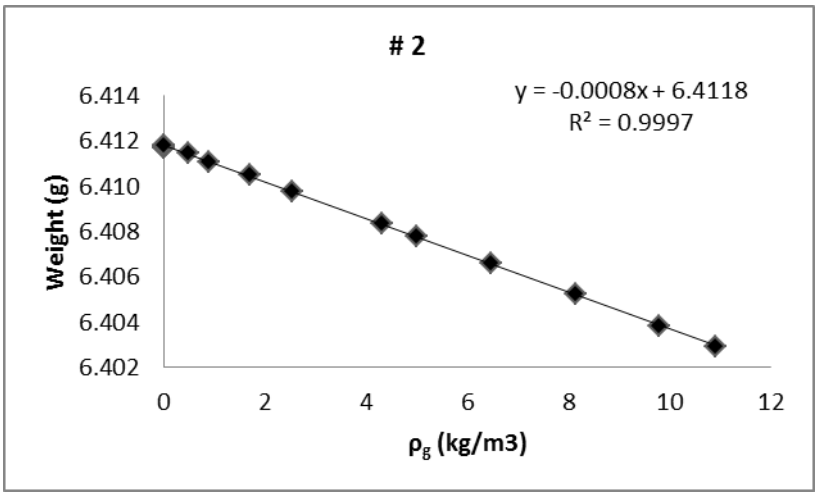

Figure 4.4- Blank calibration of sample holder #2 used in the adsorption, using helium at 293.63K.

Table 4.1 - Blank calibration of the measuring cells.

Sample holder	Conditions	m_h (g)	V_h (cm^3)	ρ_h (g/cm^3)
# 1	293.78 K. H_e	5.574	0.703	7.931
# 2	293.78 K. H_e	6.412	0.808	7.934

The determination of the mass and the density of the carbon sample (m_s and ρ_s) was performed through high temperature (353.15K) measurements [22]. It is assumed that helium acts as a probe molecule that penetrates into all accessible pore volume of the carbon without being adsorbed.

$$m - m_h - \frac{m_h}{\rho_h}\rho_g = m_s - \frac{m_s}{\rho_s}\rho_g \qquad \textbf{(Equation 4.4)}$$

Figure 4.5 shows the helium measurements performed for ANGUARD 6 and the ACHM. The results obtained from the data analysis are listed in **Table 4.2**.

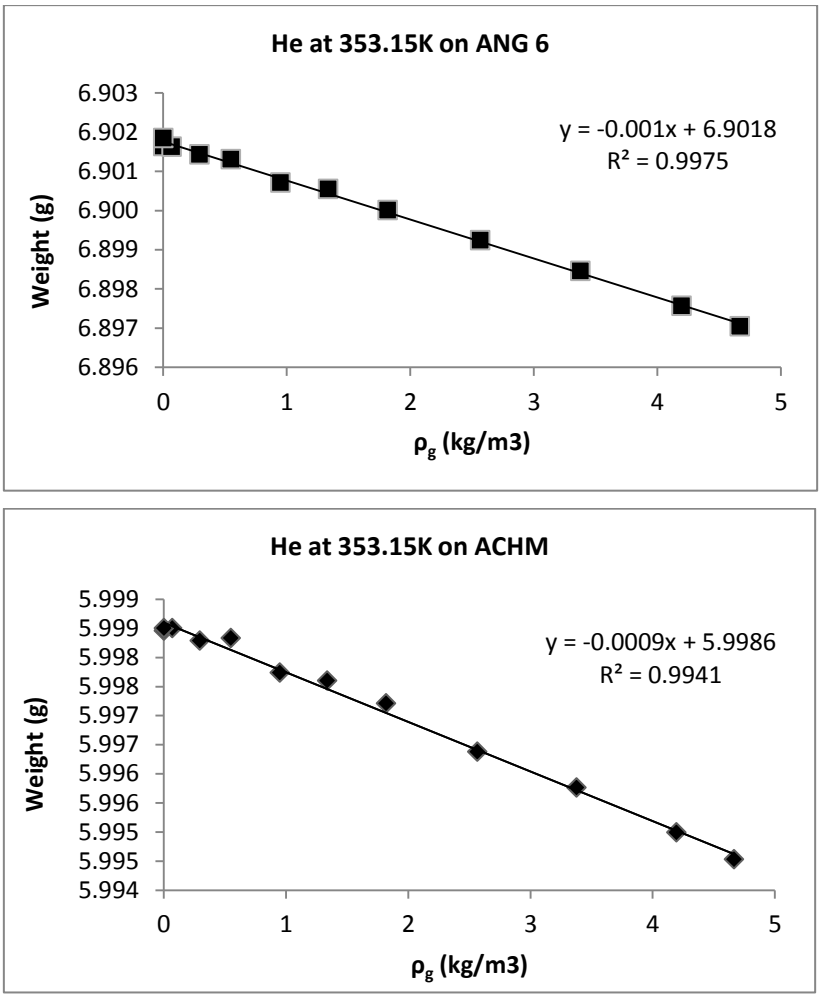

Figure 4.5 - Helium measurements on ANGUARD 6 (top) and ACHM (bottom) at 353.15K.

The values of weight and gas density, for both adsorbents are presented in **APPENDIX B, Table B.1.**

Table 4.2 - Results obtained from helium measurements for ANGUARD 6 and ACHM.

Sample	Conditions	m_s (g)	ρ_s (g/cm^3)
ANGUARD 6	353.15 K, H_e	0.490	2.622
ACHM	353.15 K, H_e	0.424	2.847

The net adsorption q_{net} can be calculated by **(Equation** 4.5. The excess amount q_{ex} is related with q_{net} through **Equation 4.6** [17]:

$$q_{net} = \frac{m - m_s - m_h + V_h \rho_g}{m_s} \qquad \textbf{(Equation 4.5)}$$

$$q_{net} = q_{ex} - \frac{\rho_g}{\rho_s}$$ **(Equation 4.6)**

Finally, the absolute amount adsorption (or total amount adsorbed), q_t can be calculated by the relation between q_{ex} and q_{net} by [30]:

$$q_t = q_{ex} + V_p \rho_g = q_{net} + (V_p + V_s) \rho_g$$ **(Equation 4.7)**

Where V_p is the accessible pore volume of the adsorbent and $V_s = \frac{1}{\rho_s}$ is the specific adsorbent volume impenetrable to the adsorbate. For ANGUARD 6, V_p is 0.98 cm^3/g, calculated in Chapter 3 by the Horvath-Kawazoe method.

During this study the V_p of the ACHM was not determined. Therefore, a V_p value reported in the literature was employed. The V_p used is 0.98 cm^3/g. This is the value reported in the literature for a similar ACHM also manufactured by Mast Carbon (UK) [10].

As an example**, Figure 4.6** illustrates the net, excess and total amounts adsorbed for nitrogen at 303.15K for ANGUARD 6. It is possible to see that in the low pressure region the values do not shown significant difference. On the other hand, when the pressure increases the values diverge from each other. For the high pressure region, the net adsorption is the lowest of the three quantities, followed by excess adsorption and total adsorption. The same trend was obtained for all the isotherms measured independently from the temperature and adsorbate employed. All the data is presented in **APPENDIX B**, in, **Figure B.1** to **Figure B.4. Table B.2** to **Table B.5** shows the experimental values of q_{net}, q_{ex} and q_t for each pure gas.

Also it can be observed that as predicted in Chapter 3, the isotherms obtained are *Type I*, which is characteristic of microporous adsorbents. Given that physical adsorption is an exothermic phenomenon, the slope of the curvature of the adsorption isotherms will decrease with the increasing of the temperature [22].

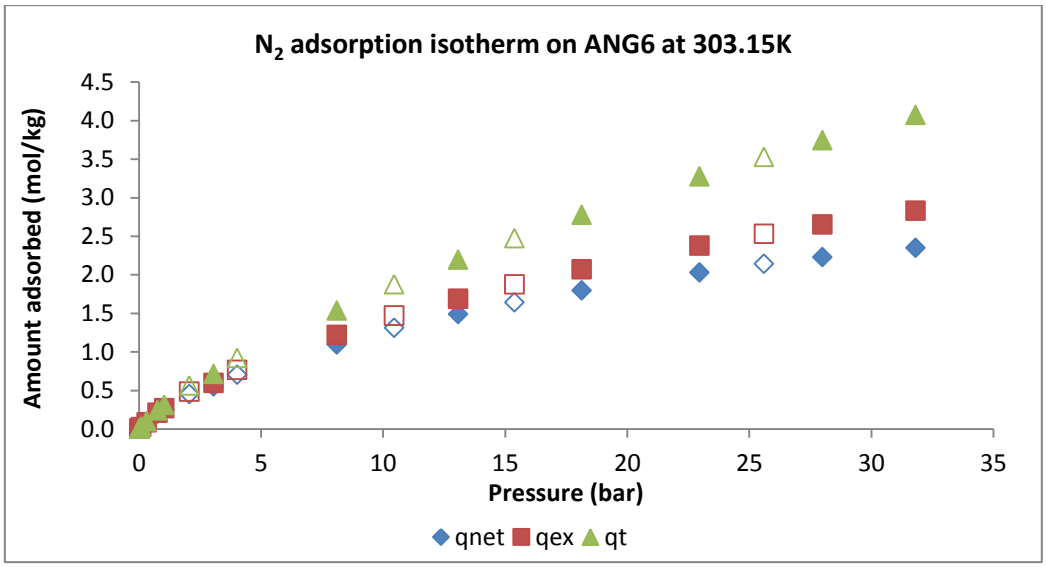

Figure 4.6 - Net (◊), excess (□) and total (Δ) amount adsorbed for nitrogen (N_2) at 303.15K for ANGUARD 6. The solid symbols represent adsorption and the open desorption.

4.3.1. Sips Isotherm Model

Knowledge of the adsorption equilibrium and heat of adsorption are essential for proper design of any gas-phase adsorption process [22]. In fact, in adsorption separation processes, the heat of adsorption is very important since during the process the heat is released and the energy is partly absorbed by the solid adsorbent and partly is dissipated to the surrounding. The portion absorbed by the solid increases the particle temperature, decreasing its local capacity and broadening the mass transfer zone [36].

Several isotherm models are available to correlate experimentally obtained data. The Sips isotherm model (or Langmuir-Freundlich model) is an extension of the Freundlich equation, given by:

$$q_t = q_{ts} \frac{(bP)^{\frac{1}{n}}}{1 + (bP)^{\frac{1}{n}}} \qquad \textbf{(Equation 4.8)}$$

Where q_t is the amount adsorbed in mole per unit mass or volume, q_{ts} is the maximum amount adsorbed, b is the affinity constant and measure how strong the adsorbate molecule is attracted on to a surface, P is the pressure, the parameter n, usually greater than the unity, characterizes the interaction between adsorbate/adsorbent and its magnitude increases with the heterogeneity of the system.

The affinity constant b and the parameter n can be written in function of the temperature as:

$$b = b_0 \exp[\frac{Q}{R_g T_0}(\frac{T_0}{T} - 1)] \quad \textbf{(Equation 4.9)}$$

$$\frac{1}{n} = \frac{1}{n_0} + \alpha\,(1 - \frac{T_0}{T}) \quad \textbf{(Equation 4.10)}$$

Here b_0 is the affinity constant at a reference temperature, (T_0), n_0 is the parameter n at the same reference temperature, α is a constant parameter and R_g is the ideal gas constant.

The isosteric heat of adsorption can be obtained by applying the Van't Hoff's equation, which relates the adsorption heat effects to the temperature dependence of the adsorption isotherm,

$$(-\Delta H) = R_g\, T^2 (\frac{\partial ln P}{\partial T})_\theta \quad \textbf{(Equation 4.11)}$$

Where θ is the fractional loading ($\theta = \frac{q_t}{q_{ts}}$). In terms of the pressure, isosteric heat it is given by:

$$(-\Delta H) = Q - (\alpha R_g T_0)\, n \ln(bP) \quad \textbf{(Equation 4.12)}$$

And in terms of fractional loading,

$$(-\Delta H) = Q - (\alpha R_g T_0)\, n^2 \ln\left(\frac{\theta}{1-\theta}\right) \quad \textbf{(Equation 4.13)}$$

In the Sips isotherm model, parameter Q corresponds to the isosteric heat of adsorption at the fractional loading of 0.5.

4.3.2. Experimental Results and Discussion

The experimental adsorption equilibrium data (the absolute amount adsorbed) was fitted by the Sips adsorption isotherm model. The maximum amount adsorbed and the isosteric heat of adsorption from each pure gas was determined. The Sips isotherm model is widely used to describe data of many substances on activated carbon with good success [36].

To determine the Sips isotherm parameters for each adsorbate, the experimental adsorption data was fitted using the software TableCurve 3D, v.4.0. This software combines a powerful surface fitter that has the ability to describe three dimensional empirical data. Using this software feature the absolute amount adsorbed (mol/kg) and the pressure (bar) are plotted in order to the three working temperatures (K). From the fitted isotherm and the experimental data it was possible to determine the average relative error percentage, $ARE\ (\%)$ (**Equation 4.14**), between the experimental points and the ones given by the isotherm model.

$$ARE\% = \frac{100}{N_{exp}} \sum \frac{|q_{mod} - q_{ex}|}{q_{ex}} \qquad \textbf{(Equation 4.14)}$$

The experimental and theoretical results obtained are disclosed in the following sections.

4.3.2.1. Experimental data fitting employing Sips isotherm model

- **Nitrogen Adsorption on ANGUARD 6**

Nitrogen (ANG6)	
Parameter	**Value**
qts (mol/kg)	11.962
b_0 (bar^{-1})	0.015
Q (kJ/mol)	9.023
n_0	1.103
α	0.346
T_0 (K)	303.21
FSE	0.0268
r^2	0.9996

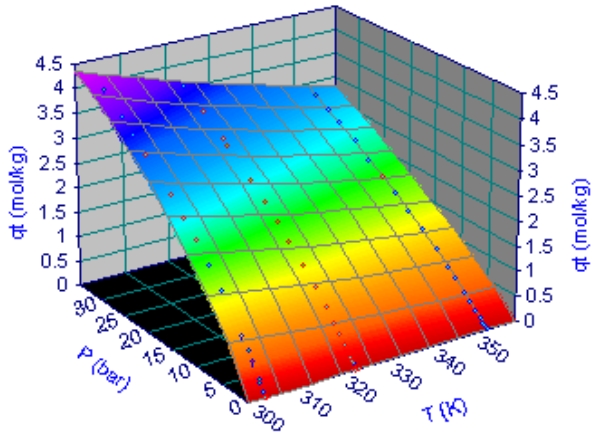

Figure 4.7 - Sips model fitting of the N_2 experimental data at 303K, 323K and 353K on ANGUARD 6 and parameters obtained. Symbols represent the experimental data and the surface is the global isotherm model.

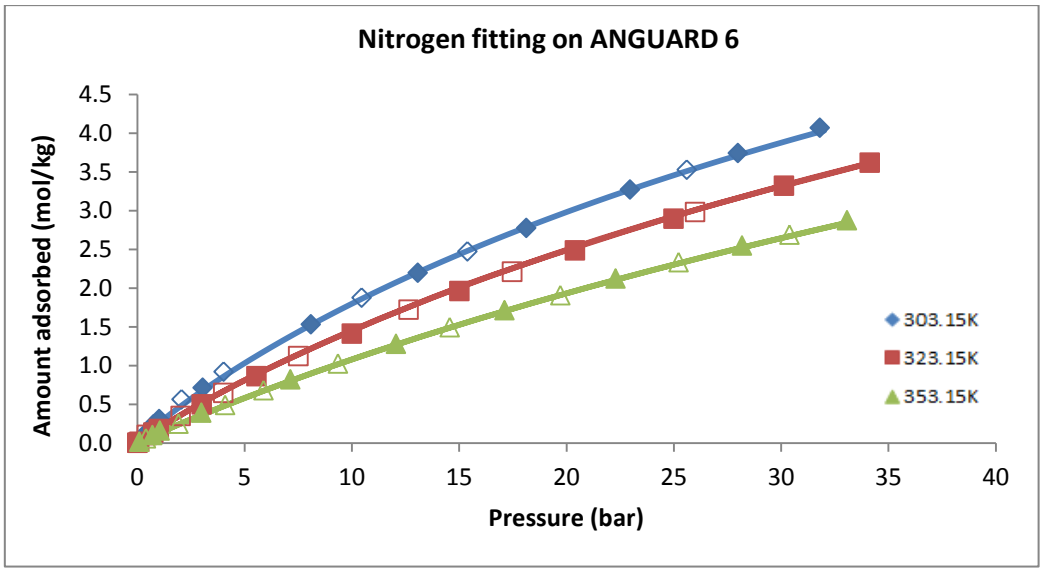

Figure 4.8 - Single component N_2 isotherms at 303K, 323K and 353K on the activated carbon ANGUARD 6.Symbols represent the experimental data (filled symbol – adsorption; empty symbol – desorption) and lines represent the fittings with the Sips model. The %ARE errors for 303.15K, 323.15K, and 353.15K are 6.98, 9.01 and 3.55, respectively. The N_2 overall ARE error is 6.51%.

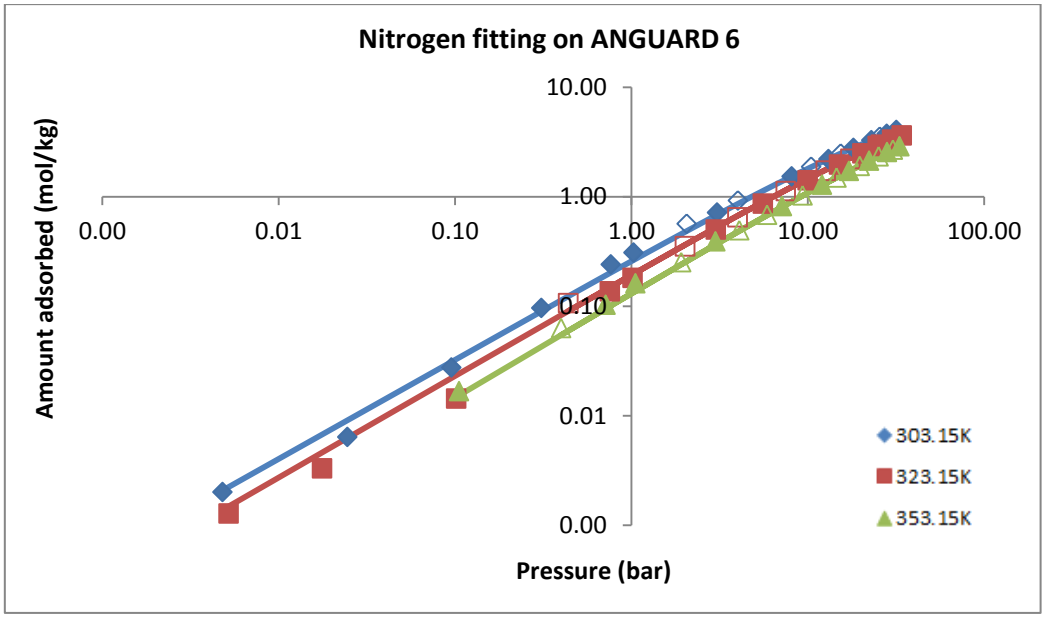

Figure 4.9 – Logarithmic representation of the single component N_2 isotherms at 303K, 323K and 353K on the activated carbon ANGUARD 6.Symbols represent the experimental data (filled symbol – adsorption; empty symbol – desorption) and lines represent the fittings with the Sips model. The %ARE errors for 303.15K, 323.15K, and 353.15K are 6.98, 9.01 and 3.55, respectively. The N_2 overall ARE error is 6.51%.

- **Butane Adsorption on ANGUARD 6**

Butane	
Parameter	**Value**
qts (mol/kg)	17.117
b_0 (bar^{-1})	0.447
Q (kJ/mol)	29.580
n_0	2.409
α	0.336
T_0 (K)	303.19
FSE	0.1426
r^2	0.9971

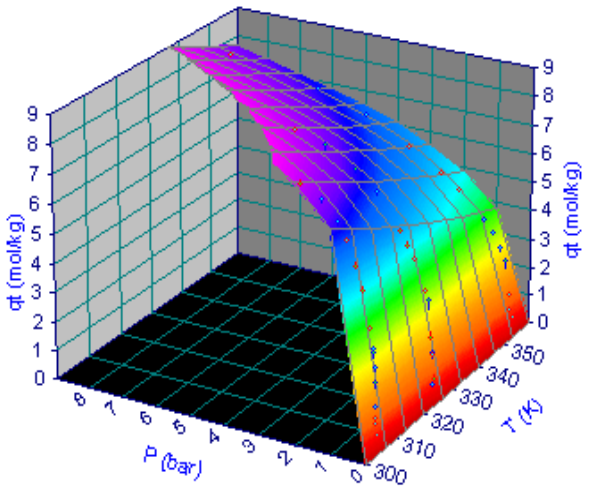

Figure 4.10 - Sips model fitting of the C_4H_{10} experimental data at 303K, 323K and 353K on ANGUARD 6 and parameters obtained. Symbols represent the experimental data and the surface is the global isotherm model.

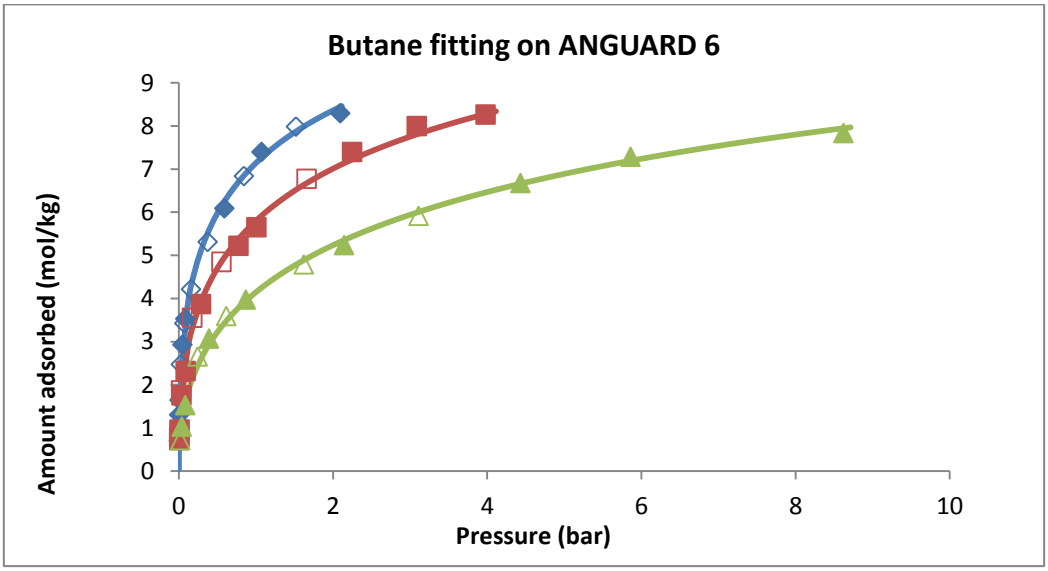

Figure 4.11 - Single component C_4H_{10} isotherms at 303K, 323K and 353K on the activated carbon ANGUARD 6.Symbols represent the experimental data (filled symbol – adsorption; empty symbol – desorption) and lines represent the fittings with the Sips model. The %ARE errors for 303.15K, 323.15K, and 353.15K are 3.90, 6.38 and 3.62, respectively. The C_4H_{10} overall ARE error is 4.63%.

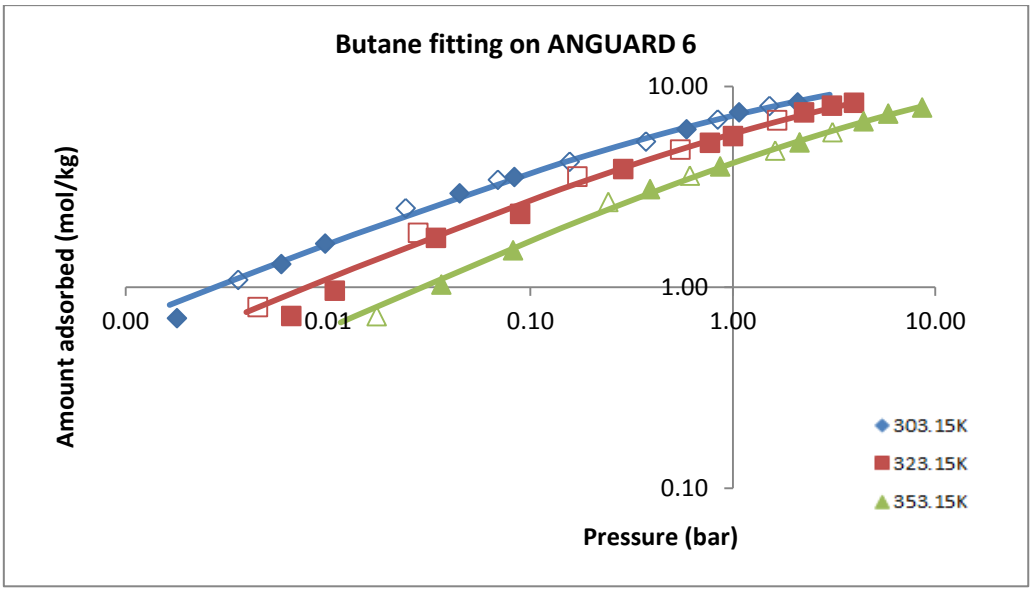

Figure 4.12 - Logarithmic representation of the single component C_4H_{10} isotherms at 303K, 323K and 353K on the activated carbon ANGUARD 6.Symbols represent the experimental data (filled symbol – adsorption; empty symbol – desorption) and lines represent the fittings with the Sips model. The %ARE errors for 303.15K, 323.15K, and 353.15K are 3.90, 6.38 and 3.62, respectively. The C_4H_{10} overall ARE error is 4.63%.

- **Carbon Dioxide Adsorption on ANGUARD 6**

Carbon Dioxide (ANG6)	
Parameter	**Value**
qts (mol/kg)	21.660
b_0 (bar^{-1})	0.040
Q (kJ/mol)	19.800
n_0	1.094
α	5.01E-05
T_0 (K)	303.22
FSE	0.1798
r^2	0.9979

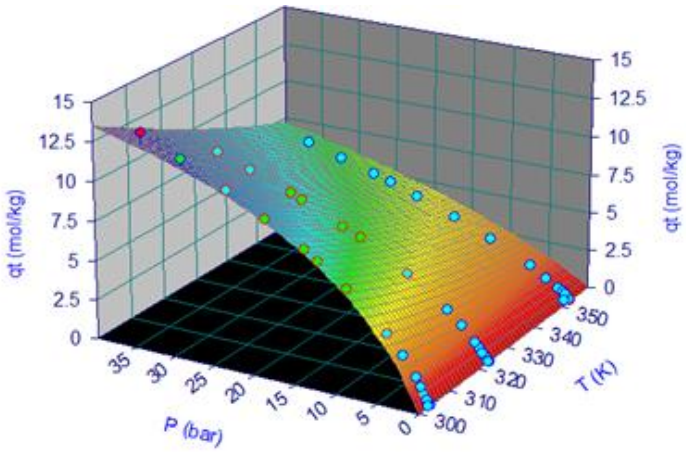

Figure 4.13- Sips model fitting of the CO_2 experimental data at 303K, 323K and 353K on ANGUARD 6 and parameters obtained. Symbols represent the experimental data and the surface is the global isotherm model.

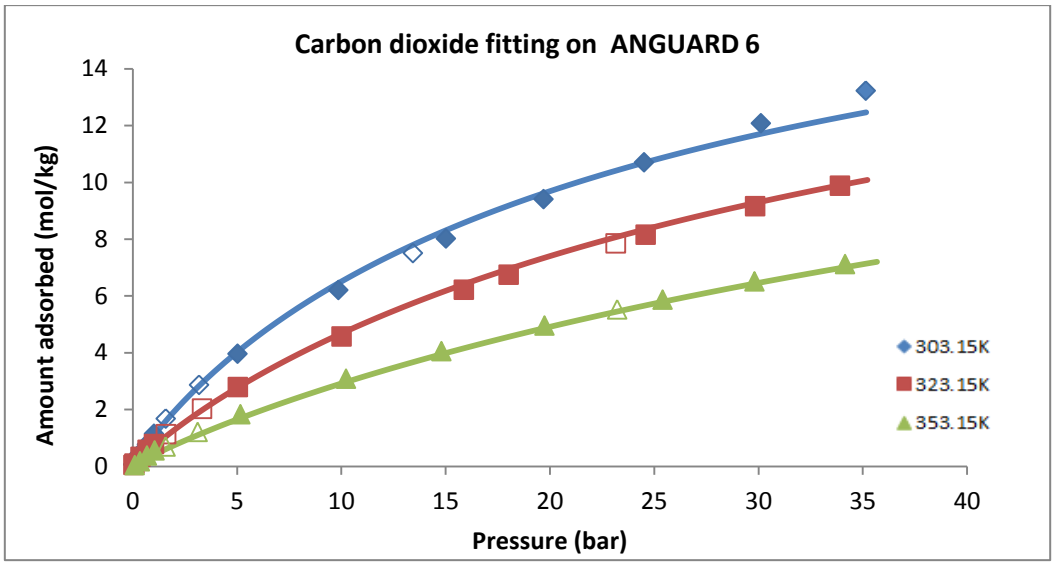

Figure 4.14 - Single component CO_2 isotherms at 303K, 323K and 353K on the activated carbon ANGUARD 6.Symbols represent the experimental data (filled symbol – adsorption; empty symbol – desorption) and lines represent the fittings with the Sips model. The %ARE errors for 303.15K, 323.15K, and 353.15K are 6.10, 6.20 and 8.45, respectively. The CO_2 overall ARE error is 6.92%.

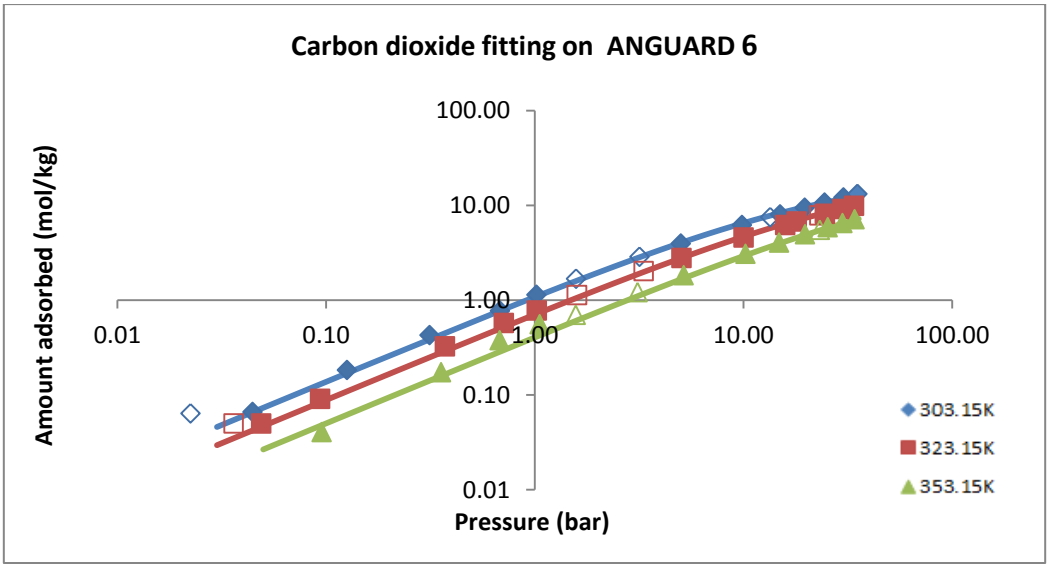

Figure 4.15 - Logarithmic representation of the single component CO_2 isotherms at 303K, 323K and 353K on the activated carbon ANGUARD 6.Symbols represent the experimental data (filled symbol – adsorption; empty symbol – desorption) and lines represent the fittings with the Sips model. The %ARE errors for 303.15K, 323.15K, and 353.15K are 6.10, 6.20 and 8.45, respectively. The CO_2 overall ARE error is 6.92%.

- **Carbon Dioxide Adsorption on ACHM**

Carbon Dioxide (ACHM)	
Parameter	Value
qts (mol/kg)	11.795
b_0 (bar^{-1})	0.239
Q (kJ/mol)	22.848
n_0	1.232
α	1.68E-06
T_0 (K)	303.22
FSE	0.1001
r^2	0.9992

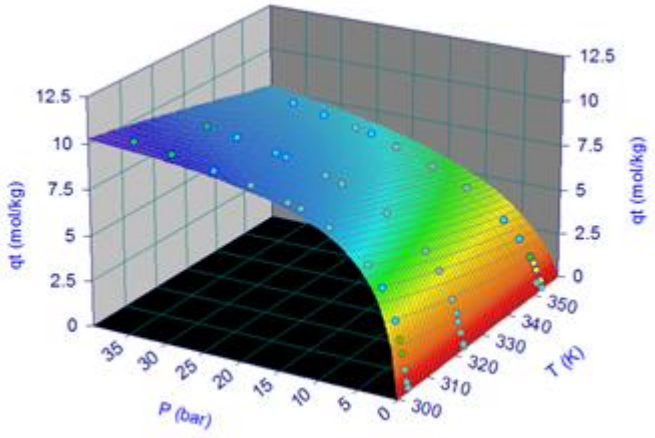

Figure 4.16 - Sips model fitting of the CO_2 experimental data at 303K, 323K and 353K on ACHM and parameters obtained. Symbols represent the experimental data and the surface is the global isotherm model.

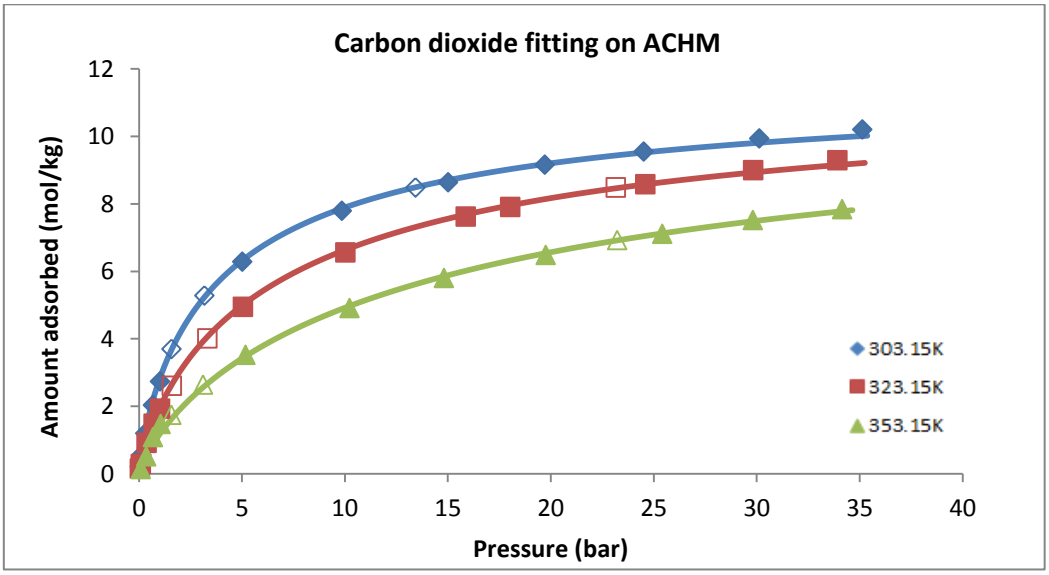

Figure 4.17 - Single component CO_2 isotherms at 303K, 323K and 353K on the activated carbon ACHM. Symbols represent the experimental data (filled symbol – adsorption; empty symbol – desorption) and lines represent the fittings with the Sips model. The %ARE errors for 303.15K, 323.15K, and 353.15K are 5.29, 4.33 and 6.49, respectively. The CO_2 overall ARE error is 5.37%.

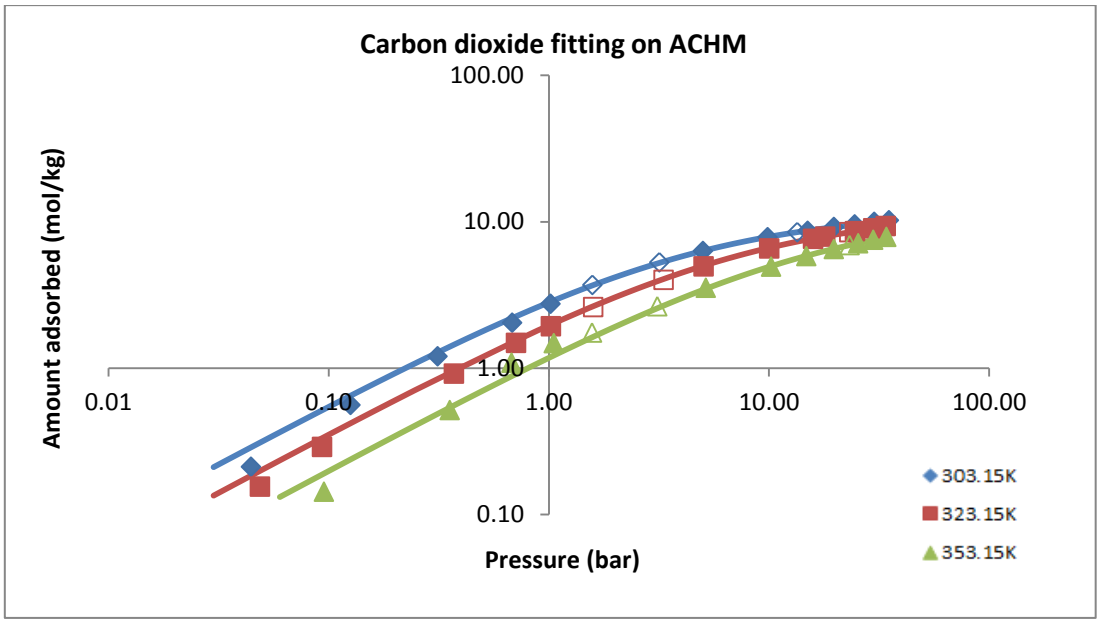

Figure 4.18 - Logarithmic representation of the single component CO_2 isotherms at 303K, 323K and 353K on the activated carbon ACHM. Symbols represent the experimental data (filled symbol – adsorption; empty symbol – desorption) and lines represent the fittings with the Sips model. The %ARE errors for 303.15K, 323.15K, and 353.15K are 5.29, 4.33 and 6.49, respectively. The CO_2 overall ARE error is 5.37%.

Through the several fittings presented between **Figure 4.7** to **Figure 4.18** it is possible to see the good agreement between the fittings with the Sips isotherm model and the experimental data through all the pressure range studied (including the low pressure region). This information is corroborated by the obtained values of r^2 (the correlation coefficient), that are close to 1 and the values the fit standard error (FSE), which are very small. These parameters of evaluation of the goodness of the fitting are showed in **Table 4.3**, along with the fitting parameters for each adsorbate studied.

Table 4.3 - Parameters obtained from Sips isotherm models for the pure gases in ANGUARD 6 and ACHM.

	ANGUARD 6			ACHM
Parameter	Nitrogen	Butane	Carbon Dioxide	Carbon Dioxide
qts (mol/kg)	11.96	17.12	21.66	11.80
b_0 (bar^{-1})	0.01	0.45	0.04	0.24
Q (kJ/mol)	9.02	29.58	19.80	22.85
n_0	1.10	2.41	1.09	1.23
α	0.346	0.336	5.01E-05	1.68E-06
T_0 (K)	303.21	303.19	303.22	303.22
FSE	0.0268	0.1426	0.1798	0.1001
r^2	0.9996	0.9971	0.9979	0.9992

4.3.2.2. Isosteric Heat of Adsorption employing Sips isotherm model

- **Nitrogen Isosteric Heat of Adsorption on ANGUARD 6**

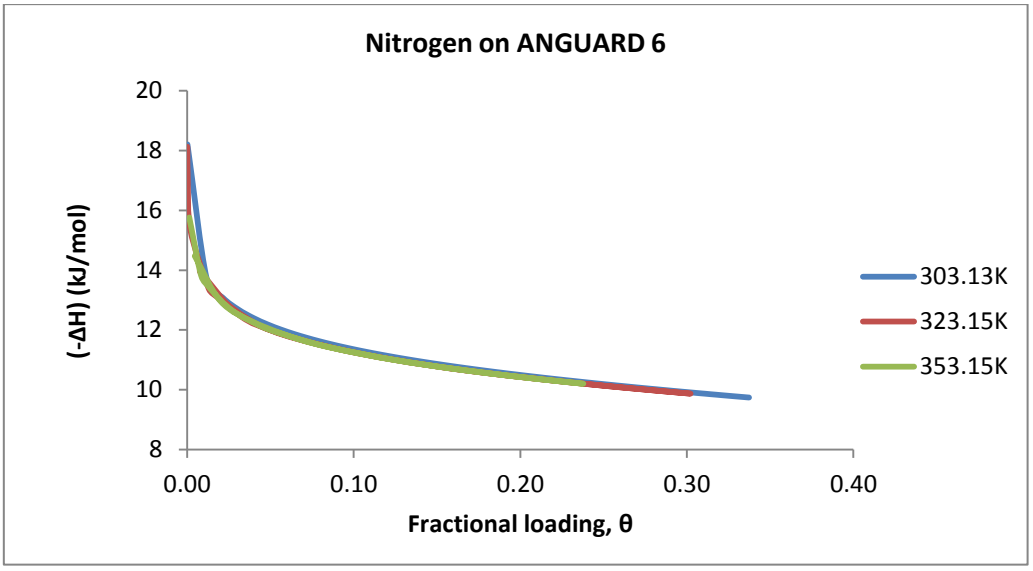

Figure 4.19 - Single-component isosteric heat of adsorption for N_2 at 303.15K, 323.15K and 353.15K as a function of fractional loading on the activated carbon ANGUARD 6, predicted by Sips isotherm model.

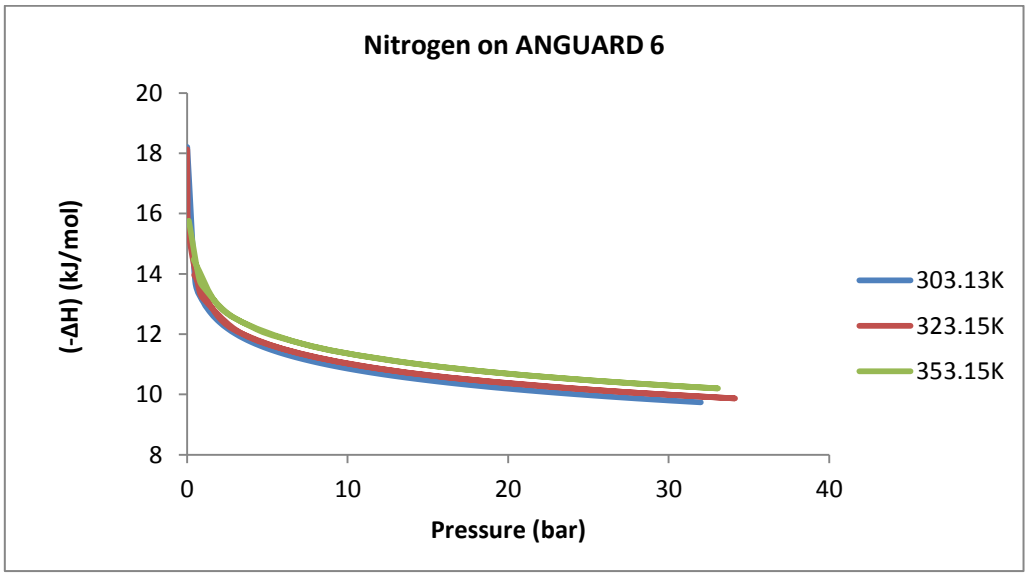

Figure 4.20 - Single-component isosteric heat of adsorption for N_2 at 303.15K, 323.15K and 353.15K as a function of equilibrium pressure on the activated carbon ANGUARD 6, predicted by Sips isotherm model.

- **Butane Isosteric Heat of Adsorption on ANGUARD 6**

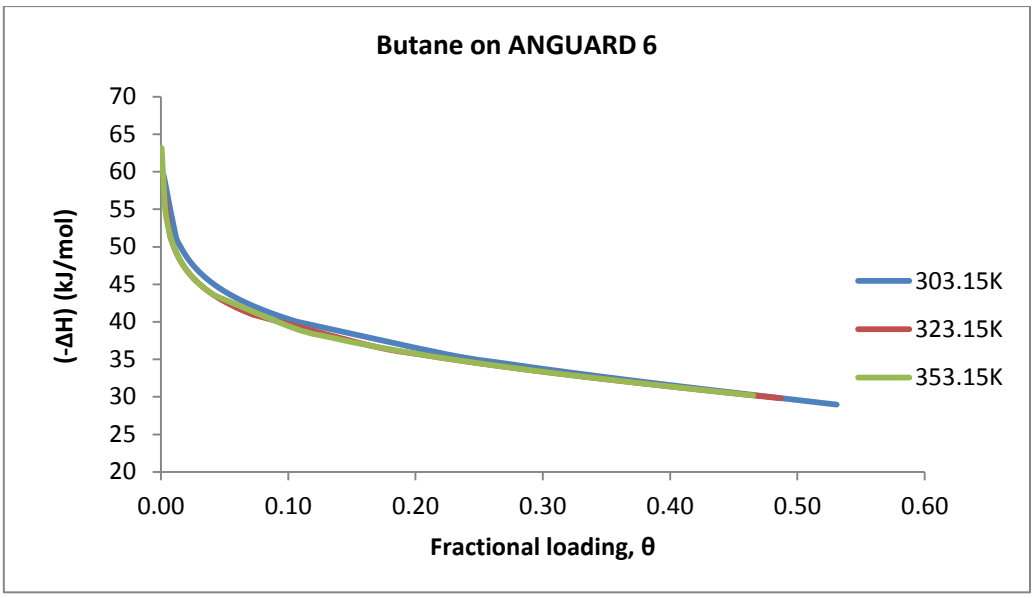

Figure 4.21 - Single-component isosteric heat of adsorption for C_4H_{10} at 303.15K, 323.15K and 353.15K as a function of fractional loading on the activated carbon ANGUARD 6, predicted by Sips isotherm model.

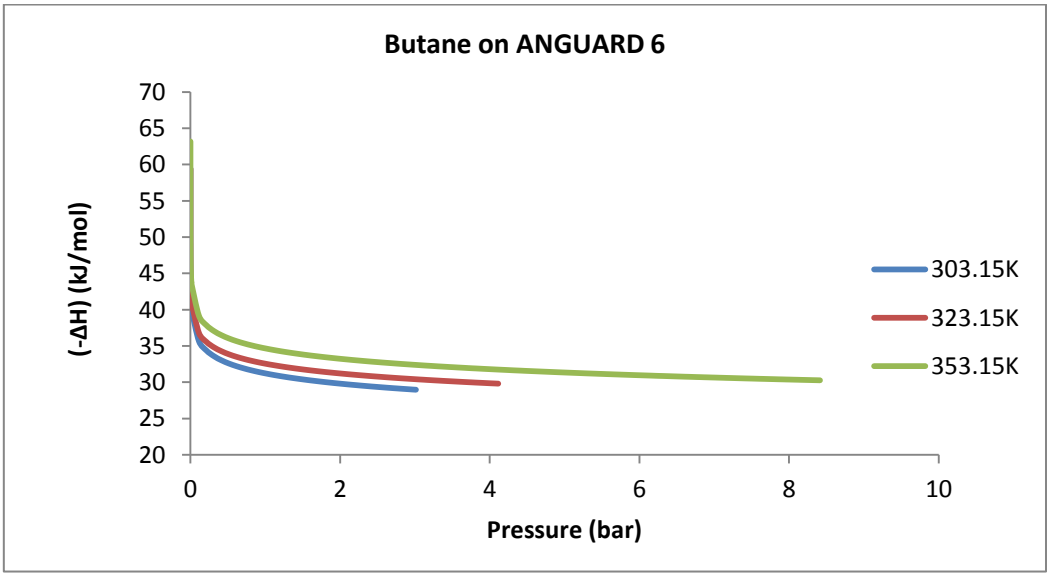

Figure 4.22 - Single-component isosteric heat of adsorption for C_4H_{10} at 303.15K, 323.15K and 353.15K as a function of equilibrium pressure on the activated carbon ANGUARD 6, predicted by Sips isotherm model.

- **Carbon Dioxide Isosteric Heat of Adsorption on ANGUARD 6**

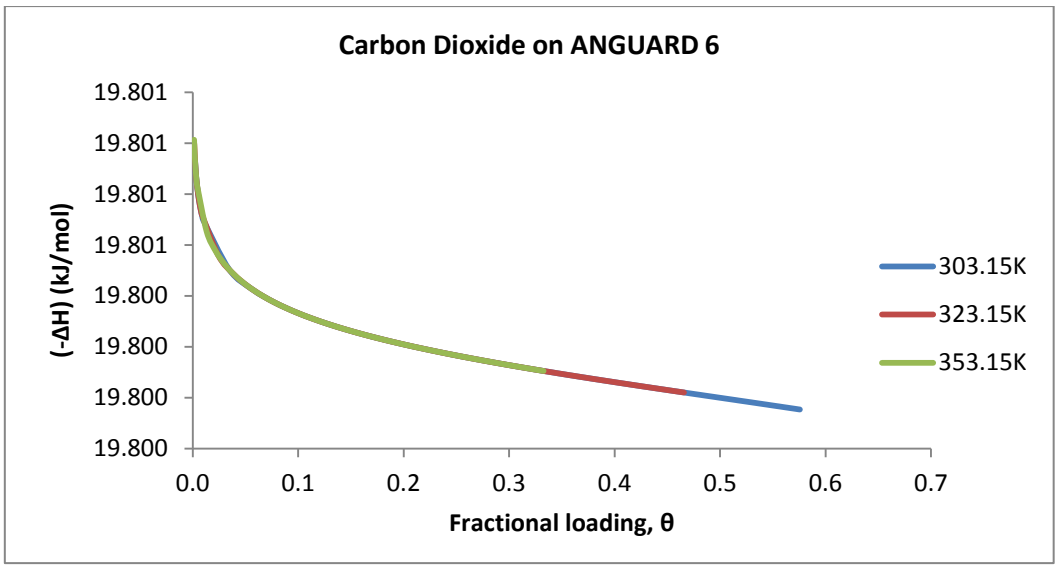

Figure 4.23 - Single-component isosteric heat of adsorption for CO_2 at 303.15K, 323.15K and 353.15K as a function of fractional loading on the activated carbon ANGUARD 6, predicted by Sips isotherm model.

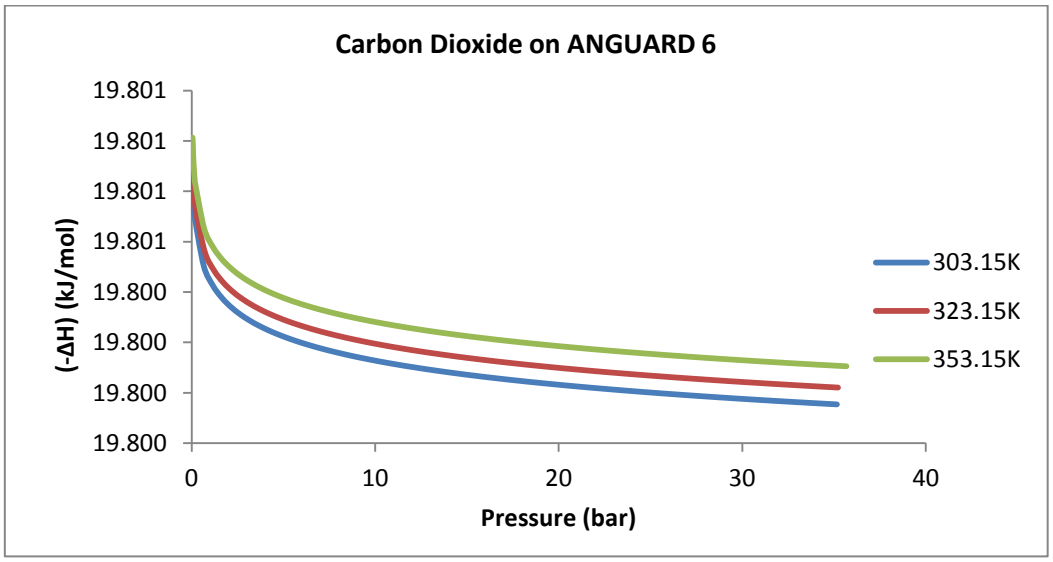

Figure 4.24 - Single-component isosteric heat of adsorption for CO_2 at 303.15K, 323.15K and 353.15K as a function of equilibrium pressure on the activated carbon ANGUARD 6, predicted by Sips isotherm model.

- **Carbon Dioxide Isosteric Heat of Adsorption on ACHM**

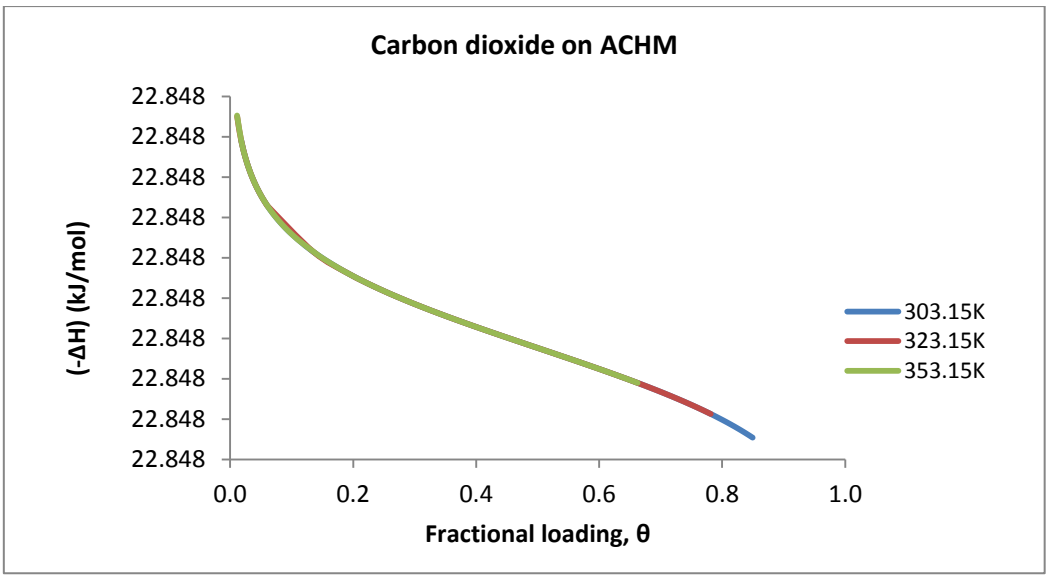

Figure 4.25 - Single-component isosteric heat of adsorption for CO_2 at 303.15K, 323.15K and 353.15K as a function of fractional loading on the activated carbon ACHM, predicted by Sips isotherm model.

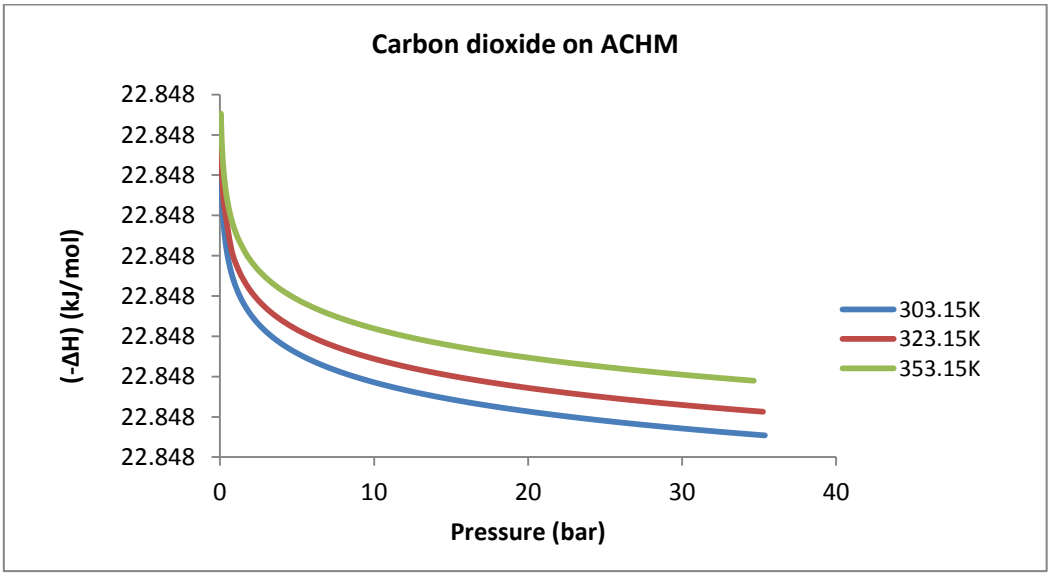

Figure 4.26 - Single-component isosteric heat of adsorption for CO_2 at 303.15K, 323.15K and 353.15K as a function of equilibrium pressure on the activated carbon ACHM, predicted by Sips isotherm model.

From **Figure 4.19** to **Figure 4.26**, it is possible to visualize the variation of the isosteric heat of adsorption for each gas with the fractional loading and with pressure. For both cases, the heat of adsorption decreases with the increasing of the fractional loading and with pressure. This fact is related with the definition of isosteric heat. Activated carbons are characterized by heterogeneous surfaces with a distribution of adsorption sites of different energies. Since the adsorbate molecules begin to adhere to the surface sites with the highest energy, more energy is released at lower surface coverage values. When those sites are totally fulfilled with adsorbate, the gas molecules will be adsorbed on the remaining sites, with lower energy. So at lower coverage, more energy is released reason why the isosteric heat of adsorption is higher for lower amounts adsorbed and decreases with the enhancement of loading and also pressure [22]. In spite of forming a plateau as the previous adsorbates, it can be seen in **Figure 4.23** to **Figure 4.26** that of the values of isosteric heats of adsorption for carbon dioxide, in ANGUARD 6 and in ACHM almost not vary. This is due to the values of parameter α obtained for the two adsorbates (consult **Table 4.3**). Since the α values are almost zero, the contribution of the fractional loading and of the pressure is practical nil, reason why the values of isosteric heat of adsorption almost not vary (see **Equation 4.12** and **Equation 4.13**).

4.3.2.3. Data interpretation from Sips isotherm model

Starting by the maximum amount adsorbed, q_{ts}, from **Table 4.3** it is possible to see that for ANGUARD 6, CO_2 has the highest saturation amount adsorbed, 21.66 mol/kg, followed by C_4H_{10}, 17.12mol/kg and finally by N_2 with 11.96 mol/kg. For comparison purposes the isotherms of CO_2, N_2 and C_4H_{10} on ANGUARD 6 at 303.15K are showed in in **Figure 4.27.**

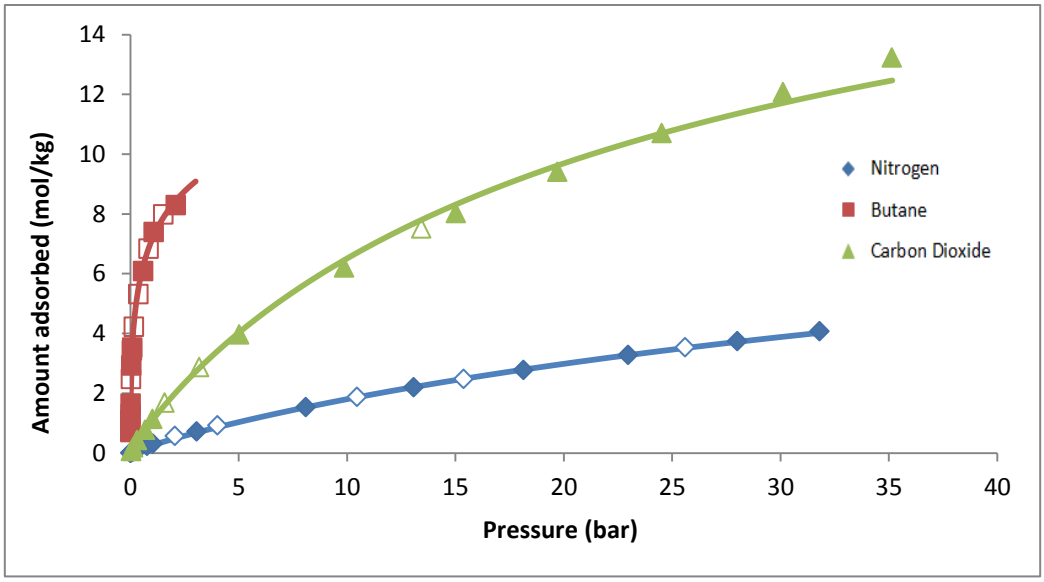

Figure 4.27 - Single-component adsorption isotherms of N_2, C_4H_{10} and CO_2 on ANGUARD 6 at 303.15 K. The symbols represent the experimental data (filled symbol – adsorption; empty symbol – desorption) and the lines represent the Sips model isotherm fitting.

The data shows that at low pressures, C_4H_{10} is significantly more adsorbed than CO_2 and N_2. Despite this fact, the CO_2 adsorption increases significantly with the pressure increase, especially when compared with the capacity of the adsorbent towards N_2. This indicates that this activated carbon has potential to perform CO_2/N_2 separation. To evaluate this potential the equilibrium selectivity of the activated carbon ANGUARD 6 for the CO_2/N_2 separation was evaluated. Adsorption equilibrium selectivity results from a ratio between q_i, the adsorbed amount of the more adsorbed species and the adsorbed amount of the less adsorb quantity, q_j.

$$\alpha_{i/j} = \frac{q_i}{q_j} \qquad \textbf{(Equation 4.15)}$$

Figure 4.28 shows the equilibrium selectivity for the CO_2/N_2 separation on ANGUARD 6. It can be observed that the selectivity for carbon dioxide decreases with the increasing of pressure. The plot shows that the selectivity of CO_2 over N_2 is more favored at low pressures, although it is known that the amount adsorbed increases significantly with pressure and both these parameters must be considered when designing adsorption-based separation processes.

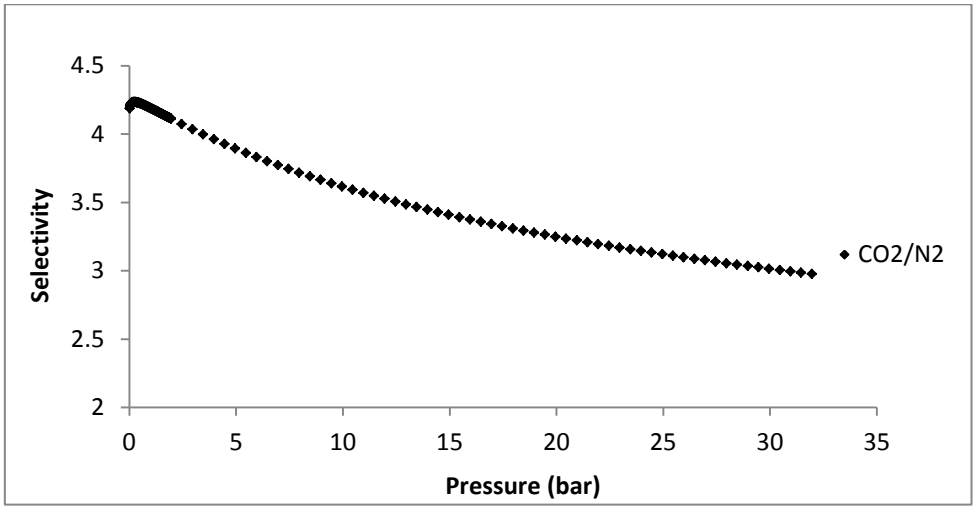

Figure 4.28 - Selectivity of CO_2/N_2 as a function of pressure at 303.15K.

The heats of adsorption, Q, predicted by the Sips isotherm model are 9.02 kJ/mol, 29.58 kJ/mol, 19.80 kJ/mol respectively for N_2, C_4H_{10} and CO_2 dioxide on ANGUARD 6 and 22.85 kJ/mol for carbon dioxide on the ACHM. This means that the adsorbate molecules of butane are the ones that release a higher amount of energy in the adsorption process.

For both activated carbons, for the four adsorbates the value of the Sips model parameter n is always greater than the unit. This parameter n regards the system heterogeneity. The larger is this parameter, the higher is the degree of heterogeneity. However,

this information does not point to what is the source of the heterogeneity, whether it be the solid structural property, the solid energetically properties or the adsorbate properties [36]. The higher value of parameter n was obtained for butane on ANGUARD 6 (n = 2.41).

This same parameter n influences the curvature of the adsorption isotherm. According to the literature [36], the larger is the value of n, the more nonlinear is the adsorption isotherm. When the parameter n is getting larger than 10, the adsorption isotherm is approaching a so-called rectangular isotherm (or irreversible isotherm). The term "irreversible isotherm" is normally used because the pressure needs to be decreased to an extremely low value before adsorbate molecules would desorb from the surface. Such dramatic pressure decrease is quite energy intensive and will therefore affect the energy consumption and cost of a separation involving adsorbate-adsorbents with such isotherms. **Figure 4.29** shows the adsorption isotherm for each adsorbate and its corresponding values of n parameter. It is possible to visualize that butane has the squarest adsorption isotherm.

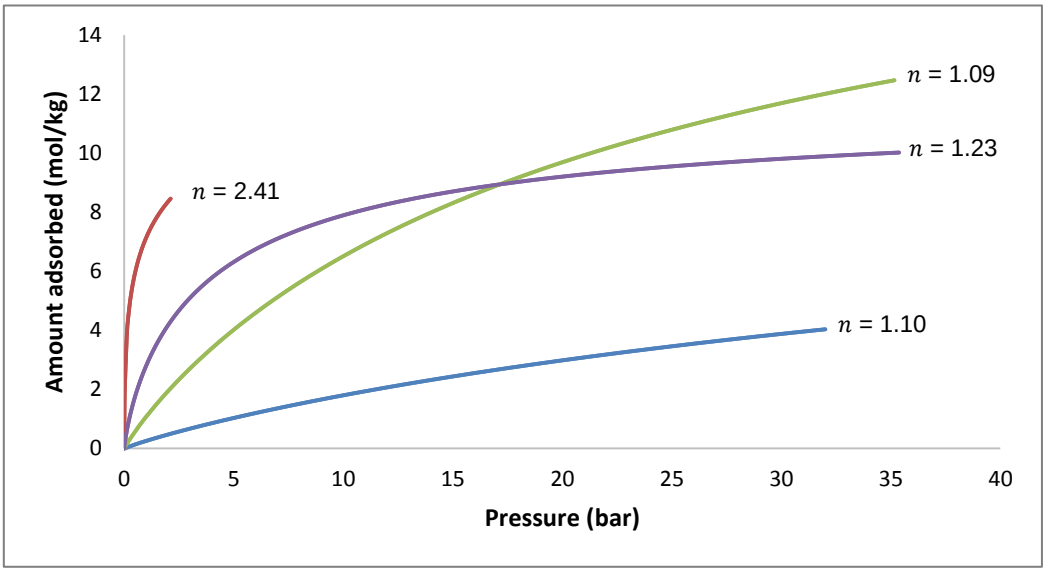

Figure 4.29 - Single-component adsorption isotherms for N_2 (blue line), CO_2 (green line), C_4H_{10} (red line) on ANGUARD 6 and CO_2 (purple line) on ACHM 6 at 303.15 K.

Through **Table 4.3**, it is also possible to see that butane has the highest value of b_0, the affinity constant for a reference temperature on ANGUARD 6. This means that the molecules of butane are the ones that are more attracted to the surface of this activated carbon. Butane is followed by carbon dioxide and nitrogen. Making a comparison between with the value of b_0 obtained for CO_2 on the ACHM, it can be concluded that the molecules of this adsorbate (CO_2) have more affinity for to the surface of the monolith than for the surface of ANGUARD 6.

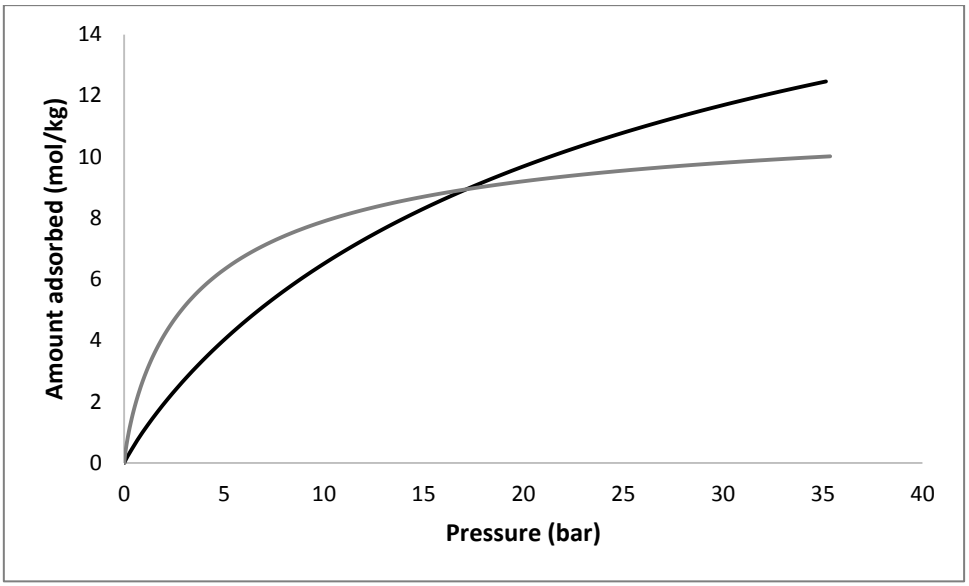

Figure 4.30 - Single-component adsorption isotherms for of CO_2 on ANGUARD 6 and CO_2 on ACHM 6 at 303.15 K. The amount adsorbed is represented in moles of carbon dioxide by mass of carbon sample.

Figure 4.30 presents the CO_2 isotherms at 303.15K of the two activated carbon samples studied. It can be clearly observed that the ACHM adsorbs more CO_2 at low pressures while for higher pressures the ANGUARD 6 activated carbon presents higher adsorption capacity towards CO_2. In fact, the isotherms even cross at around 18 bar.

When the amount adsorbed is compared not by mass of carbon but by volume, a similar trend is observed. The calculus involved in the determination of the bulk densities for ANGUARD 6 and ACHM can be consulted in **APPENDIX A.10**. **Figure 4.31** shows that at low pressures ACHM adsorbs more CO_2 than ANGUARD 6, but around 29 bar, where the adsorption isotherms cross, the situation reverses.

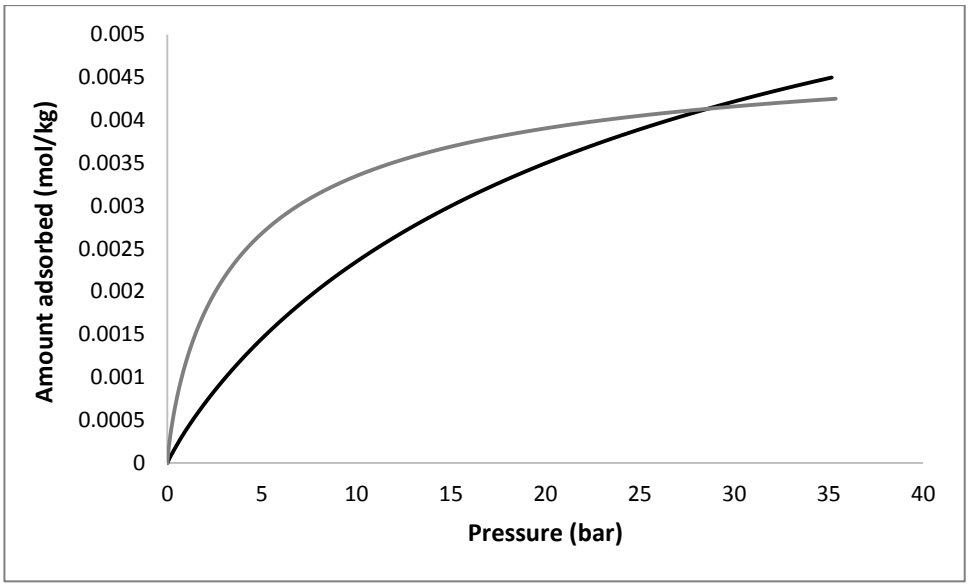

Figure 4.31 - Single-component adsorption isotherms for of CO_2 on ANGUARD 6 and CO_2 on ACHM 6 at 303.15 K. The amount adsorbed is represented in moles of carbon dioxide by volume of carbon sample.

The isotherm of CO_2 on the honeycomb monolith is much squarer than the ANGUARD 6 isotherm. The isotherm shapes is very important when designing a separation process as Pressure Swing Adsorption (PSA). PSA is widely study adsorption-based process [62] in which the adsorbed species are desorbed by decreasing the system pressure [14], [28]. Therefore, if the isotherm presents a square shape an important amount of energy must be spent in order to decrease the pressure enough to ensure desorption of the retained compound.

4.4. Summary

In this chapter adsorption equilibrium of carbon dioxide (CO_2), nitrogen (N_2) and butane (C_4H_{10}) at 303.15K, 323.15K and 353.15K and helium (H_e) pycnometry at 353.15K, in a range of 0 – 35 bar, on ANGUARD 6 activated carbon was presented. Adsorption equilibrium of CO_2 on an activated carbon honeycomb monolith, at the same temperatures and pressure range, was also disclosed.

The experimental adsorption equilibrium results obtained showed that all the adsorption isotherms obtained can be classified as IUPAC *Type I*, characteristic from microporous adsorbents.

The adsorption experimental data from each pure gas was fitted employing the Sips isotherm model. This fitting allowed the estimation of the Sips model parameters. With these parameters the fractional loading, θ and the isosteric heat of adsorption, $(-\Delta H)$ could be calculated.

The isosteric heats of adsorption as a function of the fractional loading and pressure were also determined. The isosteric heat decreases with the increase of the fractional loading

and with the increasing of pressure for all the adsorbate species studied. In case of CO_2, this dependence is almost nil due to the values of parameter α.

For ANGUARD 6, the higher q_{ts} estimated from the Sips model corresponded to carbon dioxide. The q_{ts} obtained for CO_2 on ANGUARD 6 was 21.66 mol/kg while the q_{ts} obtained for CO_2 on the honeycomb monolith was only 11.80 mol/kg. This indicates that the ANGUARD 6 can adsorb more CO_2 than the ACHM for sufficiently high pressures. This fact was also confirmed by comparison of isotherms at the same temperature (303.15 K). Although the ACHM adsorbs more CO_2 at low pressures (above 18 bar when compared by mass and above 29 bar when compared by volume) the isotherms of CO_2 on both carbons cross, and ANGUARD 6 is able to adsorb more CO_2. Also the isotherm of CO_2 on the honeycomb monolith is much squarer than the ANGUARD 6 isotherm, which indicates that to ensure desorption of the retained compound, a great amount of energy must be spent to decrease the pressure.

Chapter 5

5. Conclusions and Suggestions for Future Work

5.1. Conclusions

The work developed within this thesis was divided in two parts:

a) Adsorbent characterization of two activated carbons: ANGUARD 6, which is an activated carbon in the form of extrudates, supplied by Sutcliffe Speakman Carbons Ltd. (UK) and an honeycomb monolith from Mast Carbon International Limited (UK);
b) Single-component adsorption equilibrium measurements of pure gases (carbon dioxide, nitrogen and butane), performed in a magnetic suspension microbalance, by the gravimetric method.

To characterize the activated carbons several methods were used. Surface chemistry of both carbons was analyzed using the Point of Zero Change and Bohem tiration methods. The results obtained indicated that both adsorbents have an amphoteric surface, characterized by basic groups (chromene, ketone and pyrones) and by acidic groups (carboxylic groups, phenols, but not by lactonic groups).

Thermogravimetric analysis (TGA) of the ANGUARD 6 sample was also performed. The TGA curve showed that the weight of ANGUARD 6 decreases steeply at 50ºC (323.15K), losing at least 3% of its weight. From 50ºC (323.15K) to 550ºC (823.15K) the weight decreases slowly and above 600ºC (873.15K), the sample starts to decompose.

Adsorption of nitrogen at 77K was also measured for ANGUARD 6 (at this point the purchased honeycomb monolith was not yet available). From the adsorption isotherm several physical proprieties of the adsorbent were determined. The BET Surface Area method determined that ANGUARD 6 has an internal surface area of 1699.79 m²/g. The t-plot method gave an external surface area of 52.50 m²/g and a micropore surface area of 1647.29 m²/g. The Horvath-Kawazoe (HK) method ensured the determination of the pore size distribution for the microporous adsorbent, indicating that ANGUARD 6 is mostly comprised by micropores but also have a small amount of mesopores, with sizes slightly above 20 $\dot{A}$. Also, this method allowed the determination of the pore volume, used in the determination of the absolute amount

adsorbed (V_p = 0.98 cm^3/g). The Density Functional Theory method confirmed the pore size distribution obtained by HK method.

Mercury porosimetry was also performed for ANGUARD 6. The volume occupied by the mesopores and macropores were determined (0.87 cm^3/g). Combining this volume, with the micropore volume, the total pore volume ANGUARD 6 was determined (V_t= 1.85 cm^3/g).

The second part of this work consisted in the adsorption equilibrium measurements of three gases: carbon dioxide (CO_2), nitrogen (N_2) and butane (C_4H_{10}) on ANGUARD 6. Adsorption equilibrium of CO_2 on the honeycomb monolith was also measured. The experiments were made at 303.15K, 323.15K and 353.15K in a pressure range of 0-35 bar. The experiments were performed by the gravimetric method, using a magnetic suspension microbalance from Rubotherm GmbH.

The net, excess and total amount adsorbed were calculated to each pure gas. The isotherms obtained can be classified as IUPAC *Type I*, typical for microporous adsorbents. The total amount adsorbed was fitted with the Sips isotherm model. The fitting obtained were good and allowed the determination of the Sips model parameters.

The isosteric heat was also studied for all the adsorbates studied. The isosteric heat decreased with the fractional loading and with pressure for all the species studied.

ANGUARD 6 presents a high surface area and micropore volume. This adsorbent also demonstrated to have a good adsorption capacity towards CO_2 and proved to be selective for CO_2/N_2 separation. Therefore, ANGUARD 6 can be envisioned as a potential adsorbent to be employed in the capture of CO_2 from flue gases emitted from fossil fueled power stations. More specifically, ANGUARD 6 can be a good candidate to be used in PSA technology as an alternative to amine scrubbing in the post-combustion CO_2 capture process.

5.2. Suggestions for Future Work

Despite the work already developed and disclosed in the pages of this dissertation, there is still work to be developed regarding the measurement of adsorption properties of the materials employed.

The activated carbon honeycomb monolith was only available in the final part of this work and, therefore, its characterization could not be concluded. Thus, its characterization should be concluded in order to evaluate properties as its pore volume, surface area and pore size distribution.

Also, measurement of the adsorption equilibrium of methane (CH_4) on both adsorbents would be interesting. Biogas is, nowadays, an interesting energy source and since biogas is mainly constituted by CH_4 and CO_2 it would be interesting to evaluate the adsorption properties of both adsorbents towards CH_4. This way, the potential use of the adsorbents on biogas upgrading can be evaluated.

Finally, determination of the adsorption kinetics of the pure gases in the two activated carbons should be accomplished. The design of adsorption separation processes depends not only on the knowledge of the adsorption equilibrium, but also depends strongly on its kinetics. For this reason, the study of the kinetics of CO_2, N_2 and CH_4 on ANGUARD 6 and the ACHM should be performed in the near future.

References

[1] Shen C., Grande C. A., Li P., Yu J., Rodrigues A. E., "Adsorption equilibria and kinetics of CO2 and N2 in activated carbon beads," *Chemical Engineering Journal,* vol. 160, pp. 398-407, 2010.

[2] EPA - United States Environmental Protection Agency, "Overview of Greenhouse Gases," 27th January 2014. [Online]. Available: http://www.epa.gov/. [Accessed 2014 March 3rd].

[3] European Comission , "Energy Efficiency," 2014. [Online]. Available: http://ec.europa.eu/. [Accessed 2014 March 15th].

[4] Aker Solutions, "Aker Solutions to perform world's first tests for capture of CO2 from cement industry," 2014. [Online]. Available: http://www.akersolutions.com/. [Accessed 15 March 2014].

[5] ICO2N, "What is CCS," 2014. [Online]. Available: http://www.ico2n.com/. [Accessed 5th March 2014].

[6] Bellona Environmental CCS Team, "Carbon Capture and Storage," 2014. [Online]. Available: http://bellona.org/ccs/technology/capture/pre-combustion. [Accessed 5th March 2014].

[7] Gregory L. B., Scharmann W. G., "Carbon Dioxide Scrubbing by Amine Solutions - Adsorption and Extraction Symposium," *Ind. Eng. Chem,* p. 514–519, May 1937.

[8] Ribeiro, R. P. P. L., "Electric Swing Adsorption for Gas Separation and Purification," Porto, 2013.

[9] Kutz M., "Clean Power Generation from Coal - CO2 Capture," in *Environmentally Conscious Alternative Energy Production*, John Wiley & Sons, 2007, p. (255) 308.

[10] Ribeiro R. P., Sauer T. P., Lopes F. V., Moreira R. F., Grande C. A., Rodrigues A. E., "Adsorption of CO2, CH4 and N2 in Activated Carbon Honeycomb Monolith," *J. Chem. Eng.,* vol. 53, pp. 2311-2317, 9th April 2008.

[11] Condon, James B., Surface Area and Porosity by Physisorption: Measurements and Theory, Roane State Community College: Elsevier, 2006.

[12] Olds W., Xue Y.,, "Remediation of PAH Contaminated Soils and Groundwater using Activated Carbon," no. ENNR 429: Midyear Report, 2009.

[13] Rouquerol F., Rouquerol J., Sing K., Adsorption by Powders and Porous Solids: Principles, Methodology and Applications, San Diego, USA: Academic Press, 1999.

[14] Ruthven, D. M., Principles of Adsorption and Adsorption Processes, New York: John Wiley & Sons, Inc., 1984.

[15] Esteves, I. A. A. C., "Gas Separation Processes by Integrated Adsorption and Permeation Technologies," Lisboa, 2005.

[16] Lowell S., Shields J. E., Thomas M. A., Matthias T., Characterization of Porous Solids and Powders: Surface Area, Pore Size and Density, Particle Technology Series, pp. 145-148.

[17] Gumma S., Talu O., "Net Adsorption: A Thermodynamic Framework for Supercritical Gas Adsorption and Storage in Porous Solids," vol. 26, pp. 17013-17023, 2010.

[18] Ullmann's Encyclopedia of Industrial Chemistry, Seventh ed., John Wiley & Sons, Inc..

[19] United Nations Framework Convention on Climate Change, "Kyoto Protocol," 2014. [Online]. Available: http://unfccc.int/kyoto_protocol/. [Accessed 5th March 2014].

[20] "CO2Now.org," CO2Now.org, 2014. [Online]. Available: http://co2now.org/. [Accessed 5th March 2014].

[21] Encyclopedia Britannica , "Butane," 2014. [Online]. Available: http://www.britannica.com/. [Accessed 2nd March 2014].

[22] Esteves, I.A.A.C. et al., "Adsorption of natural gas and biogas components on activated carbon," 2008.

[23] Rouquerol J. et al., "Recommendations for the characterization of porous solids," Pure & Appl. Chern., Great Britain, 1994.

[24] Grande, C. A., "Biogas Upgrading by Pressure Swing Adsorption, Biofuel's Engineering Process Technology," 2011.

[25] Keller J.U., Staudt R.,, Gas Adsorption Equilibria: Experimental Methods and Adsorptive Isotherms, Germany: Springer Science + Business Media, Inc., 2005.

[26] Nagano, S.; Tamon, H.; Adzumi, T.; Nakagawa, K.; Suzuki, T., vol. 38, Carbon, 2000, p. 915.

[27] Coulson J. M., Richardson J. F., Tecnologia Química, vol. III, Fundação Calouste Gulbenkian, 1982.

[28] Yang, R. T., Adsorbents: Fundamentals and Applications, Hoboken, New Jersey: John Wiley & Sons, Inc., 2003.

[29] Bell, R.G., "Zeolites - British Zeolite Association," British Zeolite Association, May 2001. [Online]. Available: http://bza.org. [Accessed 26th November 2013].

[30] Lyubchyk A., "Gas Adsorption in the MIL-53(Al) Metal Organic Framework. Experiments and Molecular Simulation.," 2013.

[31] MOF technologies, "MOF technologies," MOF Technologies Ltd, 2012. [Online]. Available: http://moftechnologies.com/. [Accessed 26th November 2013].

[32] Lyubchyk A., Esteves I. A. A. C. , Cruz F. J. A. L. , Mota J. P. B., "Experimental and Theoretical Studies of Supercritical Methane Adsorption in the MIL-53(Al) Metal Organic Framework," *The Journal of Physical Chemistry C,* vol. 115, p. 20628 – 20638, 2011.

[33] Ribeiro, A.M.; Campo, M.C.; Narin, G.; Santos, J.C.; Ferreira, A.; Chang, J.-S.; Hwang, Y.K.; Seo, Y.-K.; Lee, U.H.; Loureiro, J.M., et al., "Pressure Swing Adsorption Process for

the Separation of Nitrogen and Propylene with a MOF Adsorbent MIL-100(Fe)," *Separation and Purification Technology,* vol. 110, pp. 101-111, 2013.

[34] Cameron Carbon Incorporated, "Activated Carbon: Manufacture, Structure & Properties," Cameron Carbon Incorporated, 2006. [Online]. Available: http://cameroncarbon.com/.. [Accessed 26th November 2013].

[35] Ribeiro A. M., Loureiro J. M., "Breakthrough behaviour of water vapor on activated carbon filters," pp. 357-360, 2006.

[36] Do. D. D., Adsorption Analysis: Equilibria and Kinetics, vol. 2, Queenslan: Imperial College Press, 1998.

[37] Gorgulho H. F., et al, "Adsorção de fenol sobre carvão activado em meio alcalino," vol. 29, pp. 1226-1232, 2006.

[38] Carbon Activated Corp., "Carbon Activated Corp.," Carbon Activated Corp., 2013. [Online]. Available: http://activatedcarbon.com/. [Accessed 26th November 2013].

[39] DESOTEC Activated Carbon, "DESOTEC Activated Carbon," DESOTEC Activated Carbon, 2013. [Online]. Available: http://desotec.com/. [Accessed 26th November 2013].

[40] Thomas Publishing Company, "Producing Activated Carbon," Thomas Publishing Company, 2013. [Online]. Available: http://thomasnet.com/. [Accessed 26th November 2013].

[41] Sun J., Brady T. A., Rood M. J., Rostam-Abadi M., Lizzio A. A., "Adsorbed natural gas storage with activated carbon," pp. 246-250.

[42] Sushrut Chemicals, "Activated Carbon," 2006. [Online]. Available: http://sushrutchemicals.com/.. [Accessed 3rd December 2013].

[43] Ekpete O.A., Horsfall M. JNR, "Preparation and Characterization of Activated Carbon derived from Fluted Pumpkin Stem Waste (Telfairia occidentalis Hook F)," vol. 1, 2011.

[44] Chemviron Carbon, "Activated Carbon as a Catalyst or for Catalyst Support," 2014. [Online]. Available: http://www.chemvironcarbon.com/. [Accessed 7th March 2014].

[45] WebMD, LLC., "Activated Charcoal," 2013. [Online]. [Accessed 3rd December 2013].

[46] Lozano D., De la Casa M.A. ,Alcañiz J., Cazorla D., Linares A., "Advances in the study of methane storage in porous carbonaceous materials," *Fuel,* vol. 81, pp. 1777-1803, 2002.

[47] CABOT INC., "Cabot Norit Activated Carbon products," 2013. [Online]. [Accessed 3rd December 2013].

[48] Boehm, H. P., "Surface oxides on carbon and their analysis: a critical assessment," pp. 145-149, 2001.

[49] Shrestha Rajeshwar M., Yadav Amar P., Pokharel Bhadra P., Pradhananga Raja Ram´, "Preparation and characterization of activated carbon from lapsi (choerospondias axillaris) seed stone by chemical activation with phosphoric acid," *Research Journal of Chemical*

Sciences, vol. 2, pp. 80-86, October 2012.

[50] Figueiredo J. L., Ramôa Ribeiro F., Catálise Heterogénea, Lisboa: Fundação Calouste Gulbenkien, 1987.

[51] SING, K. S. W. et al., "Reporting Physisorption Data for Gas/solid systems with Special Reference to the Determination of Surface Area and Porosity," Pure & App. Chem., Great Britain, 1985.

[52] Aligizaki K.K., Pore Structure of Cement-Based Materials: Testing, Interpretation and Requirements, CRC Press, 2006 .

[53] Kurdi J., Tremblay A.Y., "The determination of interaction parameters in the characterization of polyetherimide gas separation membranes using the Horvath-Kawazoe model," *Desalination ,* vol. 148, p. 341–346, 8 April 2002.

[54] Horvath G, Kawazoe K., "Method for the calculation of effective pore size distribution in molecular sieve carbon," *Journal of Chemical Engineering of Japan,* 1983.

[55] Yang R. T, Rege S. U.,, "Corrected Horváth-Kawazoe Equations for Pore-Size Distribution," *AIChE Journal,* vol. 46, April 2000.

[56] Cuevas, J. C., "www.uam.es," Institut für Theoretische Festkörpephysik Universität Karlsruhe (Germany). [Online]. [Accessed 17th December 2013].

[57] Micromeritics, "Porosimetry," One Micromeritics Drive, 1st January 2001. [Online]. Available: www.micromeritics.com. [Accessed 16th December 2013].

[58] Webb P. A.,, "Volume and Density Determinations for Particle Technologists," February 2001.

[59] Eusébio, M. F. J., *Development of an universal interface for monitoring and control of chemical and biochemical processes,* Faculdade de Ciências e Tecnologia da Universidade Nova de Lisboa (FCT/UNL), Lisbon, 2006.

[60] RUBOTHERM PRÄZIONSMESSTECHKIN GmBH, SORPTION - ISOSORP - THE NEW SORPTION SUSPENSION BALANCE, p. 8.

[61] National Institute of Standards and Technology, "NIST Chemistry WebBook," 2014. [Online]. Available: http://webbook.nist.gov/chemistry/. [Accessed 2014].

[62] Ribeiro, A. M.; Santos, J.; Rodrigues, A., , "Pressure Swing Adsorption for CO2 Capture in Fischer-Tropsch Fuels Production from Biomass," *Adsorption-Journal of the International Adsorption Society ,* Vols. 17, (3), pp. 443-452, 2011.

[63] Goertzen S. L., Thériault K. D., Oickle A. M., Tarasuk A. C., "Standardization of the Bohem titration. Part I. CO2 expulsion and endpoint determination," *CARBON,* pp. 1252-1261, 2010.

[64] Goertzen S. L., Thériault K. D., Oickle A. M., Tarasuk A. C., "Standardization of the Boehm titration: Part II. Method of agitation, effect of filtering and dilute titrant," *CARBON,* p. 3313 – 3322, 2010.

APPENDIX

A. Results from Chapter 3

A.1. Calculus used in the analysis of Bohem Titrations Results

Calculus:

The determination of the number of moles of the surface functionalities (surface functional groups) at the carbon surface was obtained through the following equation [63]:

$$n_{CFS} = [B].V_B - [HCl].V_{HCl}.\frac{V_B}{V_a} \quad \textbf{(Equation A.1)}$$

Where, n_{CFS} is the number of moles of carbon surface functionalities at the carbon surface; $[B]$ and V_B are the concentration and volume of the basic solution (or acid in case of HCl) mixed with carbon. The product between the two is the number of moles of the basic solution (or acid in case of HCl) that will be available to react with the surface groups at the carbon surface; V_a is the volume of the aliquot taken from V_B; $[HCl]$ and V_{HCl} (or in case of HCl, $[NaOH]$ and V_{NaOH}) are the concentration and volume of the titrant added to the aliquot and the product is the number of moles acid (or basic) added to the aliquot and available to react with the remaining reaction base (or acid);

The quantification of the functional groups at the carbon surface can be calculated through several subtractions. The NaOH neutralizes all the acid groups (phenols, lactonic and carboxylic groups) and therefore has a n_{CFS} that includes all of these groups. Na_2CO_3 reacts with carboxylic and lactonic groups and the difference between n_{CFS}(NaOH) and n_{CFS}(Na_2CO_3) will denote the number of phenols on the surface.

In the same way, since $NaHCO_3$ reacts only with the carboxylic groups the difference between the n_{CFS}(Na_2CO_3) and n_{CFS}($NaHCO_3$) gives the quantity of lactonic groups. The quantity of carboxylic groups it is determined directly from n_{CFS}($NaHCO_3$).The quantification of the basic groups comes from the value of n_{CFS}(HCl) [63], [64].

In the case of the ACHM, like it was mention before, the amount available to perform the experiments was less than for ANGUARD 6, and for this reason only one run, **RUN D**, was performed. The same conditions as the ones used in **RUN B** were employed. Instead of 1.0 g of well-crushed activated carbon and 10 mL of each solution previously prepared, the quantities were reduced to half.

A.2. Results from Bohem Titrations

Table A.1 - Results from Bohem Titrations Experiments for RUN A – 48 hours without centrifugation (ANGUARD 6).

Solutions	Concentration (M)	pH of the aqueous solution (0.05M) (292.15K)	pH of the solution mixed with ANG 6 (titrated) (292.35K)	Volume of the titrated (mL)	Weight of ANG 6 (g)	pH of the titrant (292.25K)	Volume of the titrant (mL)	Concentration of the titrant (mol/mL)	Concentration of the titrated (mol/mL)	Concentration of the titrated (mmol/mL)
NaOH	0.05	12.15	9.91	5.1	1.015	1.71	1.5	1.000E-04	2.941E-05	0.029
$NaHCO_3$	0.05	8.32	9.01	3.8	1.007	1.71	0.9	1.000E-04	2.368E-05	0.024
Na_2CO_3	0.05	10.89	9.50	4.0	1.009	1.71	1.4	1.000E-04	3.500E-05	0.035
HCL	0.05	2.07	5.04	2.9	1.003	12.65	0.4	1.000E-04	1.379E-05	0.014

Table A.2 - Results from Bohem Titrations Experiments for RUN B – 48 hours with centrifugation (ANGUARD 6).

Solutions	Concentration (M)	pH of the aqueous solution (0.05M) (292.45K)	pH of the solution mixed with ANG 6 (titrated) (293.15K)	Volume of the titrated (mL)	Weight of ANG 6 (g)	pH of the titrant (292.25)	Volume of the titrant (mL)	Concentration of the titrant (mol/mL)	Concentration of the titrated (mol/mL)	Concentration of the titrated (mmol/mL)
NaOH	0.05	12.15	9.96	6.1	1.003	1.71	1.7	1.000E-04	2.787E-05	0.028
$NaHCO_3$	0.05	8.32	9.40	6.8	1.01	1.71	0.9	1.000E-04	1.324E-05	0.013
Na_2CO_3	0.05	10.89	9.67	6.8	1.014	1.71	3.1	1.000E-04	4.559E-05	0.046
HCL	0.05	2.07	5.12	5.5	1.006	12.65	0.3	1.000E-04	5.455E-06	0.005

Table A.3 - Results from Bohem Titrations Experiments for RUN C– 24 hours with centrifugation (ANGUARD 6).

Solutions	Concentration (M)	pH of the aqueous solution (0.05M) (292.45K)	pH of the solution mixed with ANG 6 (titrated) (293.15K)	Volume of the titrated (mL)	Weight of ANG 6 (g)	pH of the titrant (292.25K)	Volume of the titrant (mL)	Concentration of the titrant (mol/mL)	Concentration of the titrated (mol/mL)	Concentration of the titrated (mmol/mL)
NaOH	0.05	12.15	10.960	6.5	1.011	1.71	2.0	1.000E-04	3.077E-05	0.031
$NaHCO_3$	0.05	8.32	9.800	4.8	1.022	1.71	1.1	1.000E-04	2.292E-05	0.023
Na_2CO_3	0.05	10.89	10.380	6.5	1.001	1.71	3.2	1.000E-04	4.923E-05	0.049
HCL	0.05	2.07	3.840	5.3	1.000	12.65	0.6	1.000E-04	1.132E-05	0.011

Table A.4 - Results from Bohem Titrations Experiments for RUN D – 48 hours with centrifugation (ACHM).

Solutions	Concentration (M)	pH of the aqueous solution (0.05M) (292.45K)	pH of the solution mixed with ACHM (titrated) (293.15K)	Volume of the titrated (mL)	Weight of ACHM (g)	pH of the titrant (293.15K)	Volume of the titrant (mL)	Concentration of the titrant (mol/mL)	Concentration of the titrated (mol/mL)	Concentration of the titrated (mmol/mL)
NaOH	0.05	12.83	9.61	2.6	0.491	1.02	1.0	1.000E-04	3.8467E-05	0.038
$NaHCO_3$	0.05	9.01	9.87	3.0	0.504	1.02	1.1	1.000E-04	3.667E-05	0.037
Na_2CO_3	0.05	11.67	10.13	3.0	0.505	1.02	1.4	1.000E-04	4.667E-05	0.047
HCL	0.05	1.48	3.58	2.0	0.493	12.78	0.4	1.000E-04	2.000E-05	0.020

A.3. Results from N_2 adsorption at 77K

Table A.5 - N_2 adsorption isotherm at 77K for ANGUARD 6.

Relative Pressure (mmHg)	Absolute Pressure (mmHg)	Amount adsorbed (cm3/g STP)	Saturation Pressure (mmHg)
5.40E-06	0.0042	20.1990	773.3922
9.80E-06	0.0076	40.3963	
2.10E-05	0.0162	60.5900	
3.99E-05	0.0309	80.7795	
6.86E-05	0.0530	100.9655	
1.13E-04	0.0871	121.1435	
1.82E-04	0.1403	141.3116	
2.95E-04	0.2276	161.4585	
3.73E-04	0.2876	171.1009	
7.47E-04	0.5761	197.3558	
1.50E-03	1.1537	220.5257	
3.00E-03	2.3143	241.1775	
6.09E-03	4.6931	261.2856	
1.22E-02	9.4126	282.0022	770.5537
2.51E-02	19.3363	307.5154	
4.89E-02	37.7144	339.4128	
9.83E-02	75.7452	390.3850	
1.48E-01	113.9255	434.0811	
1.99E-01	153.6747	475.4101	
2.53E-01	194.8087	513.7624	
3.09E-01	238.1761	548.4652	
4.04E-01	311.7136	592.2765	
5.04E-01	388.4846	618.3242	
6.13E-01	472.3442	632.9579	
7.09E-01	546.3831	640.0570	
7.94E-01	612.1602	645.0776	
8.58E-01	661.6496	648.7496	
8.99E-01	693.1236	651.4601	
9.24E-01	712.8140	653.5630	
9.49E-01	731.7781	656.3436	
9.73E-01	750.1361	661.1551	
9.88E-01	762.0043	667.5474	
8.96E-01	691.0161	656.5646	
7.89E-01	608.5940	650.5465	
6.88E-01	530.6953	645.2773	
6.01E-01	463.4106	640.2210	771.2968
5.01E-01	386.5867	633.1470	
3.97E-01	306.3074	591.6652	
3.03E-01	233.4853	545.7287	
2.00E-01	153.9131	475.8777	
1.02E-01	78.7608	393.3008	

A.4. Results from BET Surface Area Method Analysis

BET Surface Area Report

BET Surface Area: 1699.7935 ± 16.5198 m²/g
Slope: 0.002537 ± 0.000024 g/cm³ STP
Y-Intercept: 0.000024 ± 0.000004 g/cm³ STP
C: 106.501707
Qm: 390.4700 cm³/g STP
Correlation Coefficient: 0.9997672
Molecular Cross-Sectional Area: 0.1620 nm²

Relative Pressure (P/Po)	Quantity Adsorbed (cm³/g STP)	1/[Q(Po/P - 1)]
0.025090490	307.5154	0.000084
0.048934881	339.4128	0.000152
0.098274021	390.3850	0.000279
0.147800918	434.0811	0.000400
0.199356944	475.4101	0.000524
0.252704696	513.7624	0.000658
0.308941058	548.4652	0.000815

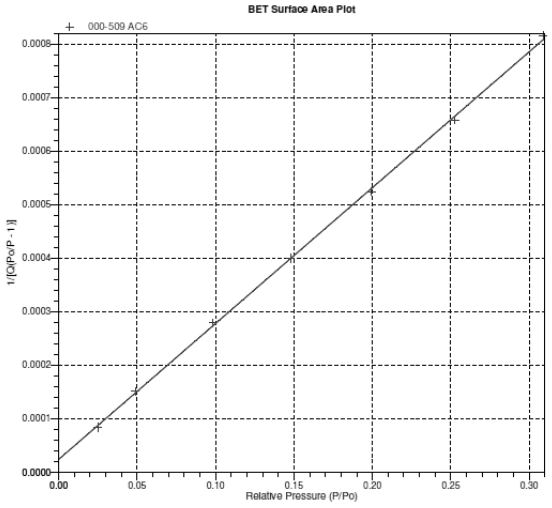

Figure A.1- BET Surface Area Report and BET Surface Area Plot for ANGUARD 6, obtained from DataMaster™, V4.00 (2004). The value of n_m^a is indicated as Qm.

A.5. Results from t-Plot Method Analysis

t-Plot Report

Micropore Volume: 0.944213 cm³/g
Micropore Area: 1647.2948 m²/g
External Surface Area: 52.4987 m²/g
Slope: 33.940212 ± 0.000000 cm³/g·nm STP
Y-Intercept: 610.430111 ± 0.000000 cm³/g STP
Correlation Coefficient: 1.000000
Surface Area Correction Factor: 1.000
Density Conversion Factor: 0.0015468
Total Surface Area (BET): 1699.7935 m²/g
Thickness Range: 0.80000 nm to 1.60000 nm
Thickness Equation: Harkins and Jura

t = [13.99 / (0.034 - log(P/Po))] ^ 0.5

Relative Pressure (P/Po)	Statistical Thickness (nm)	Quantity Adsorbed (cm³/g STP)
0.098274021	0.36649	390.3850
0.147800918	0.40232	434.0811
0.199356944	0.43647	475.4101
0.252704696	0.47072	513.7624
0.308941058	0.50706	548.4652
0.404301901	0.57220	592.2765
0.503852260	0.64944	618.3242
0.612591347	0.75285	632.9580
0.708596815	0.87291	640.0570
0.793877165	1.02084	645.0776

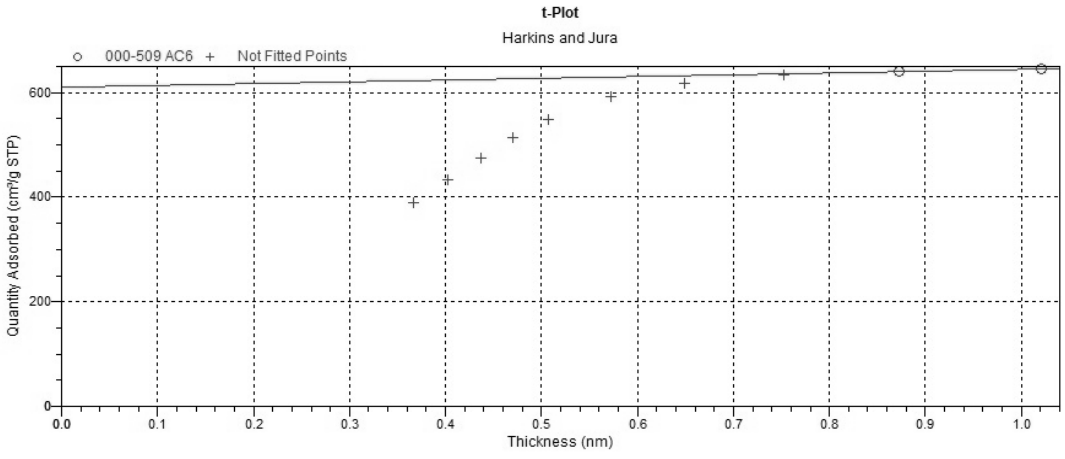

Figure A.2 - t-Plot Report and t-Plot for ANGUARD 6, obtained from DataMaster™, V4.00 (2004).

A.6. Results from Horvath-Kawazoe (HK) Method Analysis

Horvath-Kawazoe Report
Slit Pore Geometry (original HK)

Maximum Pore Volume:		0.979059 cm³/g
at Relative Pressure:		0.612591347
Median Pore Diameter:		18.4 A
Relative Pressure Range:	5.397650E-06 to	0.999999881
Diameter of Adsorptive Molecule:		3.0000 A
Diameter of Adsorptive Zero Interaction Energy:		2.5740 A
Adsorptive Density:		6.710e+14 molecules/cm²
Adsorptive Dispersion Constant:		7.777e-59
Diameter of Sample Atom:		3.4000 A
Diameter of Sample Zero Interaction Energy:		2.9180 A
Sample Density:		3.845e+15 molecules/cm²
Sample Dispersion Constant:		1.562e-58
Density Conversion Factor:		0.001547

Figure A.3 - Horvath-Kawazoe Report for ANGUARD 6, obtained from DataMaster™, V4.00 (2004).

A.7. Results from Density Functional Theory (DFT) Method Analysis

Porosity Distribution by Original Density Functional Theory
Model: N2 @ 77K on Carbon, Slit Pores
Method: Non-negative Regularization; No Smoothing

Volume in Pores	<	5.00 Å	:	0.00000 cm³/g
Total Volume in Pores	<=	1085.66 Å	:	0.86350 cm³/g
Area in Pores	>	1085.66 Å	:	15.431 m²/g
Total Area in Pores	>=	5.00 Å	:	1049.537 m²/g

Figure A.4 - Density Functional Theory results for ANGUARD 6, obtained from DataMaster™, V4.00 (2004).

A.8. Results from Mercury Porosimetry Analysis

Intrusion Data Summary

Total Intrusion Volume =	0.8689 mL/g
Total Pore Area =	104.332 m²/g
Median Pore Diameter (Volume) =	0.9008 µm
Median Pore Diameter (Area) =	0.0088 µm
Average Pore Diameter (4V/A) =	0.0333 µm
Bulk Density at 0.52 psia =	0.5624 g/mL
Apparent (skeletal) Density =	1.0999 g/mL
Porosity =	48.8681 %
Stem Volume Used =	31 %

Figure A.5 - Intrusion Data from Hg porosimetry for ANGUARD 6

A.9. Resume of the physical parameters calculated from the several characterization methods for ANGUARD 6

Table A.6 - Characterization physical parameters of ANGUARD 6.

Characterization of ANGUARD 6	
N_2 Adsorption at 77K	
Surface Area	
BET Surface Area (m^2/g):	1669.79
t-Plot External Surface Area (m^2/g):	52.50
t-Plot Micropore Area (m^2/g):	1647.29
(DFT) Area in Pores (>108.566 nm) (m^2/g):	15.43
(DFT) Total Area in Pores (≥0.500 nm) (m^2/g):	1049.54
Pore Volume	
t-Plot Micropore volume (cm^3/g):	0.94
(HK) Maximum Pore Volume (cm^3/g):	0.98
(DFT) Total Volume in Pores (≤108.566 nm) (cm^3/g):	0.86
Pore Size	
Adsorption average pore width (4V/A by BET) (nm):	2.43
(HK) Median Pore Diameter (nm):	1.84

Hg Mercury Porosimetry	
Intrusion Data Summary	
Total Intrusion Volume (cm^3/g):	0.87
Total Pore Area (m^2/g):	104.33
Medium Pore Diameter (Volume) (nm):	900.8
Medium Pore Diameter (Area) (nm):	8.8
Average Pore Diameter (4V/A) (nm):	33.3
Bulk Density at 0,51 psia (g/cm^3):	0.56
Apparent (skeletal) Density (g/cm^3):	1.10
Porosity (%)	48.87

A.10. Calculus used for the determination of the bulk densities for ANGUARD 6 and ACHM

Bulk density of ANGUARD 6

In order to determine the bulk density of ANGUARD 6, a graduated cylinder of 50 mL $\pm$ 1.0 mL was filled with the carbon pellets. The weights of the graduated cylinder and the graduated cylinder + the carbon pellets were measured. The weight of the carbon pellets was estimated by the difference.

$Weight\ of\ the\ graduated\ cylinder$ = 93.868 g

$Weight\ of\ the\ graduated\ cylinder + carbon\ pellets$ = 111.909 g

$Weight\ of\ the\ carbon\ pellets$ = 18.041 g

The bulk density was than calculated by the quotient between the weight of the carbon pellets and the volume of the graduated cylinder.

$$Bulk\ density\ of\ ANGUARD\ 6 = \frac{Weight\ of\ the\ carbon\ pellets}{Volume\ of\ the\ graduated\ cylinder} = 0.361\ g/cm^3$$

Bulk density of ACHM

Since the honeycomb monolith has a cylinder shape, it was easy to determine its volume. **Figure A.6** illustrates a piece of the ACHM and its dimensions.

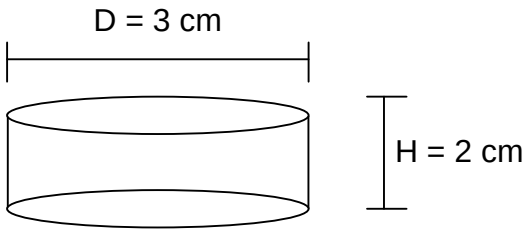

Figure A.6 - Illustration of a piece of the ACHM used for the determination of its bulk density.

After the dimensions were recorded, the piece of the ACHM was weighed.

$Weight\ of\ the\ ACHM\ piece$ = 5.997 g

$Cross\ sectional\ area\ of\ the\ ACHM\ piece = \pi r^2$ = 7.069 cm^2

$Height\ of\ the\ ACHM\ piece$ = 2 cm

$Volume\ of\ the\ ACHM\ piece = H.\pi r^2$ = 14.137 cm^3

$$Bulk\ density\ of\ ACHM = \frac{Weight\ of\ the\ ACHM\ piece}{Volume\ of\ the\ ACHM\ piece} = 0.424\ g/cm^3$$

B. Results from Chapter 4

Table B.1 - Experimental data obtained from helium measurements at 353.15K for ANGUARD 6 and ACHM.

He adsorption at 353.15K for ANG6		He adsorption at 353.15K for ACHM	
Weight (g)	**ρ_g (kg/m^3)**	**Weight (g)**	**ρ_g (kg/m^3)**
6.9016	0.0000	5.9985	0.0000
6.9016	0.0685	5.9985	0.0685
6.9014	0.2928	5.9983	0.2928
6.9007	0.9491	5.9977	0.9491
6.9000	1.8180	5.9972	1.8180
6.8985	3.3762	5.9958	3.3762
6.8976	4.1946	5.9950	4.1946
6.8970	4.6663	5.9945	4.6663
6.8992	2.5652	5.9964	2.5652
6.9006	1.3359	5.9976	1.3359
6.9013	0.5476	5.9983	0.5476
6.9019	0.0000	5.9985	0.0000

Table B.2 – Experimental nitrogen adsorption equilibrium data on the carbon sample ANGUARD 6 at 303.15K, 323.15K and 353.15K. 54 experimental data points were measured.

303.15K				323.15K				353.15K			
P (bar)	q_{net} (mol/kg)	q_{ex} (mol/kg)	q_t (mol/kg)	P (bar)	q_{net} (mol/kg)	q_{ex} (mol/kg)	q_t (mol/kg)	P (bar)	q_{net} (mol/kg)	q_{ex} (mol/kg)	q_t (mol/kg)
0.0048	0.0017	0.0018	0.0020	0.0052	0.0010	0.0011	0.0013	0.1055	0.0118	0.0132	0.0167
0.0245	0.0051	0.0055	0.0064	0.0176	0.0024	0.0027	0.0033	0.7156	0.0699	0.0792	0.1031
0.0952	0.0224	0.0238	0.0275	0.1014	0.0091	0.0106	0.0143	1.0547	0.1124	0.1261	0.1613
0.3088	0.0796	0.0843	0.0963	0.7544	0.0981	0.1088	0.1363	2.9982	0.2511	0.2900	0.3900
0.7642	0.1985	0.2101	0.2398	1.0172	0.1292	0.1436	0.1807	7.1361	0.4904	0.5829	0.8209
1.0280	0.2535	0.2690	0.3090	3.0153	0.3481	0.3909	0.5008	12.0574	0.7243	0.8806	1.2821
3.0544	0.5489	0.5952	0.7140	5.5639	0.5826	0.6616	0.8646	17.1165	0.9214	1.1431	1.7128
8.0958	1.0962	1.2189	1.5340	10.0009	0.9058	1.0478	1.4126	22.2872	1.0912	1.3799	2.1215
13.0752	1.4886	1.6867	2.1959	15.0174	1.2013	1.4144	1.9621	28.1797	1.2469	1.6112	2.5472
18.1291	1.7957	2.0706	2.7770	20.4011	1.4529	1.7424	2.4861	33.0759	1.3524	1.7795	2.8769
22.9614	2.0304	2.3787	3.2736	24.9887	1.6300	1.9844	2.8952	30.3840	1.2919	1.6845	2.6933
27.9974	2.2265	2.6512	3.7425	30.1453	1.7973	2.2246	3.3227	25.2169	1.1734	1.4996	2.3376
31.8068	2.3479	2.8305	4.0705	34.1373	1.8905	2.3744	3.6176	19.7078	1.0002	1.2553	1.9110
25.5976	2.1450	2.5333	3.5311	25.9843	1.6687	2.0372	2.9841	14.5531	0.8246	1.0133	1.4981
15.3769	1.6448	1.8779	2.4769	17.4601	1.3292	1.5770	2.2136	9.3453	0.5963	0.7175	1.0291
10.4483	1.3143	1.4726	1.8794	12.6342	1.0857	1.2651	1.7259	5.8770	0.4122	0.4885	0.6845
4.0172	0.7067	0.7676	0.9239	7.4972	0.7450	0.8515	1.1249	4.0883	0.3048	0.3579	0.4943
2.0575	0.4556	0.4867	0.5668	3.9986	0.4475	0.5042	0.6501	1.9162	0.1638	0.1887	0.2527
				2.0161	0.2508	0.2794	0.3529	0.3994	0.0447	0.0499	0.0633
				0.4383	0.0847	0.0909	0.1069				

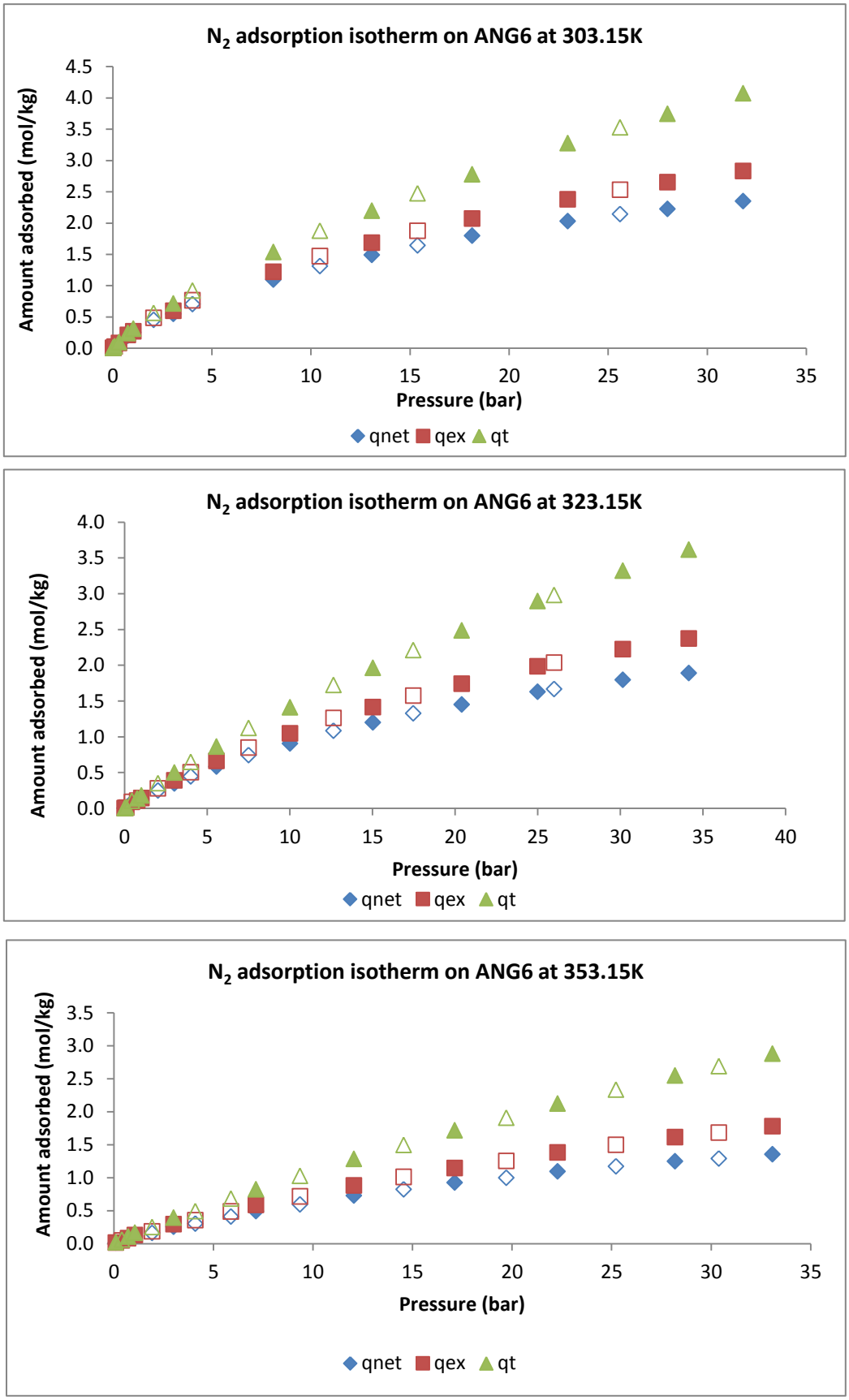

Figure B.1 - Net (◊), excess (□) and total (Δ) adsorption isotherms of nitrogen on ANGUARD 6 at 303.15K (top), 323.15K (middle) and 353.15K (bottom).

Table B.3 - Experimental butane adsorption equilibrium data on the carbon sample ANGUARD 6 at 303.15K, 323.15K and 353.15K. 40 experimental data points were measured.

303.15K				323.15K				353.15K			
P (bar)	q_{net} (mol/kg)	q_{ex} (mol/kg)	q_t (mol/kg)	P (bar)	q_{net} (mol/kg)	q_{ex} (mol/kg)	q_t (mol/kg)	P (bar)	q_{net} (mol/kg)	q_{ex} (mol/kg)	q_t (mol/kg)
0.0018	0.6981	0.6982	0.6982	0.0066	0.7175	0.7176	0.7178	0.0364	1.0252	1.0257	1.0270
0.0059	1.2985	1.2986	1.2988	0.0108	0.9571	0.9573	0.9577	0.0822	1.5183	1.5195	1.5223
0.0097	1.6463	1.6465	1.6469	0.0342	1.7557	1.7562	1.7575	0.3914	3.0472	3.0530	3.0661
0.0447	2.9250	2.9257	2.9274	0.0890	2.3123	2.3137	2.3170	0.8674	3.9330	3.9460	3.9754
0.0834	3.5221	3.5234	3.5266	0.2883	3.8531	3.8578	3.8684	2.1419	5.1309	5.1638	5.2380
0.5921	6.0561	6.0652	6.0886	0.7728	5.1751	5.1878	5.2165	4.4309	6.4442	6.5154	6.6758
1.0740	7.3356	7.3523	7.3954	1.0045	5.5960	5.6126	5.6501	8.6204	7.3348	7.4879	7.8328
2.0952	8.1699	8.2036	8.2903	2.2484	7.2691	7.3074	7.3939	5.8598	6.9672	7.0643	7.2833
1.5181	7.8986	7.9226	7.9843	3.0863	7.8173	7.8712	7.9926	3.1090	5.7599	5.8086	5.9183
0.8427	6.7919	6.8050	6.8385	3.9800	8.0334	8.1047	8.2654	1.6199	4.7123	4.7369	4.7925
0.3724	5.2927	5.2984	5.3130	1.6560	6.6846	6.7125	6.7753	0.6134	3.5661	3.5753	3.5960
0.1564	4.2081	4.2105	4.2166	0.5500	4.8201	4.8292	4.8495	0.2426	2.6475	2.6511	2.6592
0.0691	3.4227	3.4237	3.4264	0.1706	3.5435	3.5463	3.5525	0.0174	0.7175	0.7178	0.7184
0.0242	2.4727	2.4731	2.4740	0.0279	1.8670	1.8675	1.8685				
0.0036	1.0881	1.0882	1.0883	0.0045	0.7965	0.7965	0.7967				

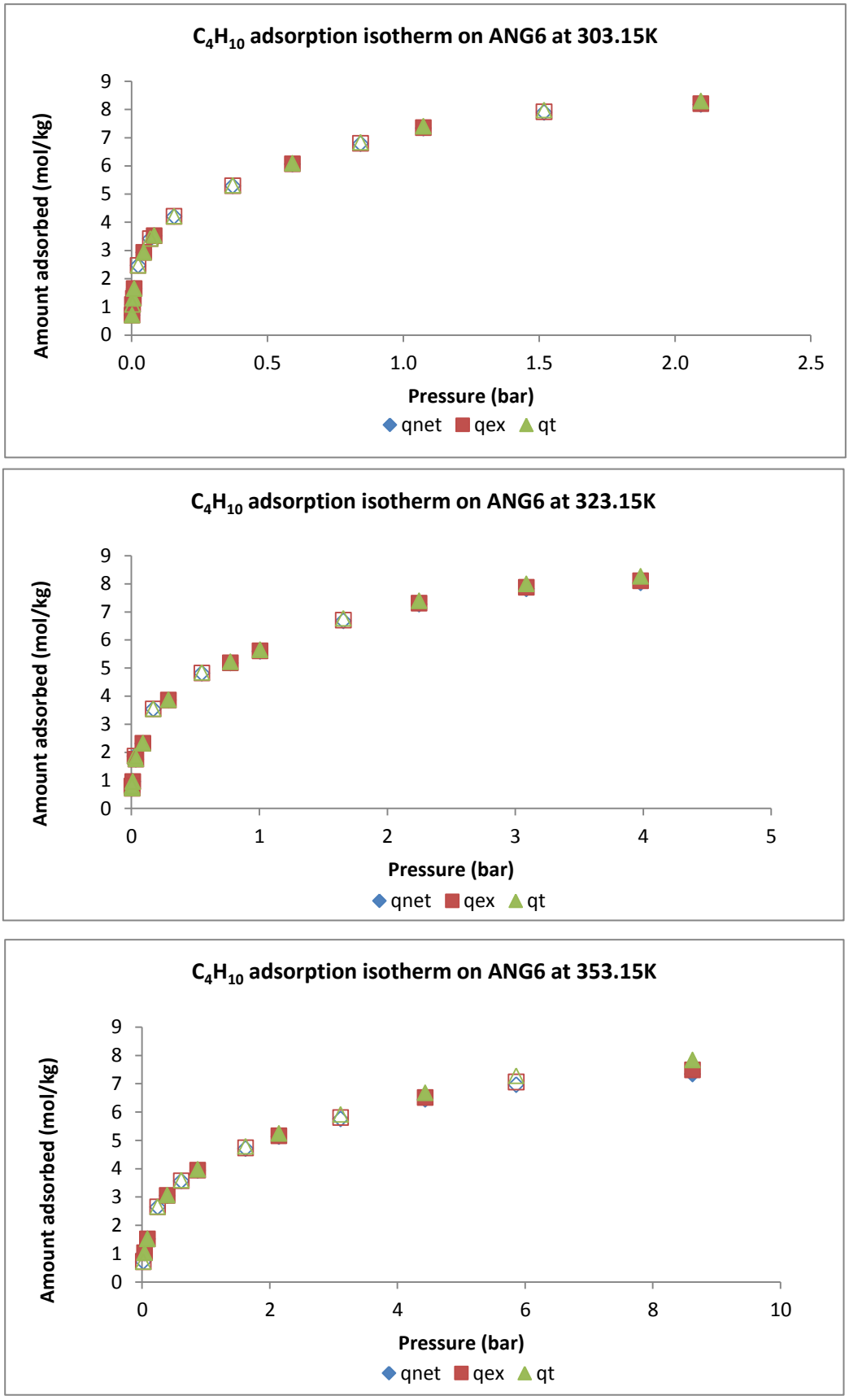

Figure B.2 -Net (◊), excess (□) and total (Δ) adsorption isotherms of butane on ANGUARD 6 at 303.15K (top), 323.15K (middle) and 353.15K (bottom).

Table B.4 - Experimental carbon dioxide adsorption equilibrium data on the carbon sample ANGUARD 6 at 303.15K, 323.15K and 353.15K. 43 experimental data points were measured.

303.15K				323.15K				353.15K			
P (bar)	q_{net} (mol/kg)	q_{ex} (mol/kg)	q_t (mol/kg)	P (bar)	q_{net} (mol/kg)	q_{ex} (mol/kg)	q_t (mol/kg)	P (bar)	q_{net} (mol/kg)	q_{ex} (mol/kg)	q_t (mol/kg)
0.0445	0.0636	0.0643	0.0660	0.0489	0.0475	0.0482	0.0500	0.0953	0.0360	0.0372	0.0404
0.1261	0.1764	0.1783	0.1832	0.0936	0.0860	0.0873	0.0907	0.3554	0.1568	0.1614	0.1733
0.3130	0.4097	0.4144	0.4266	0.3712	0.3051	0.3104	0.3239	0.6792	0.3452	0.3540	0.3767
0.6816	0.7476	0.7536	0.7692	0.7105	0.5387	0.5488	0.5748	1.0561	0.5083	0.5221	0.5574
1.0210	1.0836	1.0991	1.1390	1.0225	0.7262	0.7408	0.7782	5.1716	1.5869	1.6551	1.8302
5.0240	3.6830	3.7609	3.9610	5.0448	2.5310	2.6040	2.7916	10.2313	2.5888	2.7257	3.0774
9.8602	5.6386	5.7953	6.1978	10.0215	4.0429	4.1909	4.5711	14.8082	3.3328	3.5338	4.0502
15.0124	7.1428	7.3881	8.0185	15.8741	5.3549	5.5953	6.2128	19.7528	3.9822	4.2543	4.9535
19.7043	8.2186	8.5496	9.4001	18.0277	5.7557	6.0312	6.7393	25.4129	4.5930	4.9494	5.8652
24.5207	9.1841	9.6086	10.6993	24.5927	6.7710	7.1585	8.1542	29.8137	4.9968	5.4209	6.5109
30.1224	10.1437	10.6855	12.0775	29.8378	7.4344	7.9169	9.1566	34.1600	5.3505	5.8437	7.1110
35.1388	10.8885	11.5447	13.2308	33.9171	7.8764	8.4367	9.8764	23.2206	4.3756	4.6990	5.5301
13.4264	6.7357	6.9531	7.5119	23.1519	6.5637	6.9260	7.8572	3.1077	1.0706	1.1113	1.2160
3.1748	2.6973	2.7461	2.8714	3.3207	1.8595	1.9073	2.0299	1.5708	0.6278	0.6483	0.7010
1.5765	1.5980	1.6221	1.6838	1.5912	1.0525	1.0752	1.1336				
0.0224	0.0626	0.0630	0.0638	0.0360	0.0481	0.0486	0.0500				

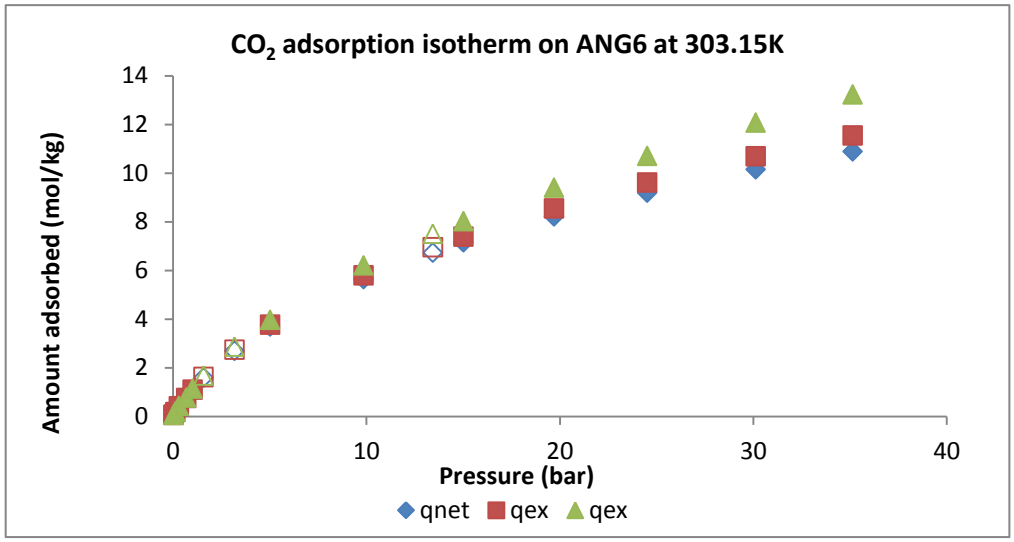

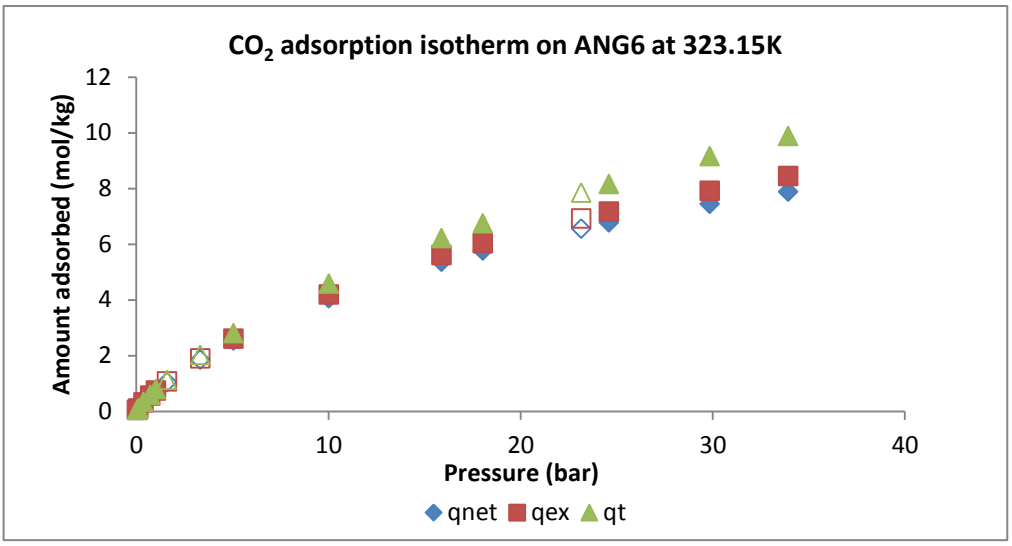

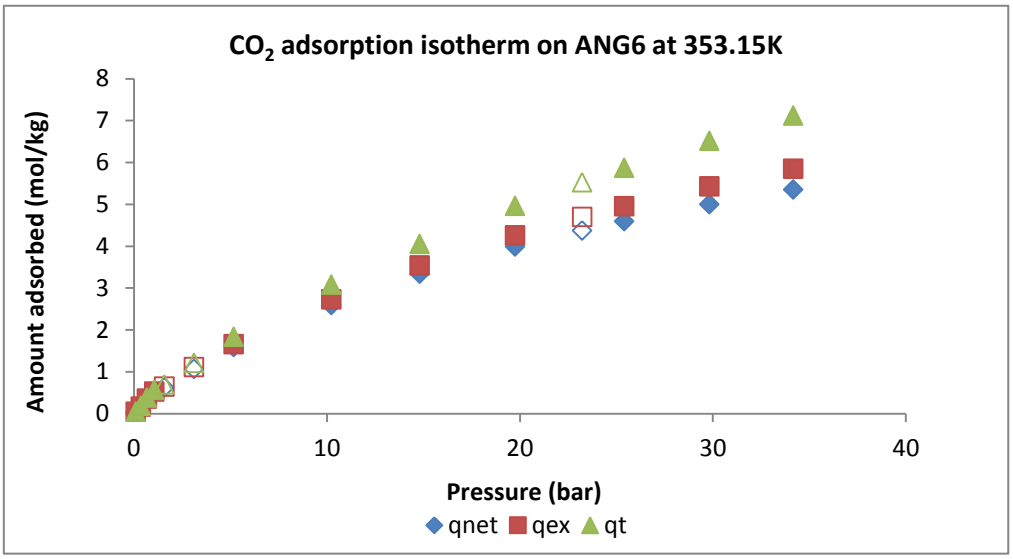

Figure B.3 - Net (◊), excess (□) and total (Δ) adsorption isotherms of carbon dioxide on ANGUARD 6 at 303.15K (top), 323.15K (middle) and 353.15K (bottom).

Table B.5 - Experimental carbon dioxide adsorption equilibrium data on ACHM at 303.15K, 323.15K and 353.15K. 41 experimental data points were measured.

303.15K				323.15K				353.15K			
P (bar)	q_{net} (mol/kg)	q_{ex} (mol/kg)	q_t (mol/kg)	P (bar)	q_{net} (mol/kg)	q_{ex} (mol/kg)	q_t (mol/kg)	P (bar)	q_{net} (mol/kg)	q_{ex} (mol/kg)	q_t (mol/kg)
0.0445	0.2084	0.2090	0.2090	0.0936	0.2832	0.2844	0.2844	0.0953	0.1377	0.1388	0.1388
0.1261	0.5503	0.5520	0.5520	0.3712	0.8957	0.9006	0.9006	0.3554	0.4973	0.5016	0.5016
0.3130	1.1820	1.1864	1.1864	0.7105	1.4487	1.4580	1.4580	0.6792	1.0534	1.0616	1.0616
0.6816	2.0122	2.0178	2.0178	1.0225	1.8759	1.8893	1.8893	1.0561	1.4246	1.4372	1.4372
1.0210	2.6879	2.7022	2.7022	5.0448	4.6886	4.7559	4.7559	5.1716	3.2839	3.3467	3.3467
5.0240	6.0145	6.0862	6.0862	10.0215	6.0383	6.1746	6.1746	10.2313	4.4303	4.5564	4.5564
9.8602	7.2441	7.3884	7.3884	15.8741	6.7796	7.0010	7.0010	14.8082	5.0933	5.2784	5.2784
15.0124	7.7803	8.0062	8.0062	18.0277	6.9377	7.1915	7.1915	19.7528	5.5262	5.7768	5.7768
19.7043	7.9952	8.3001	8.3001	24.5927	7.2193	7.5763	7.5763	25.4129	5.8598	6.1881	6.1881
24.5207	8.0591	8.4501	8.4501	29.8378	7.3046	7.7490	7.7490	29.8137	6.0267	6.4174	6.4174
30.1224	8.0314	8.5304	8.5304	33.9171	7.3298	7.8458	7.8458	34.1600	6.1140	6.5683	6.5683
35.1388	7.9005	8.5049	8.5049	23.1519	7.2130	7.5468	7.5468	23.2206	5.7941	6.0920	6.0920
13.4264	7.7225	7.9228	7.9228	3.3207	3.8471	3.8910	3.8910	3.1077	2.5038	2.5413	2.5413
3.1748	5.1124	5.1573	5.1573	1.5912	2.5311	2.5520	2.5520	1.5708	1.6783	1.6971	1.6971
1.5765	3.6160	3.6381	3.6381	0.0360	0.1290	0.1294	0.1294				

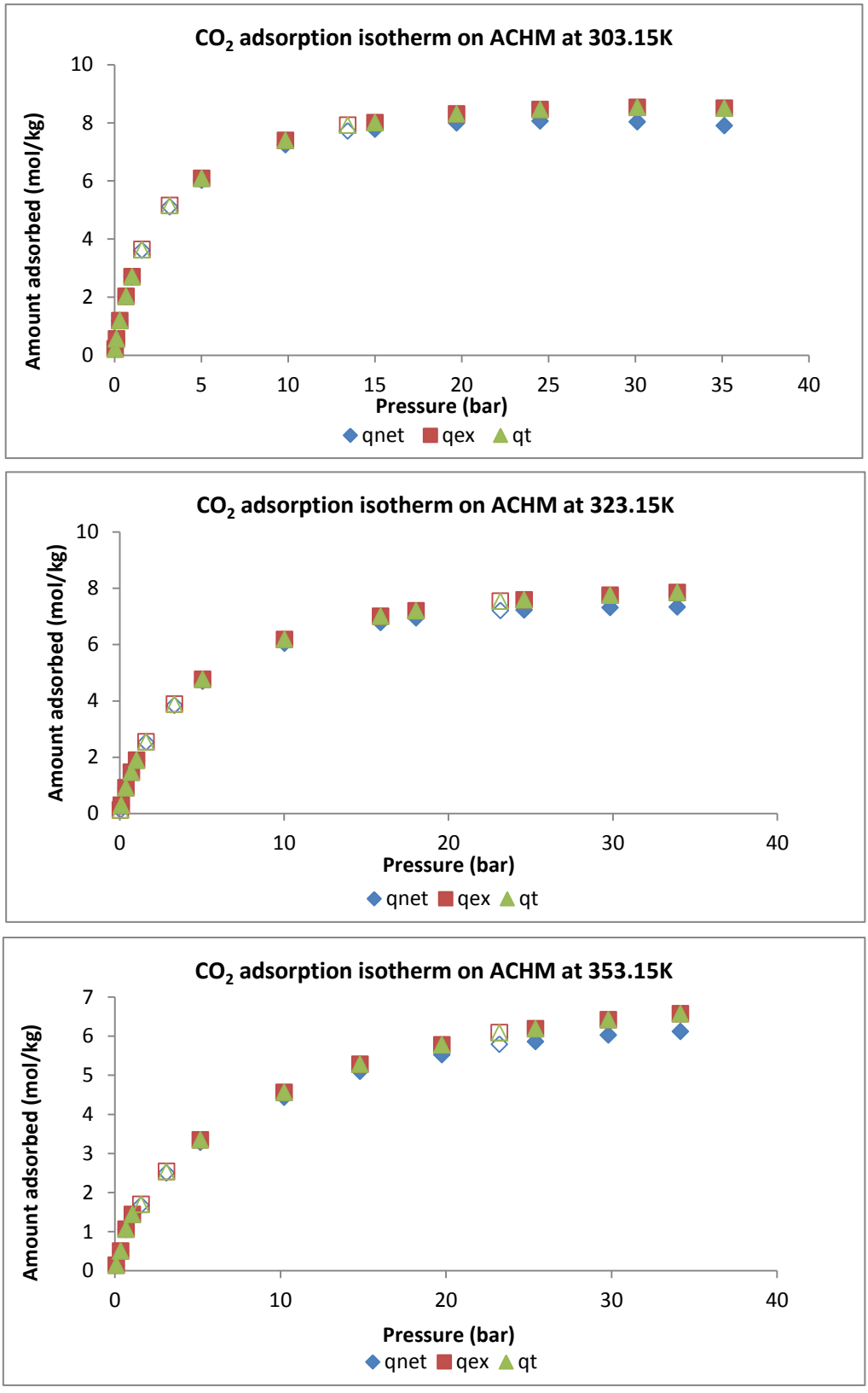

Figure B.4 - Net (◊), excess (□) and total (Δ) adsorption isotherms of carbon dioxide on the ACHM at 303.15K (top), 323.15K (middle) and 353.15K (bottom).

C. Equipment Description

C.1. Equipment Description for Adsorption Equilibrium

- **High-pressure magnetic suspension balance (MSB)**

Model: ISOSORP 2000 coupled with a Sartorius microbalance Model BP211D.
Supplier: RUBOTHERM GmbH.
Characteristics: for a maximum load of 25 g (total measuring volume, ie. suspension coupling and measuring cell with sample), the balance have a resolution of 0.01 mg, an uncertainty than 0.002% of the measured value, a reproducibility than 0.03 mg, for pressures in the range UHV - 150 bar and temperatures up to 100 ºC.

- **Vacuum Pump (VP)**

Model: EDWARDS 5 C, A65201903I
Pump Serial Number: 139482910
Supplier: EDWARDS
Characteristics: pumping speed 3.0 m^3/h, motor type: RV3 US/EUR PUMP HIGH VOLTS , 220-240 V, 50/60 Hz, Single phase, operating temperature of – 30ºC to 70ºC, maximum total pressure in high flux of 1.2×10^{-1}, maximum total pressure of 2×10^{-3}.
Pump Oil: Edwards Ultragrade 19, hydrocarbon-oil, H11025015, 1 Litre.

- **Pressure Generator**

Model: 87-6-5
Supplier: HiP
Characteristics: pressure rating of 5000 psi, capacity per stroke 60 ml with teflon packing B-208.

- **Thermostatic Bath – Refrigerator/Heater**

Model: F32-HL
Supplier: JULABO Labortechnik GmbH
Characteristics: working temperature range of -35ºC to 200ºC, temperature stability $\pm$ 0,01 ºC, cooling capacity: +20 0 -20 -30ºC to (Medium: ethanol): 0,45 0,39 0,15 0,06 KW, overall dimensions 31x42x64 cm, bath opening (WxL) 18x12 cm, bath depth 15 cm, filling volume 5.5 to 8 liters , weight 38 Kg.

Refrigerant: R134a

- **Pt100 Temperature Probes**

Model: Pt100

Supplier: RS Amidata, Spain

Characteristics: 4 wires temperature sensors with platinum resistance, that exhibit a typical resistance of 100 at 0ºC, typically measure temperatures up 850ºC, Classe B precision ±0.12- at 0.3ºC. It consists of a thin film of platinum on a plastic film inside a stainless steel involucre. The relationship between resistance and temperature is relatively linear, but curve fitting is often the most accurate way to make the RTD measurement. The probes were calibrated in the laboratory against a highly accurate Hart Scientific Pt 5613 temperature sensor with an accuracy of ±0.01 K.

- **Pressure Transducer (PT)**

Model: MKS Baratron Type 627D

Supplier: MKS Baratron

Characteristics: pressure measurements in the range from 1K Torr (1.3157bar) to as low as 0.02 Torr (0.00002 bar) Full Scale (FS). The instrument operates with ± 15 VDC (± %5) input at ≤ 250 mA, and provides 0 to 10 VDC output linear with pressure. The 627D transducer is available with optional heater status LEDs, two interface connector lock options, and a variety of fittings. The unit is capable of measuring pressure at ambient temperatures of 15ºC to 40ºC (59ºC to 104ºF).

- **Pressure Transducer (PT) (OM2)**

Model: PX01C1-150A5T

Supplier: OMEGADYNE, Inc.

Characteristics: pressure range of 0-10 bar.

- **Pressure Transducer (PT) (OM3)**

Model: PX01C1-500A5T

Supplier: OMEGADYNE, Inc.

Characteristics: pressure range of 0-35 bar.

- **Pressure Transducer (PT) (OM4)**

Model: PX03C1-3KA5T

Supplier: OMEGADYNE, Inc.

Characteristics: pressure range for 0-69 bar-138-207.

Table C.1 - Characteristic of the several pressure transducers used in this work.

Name	ACRN.	Supply (VDC)	(linearity) ACC (%F.S.)	F.S. (bar)	Output (VDC)	Ch.	Calibration Y=a+bx
Omega 1	OM1	28	0.005	1.034	0-5	0	USB6 xxx Analog Input Multi Sample
Omega 2	OM2	28	0.005	6.124	0-5	1	USB6 xxx Analog Input Multi Sample
Omega 3	OM3	28	0.005	34.83	0-5	2	USB6 xxx Analog Input Multi Sample
Omega 4	OM4	28	0.15	68.931	0-5	3	USB6 xxx Analog Input Multi Sample
Baratron	MKS	$\pm$ 15 VDC $\pm$ 5% $\leq$ 250 mA		1.005	0-10	COM 1	MKS PR 4000B
MSB					0-5	COM 4	Sartorius Rubotherm

- **Power Suppliers**

Model: PS 613
Supplier: Velleman
Characteristics: variable voltage of 0–30 V, 2.5 A DC and two fixed supplies of ±12 V and ±5 V.

- **Ball Valves**

Model: SS-43S4

Supplier: Swagelok

Characteristics: 1/8”OD fittings, Cv = 2.4, P ≤ 206 bar, 283K ≤ T ≤ 338K

- **Check Valves**

Model: SS-4C-TR-1

Supplier: Swagelok

Characteristics: 1/8”OD fittings, PTFE seals, P_{crack} = 0.06 bar, P_{max} = 206 bar.

- **Several fittings**

  Model: Swagelok types (nuts, unions, reducers, elbows, etc.)
  Supplier: Swagelok
  Characteristics: 1/8”OD fittings.

- **Computers (PC)**

  Model: Intel(R) Core(TM) i3-2100 CPU @ 3.10GHz 3.10 GHz
  Supplier: Tsunami Computers
  Characteristics: Windows 7 Professional, RAM: 8.00 Gb, System type: 64-bit Operating System.

- **Gases**

  Supplier: Air Liquide and Praxair (Portugal and Spain).
  Characteristics: Compressed Helium (H_e) (99.99%), P=200 bar from Air Liquide Alphagaz; Compressed Nitrogen (N_2), P=200 bar from Air Liquide Alphagaz; Carbon dioxide (CO_2) N48, P=80 bar from Air Liquide Alphagaz; Butano (C_4H_{10}) N35, P=0.75 bar from Air Liquide Alphagaz.

C.2. Bank of Images

Figure C.1 - Magnetic Suspension Balance (Metal version).

Figure C.3 - Unit controller for data acquisition by Rubotherm GmBH.

Figure C.2 - Pressure Transducers from MKS Baratron and Omegadyne.

Figure C.4 - Gas Bottles from Air Liquid and Praxair.

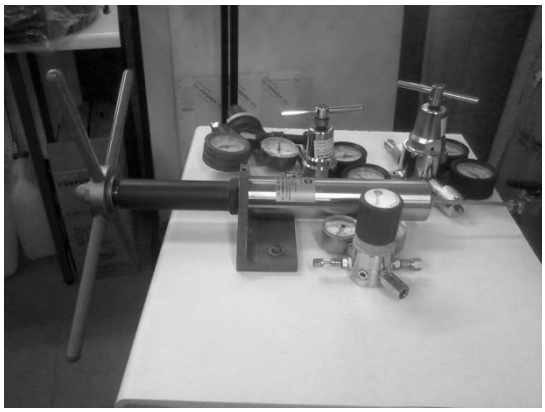

Figure C.5 - Pressure Generator from HiP.

Figure C.6 - Thermostatic Bath, Refrigerator/Heater from Julabo.

Figure C.7 - Vaccum Pump from Edwards.

Figure C.8 - Heater from Nabertherm.

Figure C.9 - Pictures of the experimental apparatus used in the equilibrium measurements.